2018-06-19

Recovery Strategies and Flow Modeling in Fractured Grosmont Carbonates with High Permeability Conduits

Cheng, Yajie

UNIVERSITY OF CALGARY

Recovery Strategies and Flow Modeling in Fractured Grosmont Carbonates with High Permeability Conduits

by

Yajie Cheng

A THESIS

SUBMITTED TO THE FACULTY OF GRADUATE STUDIES

IN PARTIAL FULFILMENT OF THE REQUIREMENTS FOR THE

DEGREE OF MASTER OF SCIENCE

GRADUATE PROGRAM IN CHEMICAL AND PETROLEUM ENGINEERING

CALGARY, ALBERTA

JUNE, 2018

Abstract

Grosmont is a large carbonate reservoir with 407 billion barrels of bitumen in place. However, it has not been commercially developed currently due to its extremely heterogeneous environment with various porosity types. A 3D heterogeneous carbonate model with high permeability conduits representing the Mclean pilot is built to investigate different recovery strategies including steam-based thermal schemes and solvent-aided methods. A vertical well CSS has severe steam override phenomenon and a SAGD process is extremely sensitive to its steam chamber which is hardly formed evenly in Grosmont. An improved hybrid SAGD in a staggered pattern that promotes lateral and downward sweep and retains more heat regardless of its steam chamber shape is presented and studied. Furthermore, a lower density and saturation temperature light solvent-aided process performs especially well in a heterogeneous carbonate reservoir with high permeability conduits. Parameter sensitivity effects are analyzed for each recovery strategy. The Brinkman-Stokes equations are tested in a 2D synthetic carbonate model, showing its possibility to describe the multi-physical flow in both free flow fractures and porous matrix. The application range and validity of Brinkman-Stokes multi-physical flow on karstified carbonates are discussed.

Acknowledgements

I would like to deliver my deepest appreciation to my supervisor Dr. Zhangxing (John) Chen, who provides consistent support and valuable suggestions to my research and study over the past several years.

My sincere gratitude also goes to the committee members, Dr. Roberto Aguilera and Dr. Qi Zhou. Thanks for their valuable suggestions.

I would like to thank Energi Simulation (formerly, Foundation CMG), National Science and Engineering Research Council of Canada (NSERC), and Alberta Innovates for all financial support and the Department of Chemical and Petroleum Engineering, Schulich School of Engineering, the University of Calgary.

Last but not least, I am thankful to the support and love from my parents and friends.

Table of Contents

List of Tables

List of Figures

Nomenclature

a	viscosity coefficient corresponding to the unit of viscosity
a_i	coefficients of a proxy model
b	viscosity coefficient corresponding to the unit of absolute temperature
BHP	bottom-hole pressure, Pa
BHT	bottom-hole temperature, °C
C	controlled injection/production operation
CDOR	calendar day oil rate, m^3 /D
$COMP_{min}$	minimum value of actual rock compressibility range, 1/Pa
$COMP_{max}$	maximum value of actual rock compressibility range, 1/Pa
$COMP_{scaled}$	scale-invariant rock compressibility
$Compress$	rock compressibility, 1/Pa
CSOR	cumulative steam oil ratio, m^3/m^3
$Cum\ \ Oil$	cumulative oil production, m^3
Cyclic SOR	steam oil ratio for each cycle, m^3/m^3
DI	fracture spacing in I direction, m
DK	fracture spacing in K direction, m
DK/DP	dual permeability/dual porosity model
EOR	enhanced oil recovery
ES-SAGD	Expanding Solvent-SAGD

FVF rock-in-fracture fraction

$HeatCap$ rock heat capability, J/(m^3*°C)

H-SAGD hybrid steam assisted gravity drainage process

K gas-liquid K-value of solvent

K permeability tenser, mD

K_f fracture permeability, mD

K_m matrix permeability, mD

K_{V1} K-value coefficient corresponding to the unit of pressure

K_{V4} K-value coefficient corresponding to the unit of temperature

K_{V5} K-value coefficient corresponding to the unit of temperature

L the length of grid block, m

n_1 unit normal vector upward

n_2 unit normal vector towards right

n_3 unit normal vector downward

n_4 unit normal vector towards left

n_i mole fraction of component i

P pre-casing leak period

p_M pressure in the matrix, Pa

p_F pressure in the fracture, Pa

p_x pressure difference in the x direction, Pa

p_y	pressure difference in the y direction, Pa
RF	recovery factor
s_{or}	residual oil saturation
T	temperature, °C
μ	fluid viscosity, cP
μ_e	effective viscosity, Cp
u_F	fluid velocity in fracture, m/s
u_M	fluid velocity in fracture, m/s
μ_i	Viscosity of the component i, Pa·s
μ_o	oil viscosity, cP
μ_s	solvent viscosity, cP
$\overline{u_x}$	average velocity of x component, m/s
$\overline{u_y}$	average velocity of y component, m/s
x_i	input sensitivity parameters

CHAPTER 1 : INTRODUCTION

Alberta produces three-quarters of Canada's oil in 2010 and holds a total of 26.9 billion cubic meters crude bitumen; however, only 4.3% of that has been recovered since 1967 (ERCB, 2011). The portion of bitumen recovery to total oil is continuously increased in recent years. Thus, the surged demand for heavy oil arouses considerable interests in bitumen-rich reservoirs. Grosmont is a large carbonate reservoir with 64537*E+06 m^3 (407 billion barrels) initial bitumen in place. Nevertheless, there is still no commercial development currently in Grosmont due to its extremely heterogeneous environment with various porosity types including fractures, matrix, vugs, breccia and karst. A 3D heterogeneous carbonate model with high permeability conduits representing the Grosmont Mclean pilot is built to investigate different recovery strategies including steam-based thermal schemes and solvent-aided methods.

Steam has enormous latent heat than water, so steam-based thermal methods have been tested as possible options for injection in Grosmont. Some pilots of cyclic steam stimulation (CSS) have achieved some great success since the 1970s whereas SAGD provides another chance to enhance bitumen recovery recently. The performance of CSS and SAGD varies in different regions or reservoirs. Therefore, different thermal recovery strategies including an improved hybrid SAGD process and parameter sensitivity effects will be discussed in a 3D carbonate model with heterogeneously distributed properties representing the Mclean pilot.

Solvent can be utilized as an additive with steam to accelerate dispersion and reduce oil viscosity, which has been widely tested in the Alberta heavy oil reservoirs with encouraging results. However, only simple experiments have been established to show the viability of solvent-aided processes on Grosmont carbonates. Therefore, numerical simulation of solvent additives for heterogeneous carbonates with high permeability conduits is investigated comprehensively to detect the recovery mechanisms, phase behavior, and optimal solvents or conditions in this paper.

Considering the existence of high permeability conduits and large-scale karst or vug related regions in this complicated carbonate reservoir, a traditional dual permeability/dual porosity numerical model with the application of Darcy's law in both fractures and matrix may no longer capture the multi-physical fluid flow. Therefore, the Brinkman-Stokes equations are employed to predict the multiple flow physics including free flow in large fractures and Darcy's flow in porous matrix. A 2D synthetic flow model is built to explore the large-fracture effects on velocity or pressure and detect the application range or validity of the Brinkman-Stokes equations on karstified carbonates. Moreover, parametric studies and up scaled treatments through effective permeability calculations provide a more detailed application method of the Brinkman-Stokes equations in future work.

CHAPTER 2 : REVIEW OF LITERATURE

2.1 Grosmont Geology Description

The upper Devonian Grosmont is a bitumen-bearing, regionally extensive carbonate formation located in northern Alberta with a southwest-northeast stratigraphic section in Fig. 2-1. It is truncated by a regional unconformity sub-crop beneath the Cretaceous Mannville Group. Grosmont displays an unconformable contact directly with an overlying Cretaceous Athabasca McMurray-Wabiskaw formation. There are four members divided: Grosmont A through D separated by discontinuous marl layers from Lower Grosmont to Upper Grosmont. C and D units contain 80% of the total Grosmont bitumen (Ezeuko, 2015). Existing platform characteristics are generated by 5 main geological successions: sedimentation, dolomitization, a fractured network, karstification and biodegradation. The Grosmont was dolomitized causing scattered molds and vugs. Most fractures were derived from rock collapse or dissolution and hence created a dynamic forebulge in the formation (Machel et al., 2012). The complex diagenetic history generates a highly heterogeneous reservoir including a variety of pore types: matrix, pervasive sub-vertical fractures, karst related vugs and breccia (Jiang, 2009). Core photographs of the fractured Grosmont carbonate are displayed in Figure 2-2 which proves the various porosity types. The sub-vertical fractures are extensively distributed in the Grosmont C and D mixed with karst-breccia clasts. Moreover, the scale features of pore vary from centimeters to meters (Hein, 2016).

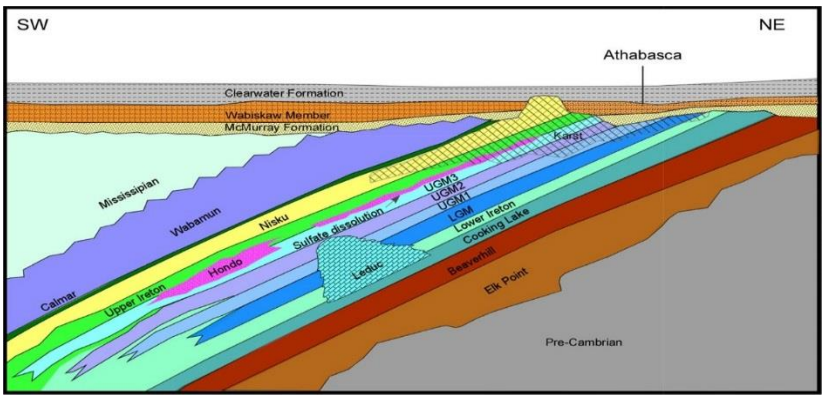

Figure 2-1 SW-NE stratigraphic section of Grosmont (Machel, 2012)

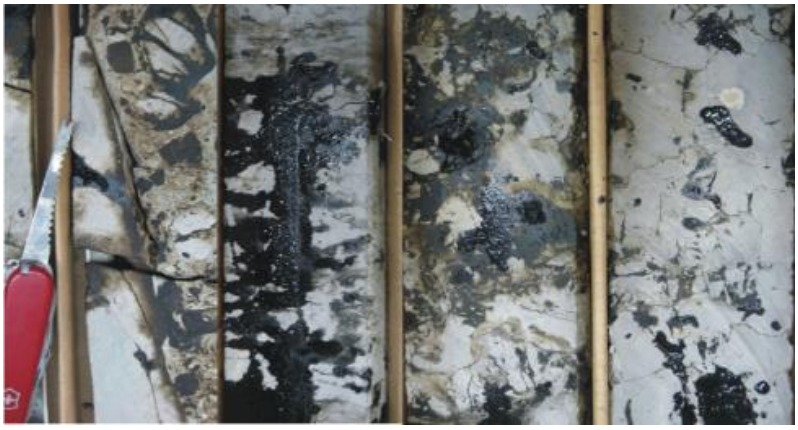

Figure 2-2 Core photographs of the fractured Grosmont carbonate (Hein, 2016)

2.2 Thermal Recovery in Grosmont

Primary recovery is extremely poor in Grosmont as a result of higher viscous oil and lower dissolved gas, especially for this seriously heterogeneous reservoir. Generally, fractured carbonates are mixed or oil wet, so steam-based thermal methods perform better than water due to enormous latent heat and late breakthrough.

2.2.1 Field Pilots

From the 1970s to the 1980s, several field pilots were conducted to test different thermal EOR (enhanced oil recovery) methods including cyclic steam stimulation, steam flooding and in situ combustion. The first attempt started in late 1974 at Chipewyan River including air injection followed by CSS in vertical wells. It showed different reservoir conditions in this area with higher steam injection pressure than that seen at McLean or Buffalo Creek. Rapid pressure depletion indicated the existence of high water saturation thief zones. A small steam slug (about 2000 m^3) and a short soak period were main reasons for poor production (UNOCAL Report 648). The pilot in the Algar area (81-17-W4) was performed by Chevron in 1976. A vertical well CSS was drilled in Grosmont D and this pilot was short owing to operation problems (Yuan, 2010).

Steam drive in Grosmont C at Buffalo Creek was operated since 1977. A steam flood process applied to two wells was proved disappointing (Yuan, 2010). However, a 12 cycles CSS test was carried out in a single vertical well leading to a great success in terms of productivity from 1980 to 1986. Oil production rates were up to 70 m^3/day while a steam-oil ratio (SOR) for some cycles appeared abnormal. An in-situ combustion process was then operated and it was hard to control the combustion front (McDougall, 2008).

The McLean test commenced after the encouraging results from previous pilots in 1982. A five-spot pattern with four observation wells was designed initially with steam flooding to a center well.

Unfortunately, steam loss owing to an interaction between wells and communication between Grosmont C and D was observed. To improve process efficiency, it turned to CSS in corner wells and achieved better results in some wells with a peak oil production rate of 100 m^3/day (Ezeuko, 2013). Steam injection pressure at McLean was observed lower than that seen in other tests. Then in 1984 the pilot was expanded to a larger five-spot pattern; however, there appeared premature steam breakthrough. Foam was used to improve steam conformance and showed incremental production (McDougall, 2008).

A Unocal Orchid pilot in 1985 drilled a single CSS well at 08-01-88-20W4. Both McLean and Orchid sites were in an area prone to karstification. A low oil rate in cycle one was attributed to a long steam cycle at a low rate. Initial lower cold water injectivity indicated that where water mobility existed, the reservoir appeared to be unbounded (UNOCAL Report 648). Laricina's Saleski project, the first solvent cyclic SAGD pilot in Grosmont, was located 350 km of northern Alberta. There were four horizontal well pairs, two pairs in the Grosmont D and two in the C. Both SAGD and a single well cyclic process were performed since 2010. The cyclic operation showed a potential to improve production because of less sensitivity to the pilot plant and artificial lift. The results, however, were not enough to eliminate SAGD as a feasible technology for the Grosmont carbonate. Great steam injectivity was observed even under a cold formation condition (Hosseininejad, 2014).

2.2.2 Numerical and Experimental Investigations

Swapan (2007) investigated different thermal recovery processes and performed sensitivity assessments in a 2D fractured carbonate model. A heterogeneous environment made the flooding process inefficient. An increase in fracture spacing led to more steam injection without oil production growth yet. Different matrix permeability showed no apparent change of production in the early time. Wettability and viscosity played important roles in the simulation results. It was shown that CSS and SAGD with staggered wells were more suitable for a lower viscosity reservoir while SAGD may be appropriate in high viscosity bitumen carbonates.

A 5 cycles Buffalo Creek pilot was history matched of production and bottom-hole temperature by Novak (2007). At first, several isotropic permeability simulation models achieved an agreement production trend with the field record, though BH (bottom hole) temperature was not matched accurately. Then heterogeneous permeability models adjusted by a genetic algorithm were introduced to obtain improved matching results.

Considering the extreme heterogeneity of Grosmont, a geostatistical model with 11 facies based on core and log data was created using Petrel software by Yuan (2010). A semi-quantitative method was used to correct permeability so that five grades of fracture intensity were designed. This due permeability/dual porosity model was validated by history matching of the first cycle of the Buffalo Creek pilot vertical well CSS process. From the numerical results, a SAGD technology

with low injection pressure in Grosmont C appeared viable with better performance and conformance compared with CSS. Warm solvent simulation results were consistent with the experimental core tests. High permeability fractures promoted the gravity drainage and solvent flow.

A multiple objects network of fractures, vugs, breccia and matrix was used with the stochastic method to build a novel carbonate Grosmont model by Ezeuko et al. (2013). Properties distribution were conducted with the conditioned-Gaussian approach. They supposed that the traditional facies modeling technique was hard to describe the extremely heterogeneous Grosmont and the presence of large permeability karst or vugs related regions offered a strong communication between non-fracture objects. Thus, control limits were established to reduce uncertainty as much as possible. Preliminary continuous injection SAGD results from the multi-objects based model showed that steam preferred to flow through high conductive objects resulting in steam channelling, so it may not be economical. Capillary forces, cycle length, injection pressure and formation compressibility played important roles in the CSS process.

Jinxiu (2013) built a DP/DK model to characterize the Grosmont carbonate and history matched the horizontal well CSS performance. Matrix permeability could be measured from the routine core analysis whereas fracture porosity and permeability would be decided by history matching and a sensitivity analysis. Simulation results implied that small vugs should be considered as a part

of matrix, in order to achieve better matching performance. Some unknown parameters in Grosmont were also acquired via the sensitivity analysis and history matching.

Yang (2014) presented a cyclic to continuous SAGD strategy based on the experience of the Saleski pilot which could maximize the recovery in future. Initially cyclic processes for individual horizontal wells located at the bottom were performed until the cycles were matured, and then were turned to continuous steam injection at the top and production from the bottom well. Three main mechanisms were found including thermal expansion, spontaneous imbibition and gravity drainage. The influence of low porosity in Grosmont could be compensated for by lower water saturation. Then a cyclic operation follow-up project of Saleski Phase 1 was designed.

Song (2015) tested various steam injection strategies and observed a high steam-oil ratio using Yuan's model (2010). She insisted that the performance of SAGD and horizontal CSS would be influenced by unconformable steam chambers. After several numerical studies, vertical injector-horizontal producer steam flood achieved the best results due to gravity flow and delayed steam breakthrough.

2.3 Hybrid SAGD

To improve the performance, several variations of SAGD operation have been presented such as fast SAGD, hybrid SAGD and follow-up process. A regular hybrid SAGD combining the

advantages of both CSS and SAGD has achieved encouraging results in Clearwater formation by Coskuner (2009).

SAGD as a follow up process to vertical well cyclic steam stimulation was implemented on the Liaohe Oilfield in China which is a thick and high permeability bitumen reservoir with top water. Due to a low recovery factor and high remaining oil saturation between wells after CSS, the follow-up SAGD process in horizontal wells was designed and predicted over 50% oil recovery in this formation through numerical studies (Liu, et al., 2003). Later a field pilot of follow-up SAGD with 2 horizontal and 12 vertical wells was tested. Thermal communication between horizontal and vertical wells should be established before switching to SAGD. A production decline was observed during the vertical CSS from 2000 to 2003 and then a follow-up process was applied to reverse the decay trend. The ultimate bitumen recovery factor for this pilot could reach up to 56% (Yang, 2006).

Jiang (2006) investigated a follow-up process after cyclic steam stimulation to improve bitumen recovery in the Clearwater formation with a thin and complex stratigraphy. Infill wells were drilled between current CSS horizontal wells to mimic the gravity drainage process, and hence achieved additional 20%-30% bitumen recovery. Also, a combination of CSS and SAGD with four horizontal wells operated by periodically injection or production was evaluated in a homogeneous

model by Ghanbari (2011), which presented more oil and better injectivity than conventional SAGD.

Coskuner (2009) introduced a novel hybrid SAGD (HSAGD) method whose well patterns were derived from the fast SAGD, but a totally different operation strategy. At first, CSS was performed in both SAGD injectors and offset horizontal wells until steam chambers contacted each other. Then the SAGD injector started injecting steam while SAGD producers and offset wells kept continuously producing. An analysis of numerical results in the Clearwater area suggested that this proposed hybrid method presented more oil production and less steam injection within a shorter period compared with the conventional CSS or SAGD.

Li (2011) designed a new hybrid SAGD method using only a single SAGD well which would be more viable and economic in a shallow formation. Initially, CSS was operated in offset horizontal wells until steam chambers contacted each other. At this point, the single SAGD well began injecting steam and bitumen would be produced from offset horizontal wells nearby. A numerical study in typical oil sands reservoirs showed that this new hybrid strategy improved steam chamber evolution and enhanced recovery efficiency compared with the conventional CSS.

2.4 Solvent-Aided Recovery

Solvent can be utilized as an additive with steam to accelerate dispersion and reduce oil viscosity. It has been widely tested in the Alberta heavy oil reservoirs with encouraging results.

2.4.1 Numerical and Experimental Study of ES-SAGD on Heavy Oil

Nasr et al. (2003) presented the Expanding Solvent-SAGD (ES-SAGD) process and completed experimental tests on Cold Lake bitumen. They insisted that non-condensable gas injection would not improve oil drainage in a live oil reservoir. In addition, a solvent having a closer vaporization temperature with steam achieved the best results, so C_6 had the highest drainage rate. On the other hand, Jha (2013) disagreed with Nasr and claimed that steam condensed at first due to much smaller partial pressure. Li (2010) thought that C_7 achieved better results than C_6 in a 2D Athabasca homogeneous model because of earlier condensation before steam, and hence a water film ahead would impact the solvent dissolution. However, a heavier solvent like C_{12} was hard to recycle and appeared uneconomic. ES-SAGD with butane was tested in a 3D heterogeneous permeability numerical model with finer grids near wells (Govind, 2008). Comparison of simulation results in Cold Lake and Athabasca reservoirs exhibited that solvents heavier than butane were favorable to the Athabasca heavy oil formation. If initial solution gas was considered in the model, solvent additives did not appear effective (Ardali, 2010). Moreover, Hosseininejad (2010) insisted that co-injection of NCG was not efficient in viscous bitumen. Various parameters including a solvent type and concentration, relative permeability, initial GOR, and steam trap control were evaluated

in a 2D homogeneous McMurray model by Yazdani during a solvent co-injection process (2012). There are two criteria for selecting the optimal solvent including mixture quality and mixture rate (Marciales, 2014). Keshavarz pointed out that the volatile solvent injection resulted in lower three-phase temperature and less water in vapor at a chamber edge (2015).

2.4.2 Experimental Study on Grosmont Carbonate

The cold solvent of propane and CO_2 soak experiment was performed in a Grosmont core and revealed more than 60% original oil recovery. Also, the cold solvent test in a single well of the Saleski pilot appeared high injecticvity (Edmunds, 2009). Then, a warm solvent core test displayed more oil drainage and also explored the oil in lower porosity regions (Jiang, 2009). A simulator modeling this warm solvent test was completed. It appeared that high permeability conduits in Grosmont carbonates would promote the solvent process (Yuan, 2010). During the hot solvent soak, experimental temperature was set slightly higher than the saturation condition and butane diluted more oil than propane (Pathak et al., 2012). Solvent could be utilized as a follow up process after steam, because it explored the oil in matrix of carbonates where steam is difficult to access due to wettability. At high temperature, propane performed less effectively than at intermediate temperature owing to weak solubility (Bryan, 2014). The steam-over-solvent injection strategy in fractured Grosmont cores produced 40%-90% ultimate oil. Also, hot water immersion could accelerate solvent retrieval. Distillate (C_{11}-C_{15}) achieved better results than a pure solvent in carbonates due to closer structure to oil and less asphaltene precipitation. Moreover, CO_2 could be

used as an alternative solvent in this injection strategy to save the cost (Naderi et al., 2013, 2014, 2016).

2.5 Multi-physical Flow in Carbonate Reservoir with Large Fractures or Vugs

Grosmont rock types were characterized and classified into microscopic, mesoscopic, macroscopic and megascopic porosity (Luo, 1995). A naturally fractured reservoir is extremely heterogeneous with various porosity types including fractures, matrix, vugs, breccia and karst, so that Darcy's law is no longer suitable to describe fluid flow accurately in a whole carbonate formation. The Stokes equation can be utilized to predict the free flow in large fractures or vugs while Darcy's law is still applicable in porous media. Brinkman modified Darcy's equation to capture boundary effects which avoided additional boundary problems as in the Darcy-Stokes coupling method (Brinkman, 1947). Recently, the Brinkman-Stokes (B-S) equations had been studied to predict multiple flow physics including free flow in large fractures and Darcy's flow in porous matrix. Popov (2009) presented an upscaled treatment of the B-S unified formulation through effective permeability calculations in a 2D or 3D model with different types of fractures or vugs. Marcin et al. (2011) showed that when fracture permeability was less than 4 orders of magnitude of matrix permeability, effective permeability of the entire region was governed by matrix permeability. Also, several studies on numerical solutions and algorithms for the B-S equations were discussed (Laptev, 2003; Gulbransen, 2009; He, 2015).

CHAPTER 3 : GROSMONT HETEROGENEOUS MODEL

3.1 Reservoir Simulation Model

A 3D numerical model containing 9 x 9 x 40 grid blocks with a grid size of 10 m x 10 m x 1 m is generated by the thermal simulator CMG STARS (2015). Thus, it covers around a 2 acres area with a net thickness up to 40 m. The dual porosity/dual permeability method is used to build the carbonate model and different thermal strategies or solvent additives will be tested in this region. Although there are barrier layers separating Grosmont C and D units, communication between these two members exists as the field record (UNOCAL report 648) reported. In this simulation model, Grosmont C and D are separated by discontinuous marl barrier layers where porosity is set to 0.01, vertical permeability is 0.1 mD and water saturation is 1. The basic reservoir model parameters are summarized in Table 3-1.

Sometimes the measured permeability from cores is lower than that from well tests and the porosity measurement from a core study is often smaller than that from a log analysis (Yuan, 2010). Therefore, to characterize the extremely heterogeneous Grosmont carbonate, some spatial properties distributions like porosity, permeability and saturation are derived from known core intervals or well log data in the UNOCAL Mclean pilot report. Complex secondary pore types such as karst or vug related regions existing in the Grosmont should be included in this model. Qi (2013) insisted that small scale vugs can be considered as a part of matrix, because if vugs are

combined with fractures, history data will not be matched precisely as a result of rapid oil production from fractures and steam breakthrough. Thus, karst or vugs related regions are treated as parts of matrix in this simulation model and their positions are derived by logging data as well. Furthermore, unavailable properties will be decided by stochastic simulation in a reasonable range and tuned by history matching or optimization as listed in Table 3-2. Several fracture parameters are not possible to measure accurately in such a complicated carbonate, so they will also be decided and tuned by the history matching and sensitivity analysis process.

Original reservoir matrix properties distributions of layer I=5 in this simulation model are displayed below in Figure 3-1, Figure 3-2 and Figure 3-3. Matrix porosity and permeability and oil saturation are distributed heterogeneously. Some karst or vug related regions are considered as parts of matrix in this simulation model for reasonable matching results, so several grids have larger matrix porosity and permeability values accordingly. It is visible that the discontinous mar layers seperating Grosmont C and D have a value of 0.01 for porosity, 0.1 mD for vertical permeability and 0 for oil saturation. Moreover, the main stress in the Grosmont carbonate is along the NE, so there are some connected conduits towards this direction. Thus, high matrix permeability conduits whose vertical permeability are larger than 3500 mD resulting from severe karstification are existing mainly in the left part (J=1-3) of upper Grosmont D along the I direction. The position of high permeability conduits is decided by logging data around well BD as shown

in Figure 3-3. These high permebility conduits must be considered in the simulation model due to severe karstification as recorded in the Mclean pilot.

Table 3-1 Grosmont reservoir model parameters

Parameter	Value
Reservoir Pressure,	1,100
Depth of Grid Top,	230
Reservoir Temperature, °C	11
Water Thermal Conductivity, J/(m*day*°C)	5.35e4
Oil Thermal Conductivity, J/(m*day*°C)	1.15e4
Gas Thermal Conductivity, J/(m*day*°C)	5,000
Overburden/underburden Heat Capacity, J/(m^3*°C)	2.6e6
Overburden/underburden Heat Conductivity, J/ (m*day* °C)	1.51e5
Initial Solution Gas in Oil, mole fraction	0.05

Table 3-2 Range of matrix and fracture properties

Parameter	Value
Matrix Porosity	0.1-0.3
Matrix Permeability I & J, mD	10-400
Matrix Permeability K, mD	10-400
Fracture Volume Fraction	0.01-0.06
Fracture Permeability I & J, mD	10000-25000
Fracture Permeability K, mD	10000-25000
Fracture Spacing I&J, m	0.1-3
Karst or vug related region porosity	0.2-0.6
Rock Compressibility, 1/kPa	$8e^{-}6$-$5e^{-}5$
Rock Heat Capacity, J/(m^3*°C)	2e6-4.5e6

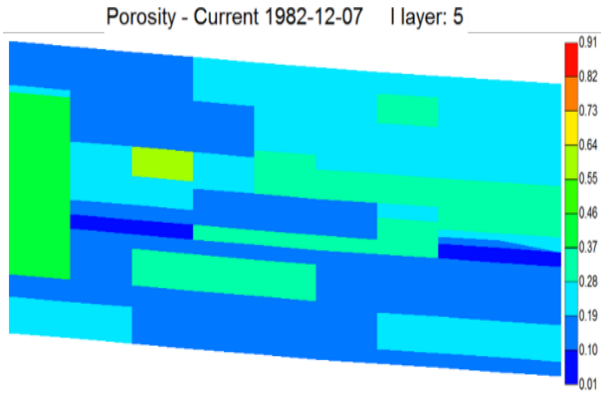

Figure 3-1 Original matrix porosity distribution of layer I=5 (1982-12-07)

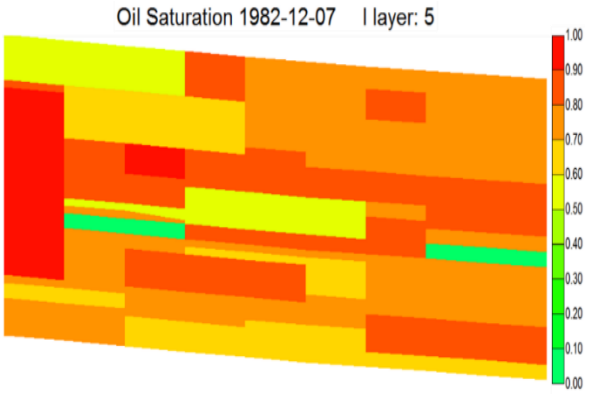

Figure 3-2 Original matrix oil saturation distribution of layer I=5 (1982-12-07)

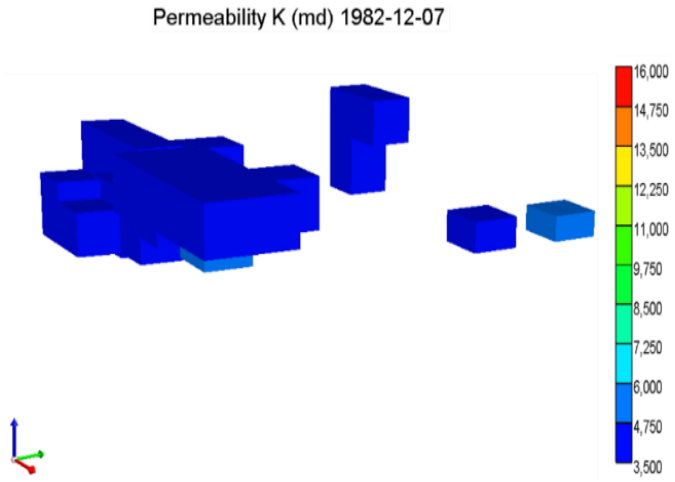

Figure 3-3 High matrix permeability conduits distribution ($K_{VERTICAL} \geq 3500$mD) mainly in the left (J=1-3) of upper Grosmont D due to severe karstification.

3.2 McLean Pilot Site

All of the basic field history data is acquired from the UNOCAL McLean pilot report. This site is located at T87-R19W4. Well configurations are designed as in Figure 3-4. 11 vertical wells are in Grosmont C, and four of them are observation wells marked as red points. A five-spot pattern spaced 110 m from the center well is drilled at first. Due to steam loss to the upper Grosmont D as a result of existing karst regions, five-spot flooding operation is changed to cyclic steam stimulation in the corner vertical wells from 1982 to 1984. Two more wells C12 and C13 are drilled after 1984 to test a larger five-spot CSS and a surfactant pilot in well C13.

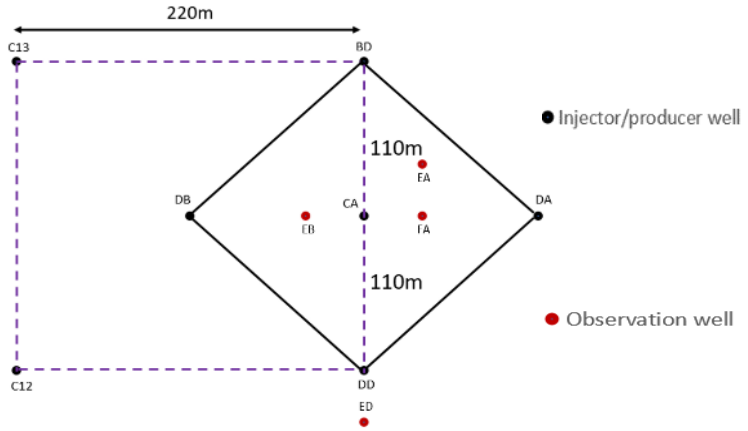

Figure 3-4 Well configurations of Mclean pilot

3.3 Fluid Physical Properties

The Grosmont carbonate is rich in highly degraded bitumen (API), more than 400 billion barrels which form the greatest potential reservoir (ERCB, 2011). A bitumen viscosity-temperature

relationship curve is shown in Figure 3-5. The ultrahigh viscosity of oil in reservoir conditions greater than 1 million cP which is not mobile can be reduced to six orders of magnitude when temperature increases.

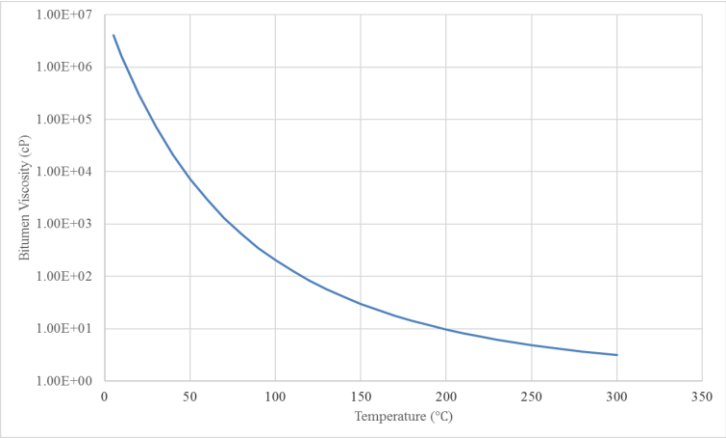

Figure 3-5 Bitumen viscosity-temperature relationship curve

Generally, a fractured carbonate is widely supposed to be oil wet, but wettability reversal to water wet is observed as temperature increases (Al-Hadhrami et al., 2001). In Table 3-3, it presents oil-water and gas-liquid relative permeability obtained from laboratory experiment data and tuned during history matching. Oil wettability is proved from oil-water relative permeability ends.

Table 3-3 Oil-water and gas-liquid relative permeability

S_w	K_{rw}	K_{row}	S_l	K_{rg}	K_{rog}
0.20	0.0000	1.0000	0.15	1.0000	0.0000
0.22	0.0000	0.7588	0.20	0.9181	0.0002
0.25	0.0001	0.5642	0.25	0.8139	0.0016
0.27	0.0006	0.4096	0.30	0.7200	0.0055
0.29	0.0020	0.2892	0.35	0.6000	0.0130
0.32	0.0049	0.1975	0.40	0.4700	0.0254
0.34	0.0102	0.1296	0.45	0.3500	0.0440
0.36	0.0190	0.0809	0.50	0.2400	0.0698
0.39	0.0324	0.0474	0.55	0.1650	0.1040
0.41	0.0518	0.0256	0.60	0.0930	0.1480
0.43	0.0790	0.0123	0.65	0.0719	0.2040
0.46	0.1157	0.0051	0.70	0.0450	0.2710
0.48	0.1638	0.0016	0.75	0.0270	0.3520
0.50	0.2257	0.0003	0.80	0.0200	0.4470
0.53	0.3035	0.0000	0.85	0.0100	0.5590
0.55	0.4000	0.0000	0.90	0.0050	0.6870
			0.95	0.0000	0.8340
			1.00	0.0000	1.0000

CHAPTER 4 : THERMAL RECOVERY STRATEGIES IN GROSMONT

Steam has enormous latent heat than water. Plenty of energy is released when steam contacts with cold oil and then condenses. A fractured carbonate is generally mixed or oil wet, so steam-based thermal methods perform better than water as viable options for injection. Commercial recovery developments have not been started yet. Some people insist that the SAGD technology performs better compared with CSS (Yuan, 2010; Song, 2015). Conversely, other simulation results and pilot tests exhibit more economic and viable results for cyclic operation (Ezeuko, 2013; Yang, 2014; Hosseininejad, 2014). However, high vertical permeability and a thick reservoir may make the gravity drainage to have great achievements as applied in the McMurray formation. Chapter 3 introduces a heterogeneous numerical model representing the Grosmont carbonate. Therefore, the validation of this model and various thermal strategies will be investigated and discussed in this chapter.

4.1 Cyclic Steam Stimulation

4.1.1 Introduction

The cyclic steam stimulation process, known as huff and puff, is comprised of three periods: steam injection, soak and production. Initially, high-temperature and high-pressure steam is injected into a well for weeks or months. Then the well should be shut in for days or weeks to allow heat distribution in a reservoir. The key to thermal based technologies is the utilization of heat to reduce oil viscosity and then make it mobile. Consequently, oil is produced from the same well during the

production period. This process can be cycled until production is no longer profitable. Cyclic steam stimulation has been applied to heavy oil reservoirs extensively and achieved excellent performance.

4.1.2 Field Performance Analysis

The initial Mclean pilot focuses on Grosmont C including five vertical wells and four observation wells and later two more wells are drilled for an expanded pattern as showed in Figure 3-4. A summary of field production history for the five vertical wells CSS process are listed in Table 4-1. All of the field data is from UNOCAL report and AccuMap database.

In this table, P means the pre-casing leak period and C is the abbreviation of controlled injection/production operation. An anomalous temperature response at the observation well EA in lower Grosmont after injection of 400 m^3 steam to well CA indicates a communication to upper Grosmont along the NE direction. This inference coincides with similar situations in the Buffalo Creek pilot. Thus, Well CA was shut in after pre-casing leak time due to severe karst related dissolution and collapse around this well. An average injected steam slug size is 7000 m^3 in each well except for the initial cycles of wells DD and BD. It is noticeable from this table marked by red color that the amount of water production from wells DA and BD is much larger than the steam injection to these wells, whereas wells DD and DB produce less water than injected in certain cycles. Between the communication wells, steam injection would reduce oil production and

increase produced water. From the field report, steaming well BD had a negative effect on the oil production of well DA. Also, pressure communication was observed between almost all wells in the Mclean pilot (UNOCAL report 648). Therefore, both production data and pressure tests confirm extensive inter-well communications in the Mclean pilot.

Continuous improvement of cyclic SOR after a number of cycles at well BD, northeastern of the well DB, is found in the table. In contrast, the first cyclic SOR is extremely high up to 255 m^3/m^3 and improved remarkably to around 5 m^3/m^3 at well DB. The performance of this well, however, is unstable for later cycles as a result of wells interference or steam channeling along the NE direction (the direction of main stress). A Calendar Day Oil Rate (CDOR) at Mclean is around 6 m^3/day. The various performance at different wells shows the heterogeneity of the Grosmont formation containing fractures and karst related regions. Poor production of some wells at Mclean is regularly likely due to large amounts of heat lost to Upper Grosmont or casing problems. In conclusion, well BD has a steady oil rate and reasonable cyclic SOR is hence chosen as the target well in later research. Also, there is no apparent difference of the reservoir condition between Mclean and Buffalo Creek through various inspections. Steam injection pressure at Mclean reveals lower compared with other sites tests.

Table 4-1 CSS field production history for five vertical wells in Mclean pilot

Well Name	CA13	DA13				DB13					DD12					BD13				
Cycles	P	P	1	2	3	P	1	2	3	C	P	1	2	3	C	P	1	2	3	C
Injection Days	14	55	28	41	55	48	30	36	53	47	99	54	41	53	27	11	25	44	53	14
Production Days		35	82	75	64	17	59	71	67	72		27	76	72	66			70	72	55
Cycle SOR		48	5	10	21	254	5.4	5.3	12	24		23	9.5	22	7.3			7.2	8.2	3.8
Cycle WOR		34	7.9	4.6	10	46	3	4	8	22		7.4	2.1	8	18			6	10	36
CDOR (m^3/D)		1.7	13	5.9	3	0.43	15	12.2	5.1	3.4		1.1	4.3	2.5	5.5			9.0	6.8	5.5
Injected Steam (m^3)	1205	7082	7088	7068	7107	7121	7119	6970	6975	9620	3502	2002	4774	6975	3722	779	4333	7397	6967	1426
Produced Bitumen (m^3)		149	1432	685	345	28	1323	1306	609	400		89	504	316	507			1022	846	379
Produced Water (m^3)		5116	11323	3128	3552	1284	3978	5215	4864	8648		666	1077	2520	8939			6137	8949	13620
Total Injected Steam (m^3)	1205	28345				37705					20975					20902				
Total Produced Bitumen (m^3)		2611				3266					909					1868				

4.1.3 Simulation Well Placements and Operation Conditions

For the vertical well CSS process, a 13 m well is drilled in the middle of the simulation model and perforated in the Grosmont C (I=5, J=5, K=27-39) below the discontinuous marl layers where porosity is 0.01, vertical permeability is set to 0.1 mD and water saturation is 1 as described before. Considering that well BD is the research target well, all operation conditions should keep consistent with the field history data. In this model, maximum injection pressure is 5000 kPa and steam quality is 80%. CSS operation starts from December 8, 1982 to October 4, 1984 including the pre-casing leak, three cycles and a controlled production period. A field steam injection rate and an actual oil production rate are imposed as the operation constraints. Injection or production duration for each cycle is different and displayed in Table 4-1.

4.1.4 Sensitivity Assessments

Some parameters have relatively large influences on production and bottom-hole pressure results. A sensitivity analysis is a technique to define how sensitive an objective function is to different variables within specific ranges. Thus, before history matching, this method is used to decide which parameters are more sensitive to the measured data.

4.1.4.1 Response Surface Designs

A response surface method (RSM) is to establish a proxy model representing the initial numerical model through a serious of experimental designs, and then the connection between parameters and an objective function can be derived. Usually, there are two types of RSMs including a linear model and a quadratic polynomial model which are listed below.

Linear proxy model:

$$y = a_0 + a_1 x_1 + \cdots + a_n x_n \tag{4-1}$$

Quadratic proxy model:

$$y = a_0 + \sum_{i=1}^{n} a_i x_i + \sum_{i=1}^{n} a_{ii}\, x_i^2 + \sum_{j<i} \sum_{i=2}^{n} a_{ij} x_i x_j \tag{4-2}$$

where a_n is the coefficient of a proxy model and x_i is the input parameter.

In order to match the field history of the Grosmont carbonate successfully, numerous reservoir parameters are tested initially including rock compressibility and heat capability, fracture spacing, fracture permeability, a fracture volume fraction and a rock in fracture fraction. CMOST (2015) software is utilized to complete the response surface methodology and a set of optimal experimental designs are automatically generated by software at this moment. Various reservoir parameters influence the performance individually or interactively making the ultimate tuned values not exclusive; however, each parameter is tested in a reasonable and practical range.

After several simulations, the proxy model equation with coefficients in terms of actual parameters for bottom-hole pressure is:

$$BHP = 1540.11 + 126.217 * DI + 8.31938E07 * Compress - 0.000193686 * HeatCap - 29.7147 * \mathrm{DK}^2 - 1.35693E12 * Compress^2 \tag{4-3}$$

The proxy equation in terms of actual parameters for cumulative oil production is:

$$Cum\ \ Oil = 911.534 + 887.129 * DI + 4.05307E07 * Compress - 1720.86 * FVF - 184.013 * DI^2 - 4.02937E11 * Compress^2 + 1525.88 * FVF^2 \quad (4\text{-}4)$$

These relationships can also be seen in the scatter plots. As the derived equation (4-3), bottom-hole pressure has an extremely strong quadratic correlation with rock compressibility and a linear relation with rock heat capability (Figure 4-1). A BHP value will rise initially and then fall gradually with the increasing compressibility whereas keep dropping with the ascending rock heat capability. The relationship of fracture spacing in the I&J direction or rock compressibility to oil production cannot be seen clearly in the scatter plot (Figure 4-2), because both fracture spacing in the I&J direction and rock compressibility have apparent linear and quadratic relationships simultaneously on cumulative oil production which can also be shown in the tornado plot (Figure 4-3).

(a) Rock compressibility

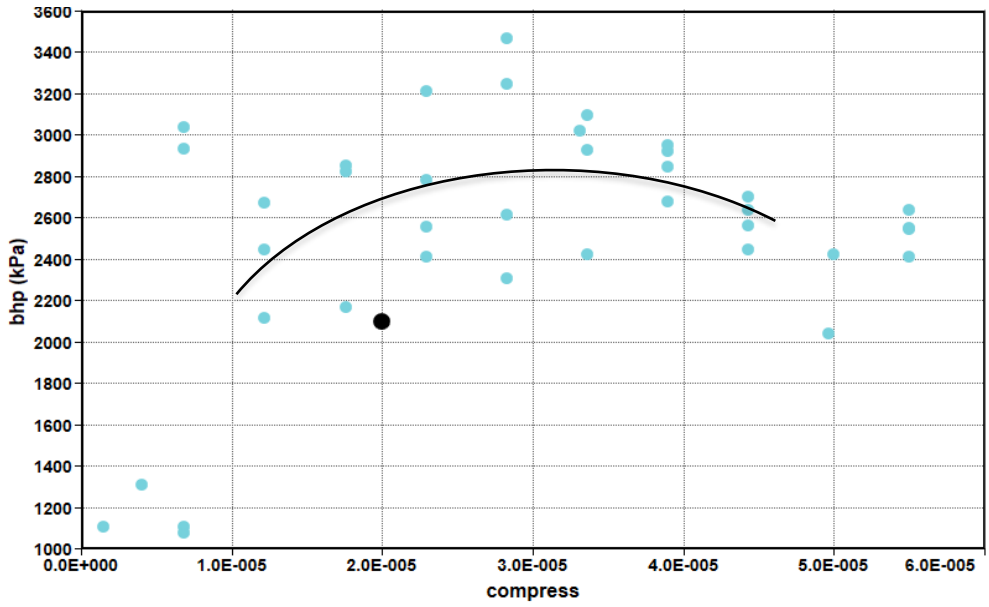

(b) Rock heat capability

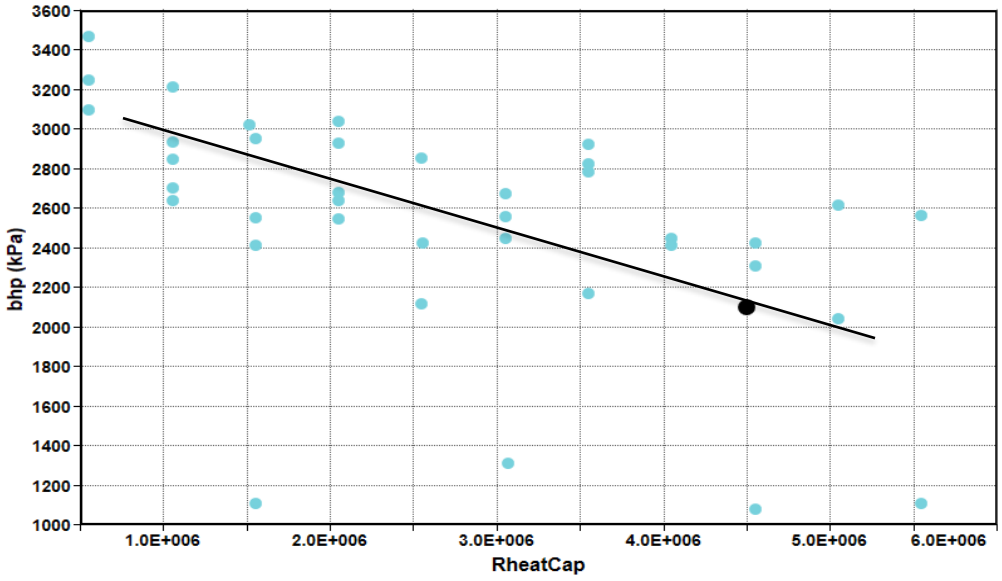

Figure 4-1 Correlation scatter plots between (a) rock compressibility, (b) rock heat capability and bottom-hole pressure

(a) Fracture spacing in I&J direction **(b) Rock compressibility**

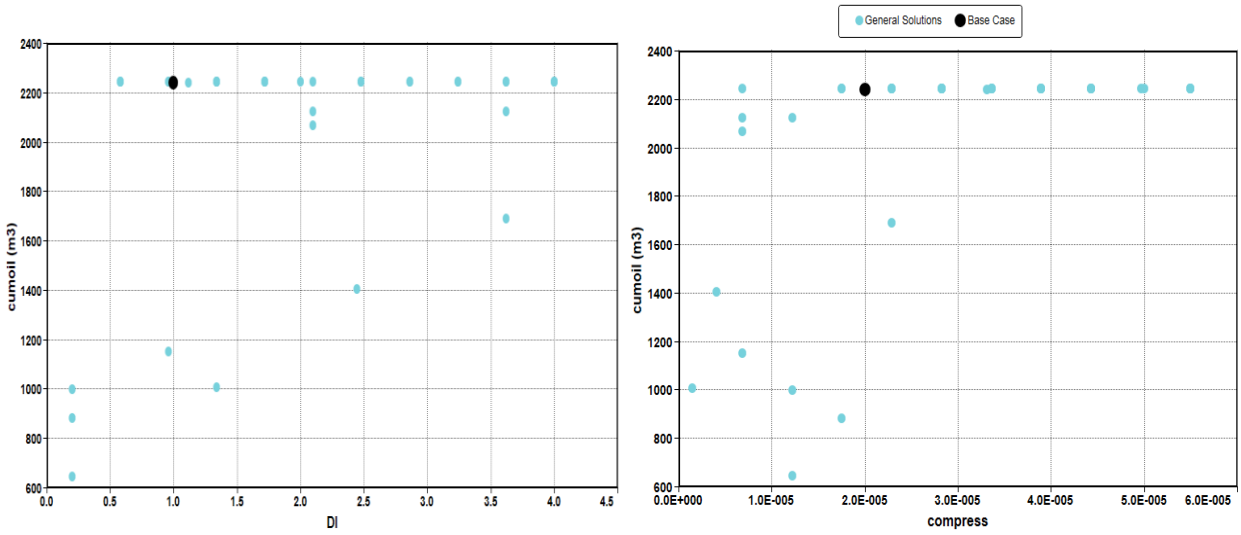

Figure 4-2 Correlation scatter plots between (a) fracture spacing in I&J direction, (b) rock compressibility and cumulative oil production

The tornado plots of effect estimates are displayed in Figures 4-3 and 4-4. A value in the plots represents the predicted response variation within the range of each parameter. A higher value suggests that the parameter is more sensitive to the objective function. Maximum or minimum means the largest or smallest objective function value of all designed experiments results. The target means the objective value of history file data. The statistically insignificant parameters are excluded in these tornado plots. Effect estimates depend on the scale of parameters apparently, and thus all parameters are normalized with a mean of 0 and a range from -1 to 1 in the CMOST software to eliminate the unit conversion problems.

Specifically, the scale-invariant rock compressibility is:

$$COMP_{scaled} = \frac{2(COMP - COMP_{min})}{COMP_{max} - COMP_{min}} - 1 \quad (4\text{-}5)$$

where $COMP_{min}$ and $COMP_{max}$ are the minimum and maximum values of the actual rock compressibility range. The scaled effects estimate is different with the coefficients in terms of the actual parameters mentioned in equation (4-3) and (4-4). Moreover, it is a half of the scaled predicted response value appearing in the tornado plot.

Analysis of these plots indicates that fracture spacing in I&J direction, rock compressibility and the rock-in-fracture fraction have relatively significant effects on the cumulative oil production, whereas parameters of rock compressibility and heat capability, and fracture spacing are important for the bottom-hole pressure in this carbonate model. As mentioned in the scatter plots, both linear and quadratic effects of fracture spacing in the I&J direction or rock compressibility play relatively important roles in oil production, which can also be observed form the response variation values in Figure 4-3. Particularly, the non-linear (quadratic) effect of compressibility*compressibility is the most sensitive effect for BHP and moderately significant for cumulative oil production. Moreover, there is no evident interaction effect between these parameters for both oil production and bottom-hole pressure which can be shown in the Sobol analysis later as well.

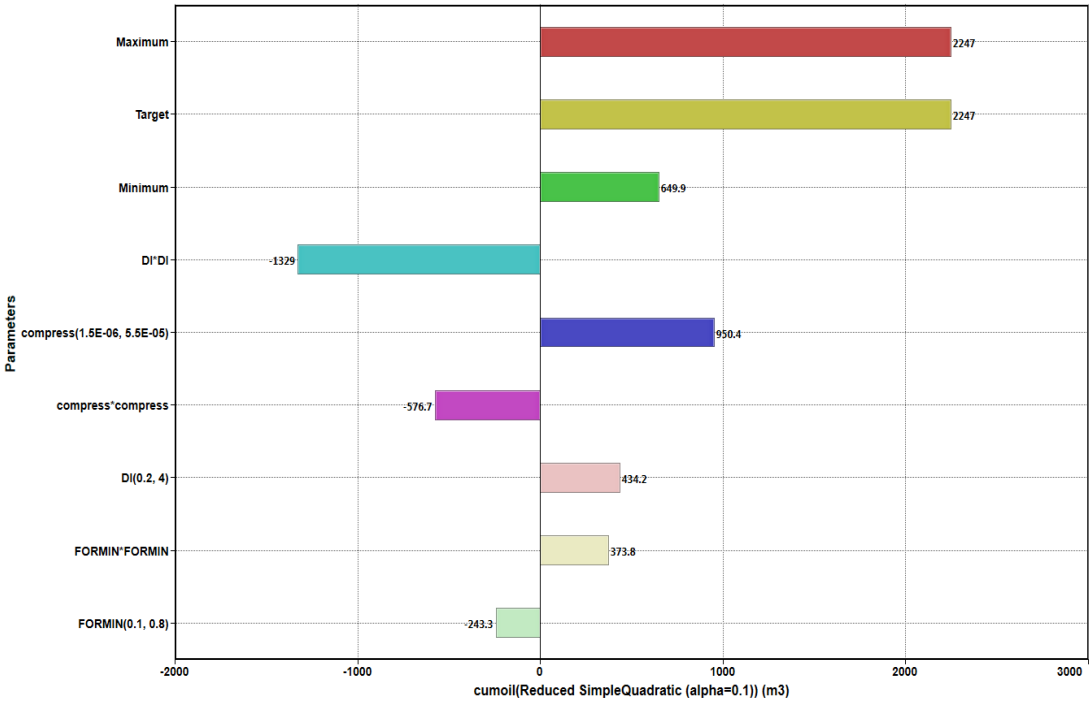

Figure 4-3 Tornado plot of effect estimates for cumulative oil production

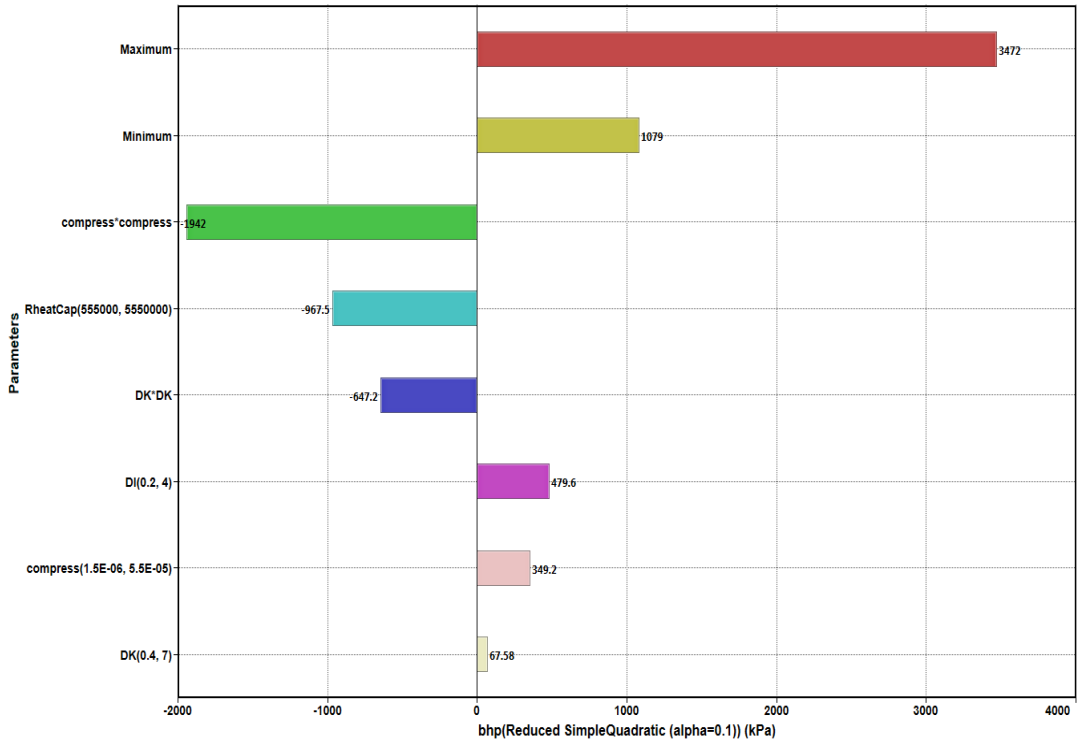

Figure 4-4 Tornado plot of effect estimates for bottom-hole pressure

A Sobol plot is a variance-based method to quantify the proportion of variance for each parameter which can contribute to the objective variance (Saltelli et al., 2010). Based on Figure 4-5, 4-6 and 4-7, rock compressibility is clearly the greatest factor to the variability of cumulative oil production, BHP and cumulative steam injection with 57%, 47% and 99% main effects individually. Fracture spacing in the I &J direction contributes much more variability to oil production (38%) and BHP (9.5%) than steam injection (0.078%), whereas rock heat capability gives less contribution to cumulative oil production (0.00022%) than BHP (39%) and steam injection (0.81%). At the same time, fracture permeability in I&J direction is less sensitive to all of the three objective functions. However, the influence of fracture permeability cannot be negligible which will be discussed later. Moreover, the interaction effects (marked by red color) for each parameter are not significant in all output responses. This result coincides with effect estimates in Figures 4-3 and 4-4 mentioned before.

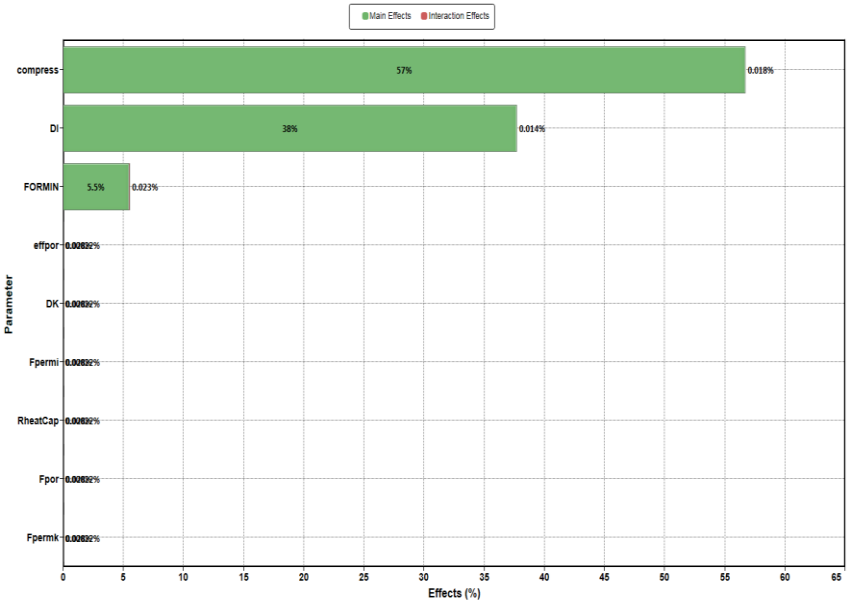

Figure 4-5 Sobol plot of cumulative oil production objective function

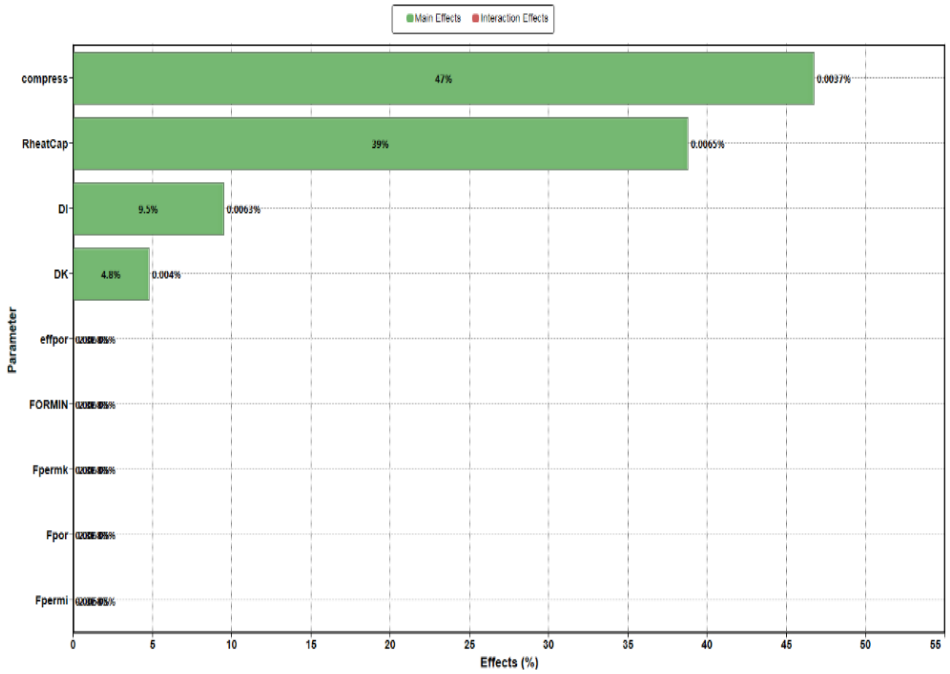

Figure 4-6 Sobol plot of bottom-hole pressure objective function

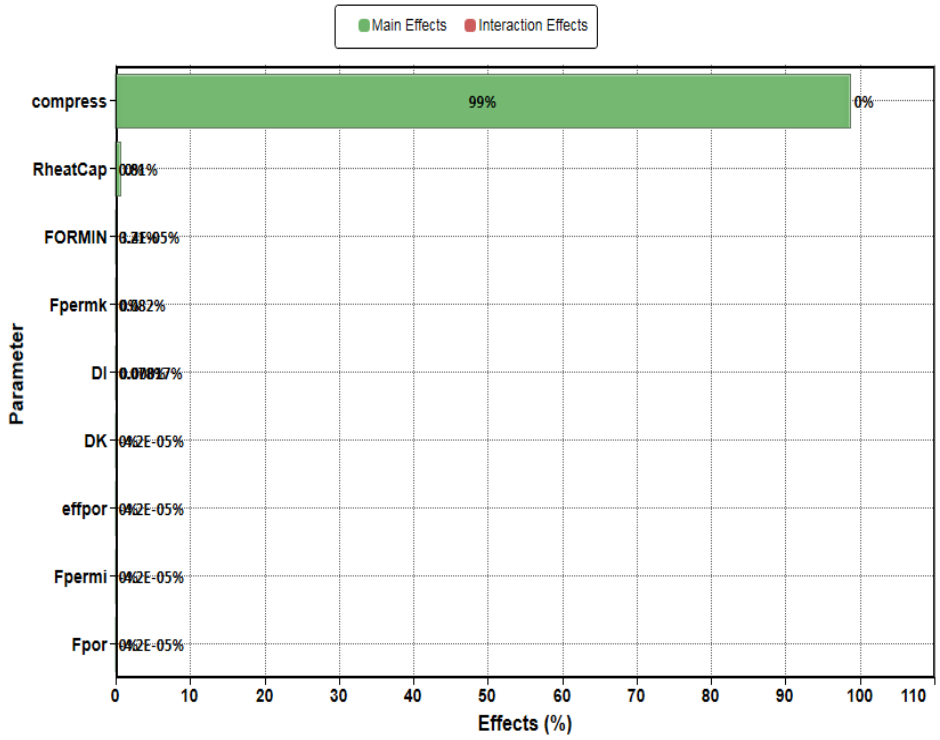

Figure 4-7 Sobol plot of cumulative steam injection objective function

4.1.4.2 Main Effects Analysis

After effects screening experiments, there is no apparent interaction between different factors and statistically insignificant parameters can be excluded in the main effects analysis. Thus, we consider sensitive factors of rock compressibility (6.85E-06, 3.89E-05 and 5.50E-05 1/kPa), fracture spacing in I&J (0.5, 1.5, 2.5m) and the rock in fracture fraction (0.17, 0.45, 0.8) to oil production, and compressibility (6.85E-06, 3.89E-05 and 5.50E-05 1/kPa), fracture spacing in I&J (0.5, 1.5, 2.5m) and rock heat capacity (9E+05, 2E+06, 4.5E+06 J/m^3* °C) to bottom-hole pressure in the main effects analysis. After factorial experimental designs, the main effects in Figures 4-8 and 4-9 agree with results provided by CMOST in which compressibility is the most important role for both oil production and BHP. As rock compressibility impacts the formation injectivity and productivity, higher rock compressibility leads to the lower pore pressure, and, consequently a decrease in BHP. Also, more oil production is attributed to better injectivity with more steam injection at a higher compressibility. Larger fracture spacing (I&J) means less high permeability fractures and improved steam channeling in the model, causing production and injector pressure growth. Enhancing the formation (rock) fraction in fractures, the void volume of oil storage and flow conduits will become small. Accordingly, oil production is declined. Increasing rock heat capacity results in low temperature around the wellbore, leading to lower BHP.

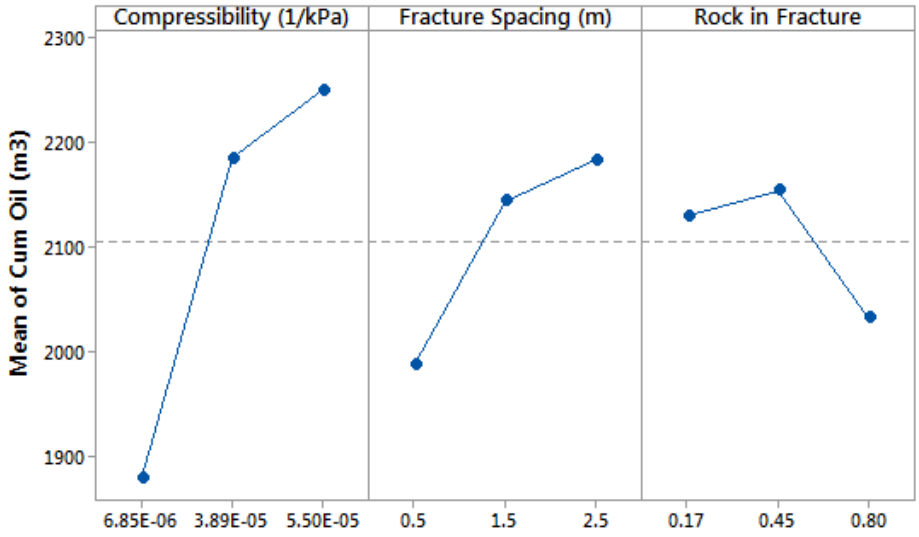

Figure 4-8 Main effects plot of cumulative oil production

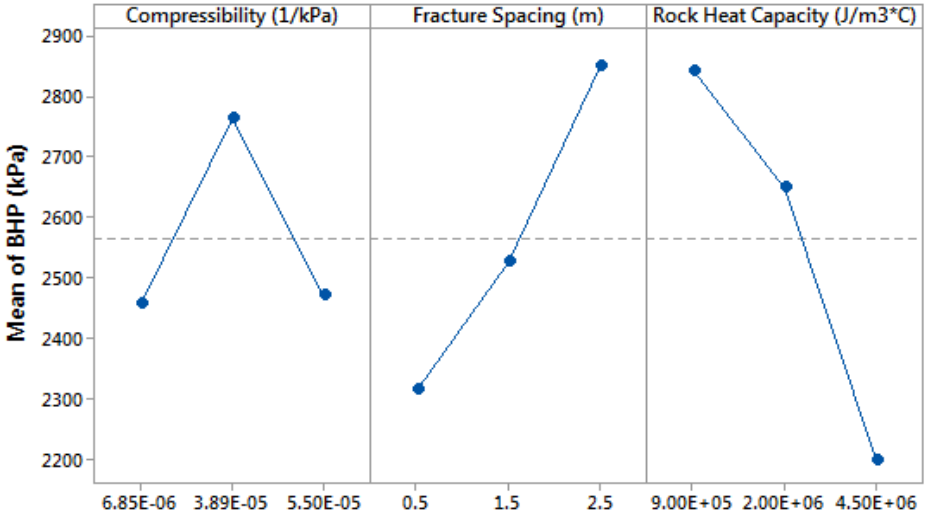

Figure 4-9 Main effects plot of bottom-hole pressure

4.1.4.3 Effects of Fracture Permeability

It is difficult to core the fractured rock and impossible to measure fracture properties accurately in such a complicated carbonate formation. Grosmont, where sub-vertical fractures are extensively

distributed, is greatly heterogeneous in permeability. Although the fracture permeability in the Sobol plots discussed before displays less sensitivity to all of the objective functions, the influence of fracture permeability is vital to simulation results. In this part, if the fracture permeability in I & J direction range narrows down to 5000-20000mD from the original 10000-35000mD and fracture permeability in the K direction is reduced to 1000-10000mD from the original 5000-20000mD, the effect estimates of some parameters will change accordingly.

Comparing the effect estimates and Sobol analysis plots of lower fracture permeability (Figures 4-10 to 4-14) with Figures 4-3 to 4-7, the quadratic effect of compressibility*compressibility becomes the most sensitive factor to both cumulative oil production and bottom-hole pressure. Effects of DI*DI and fracture permeability for oil production turn to be smaller, and meanwhile, DK*DK and fracture permeability become less sensitive to BHP in the lower fracture permeability system. Moreover, fracture spacing occupies much less percentage to all three objective functions and the rock in fracture fraction also turns to less sensitivity to oil production and steam injection when the fracture permeability range is lower. We should notice that the plots below include statistically insignificant parameters, so the values may be slightly different than those in Figures 4-3 to 4-7 excluding insignificant factors. In conclusion, most of the fracture related properties are more important and sensitive in a high fracture permeability reservoir and should be noticed during a history matching process.

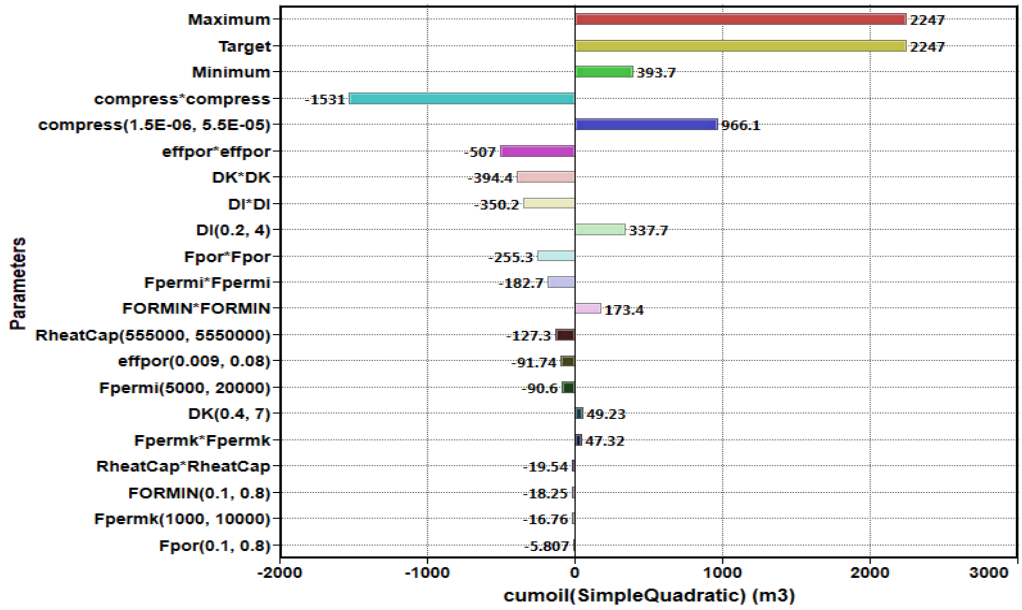

Figure 4-10 Tornado plot of cumulative oil production effect estimates (lower fracture permeability range)

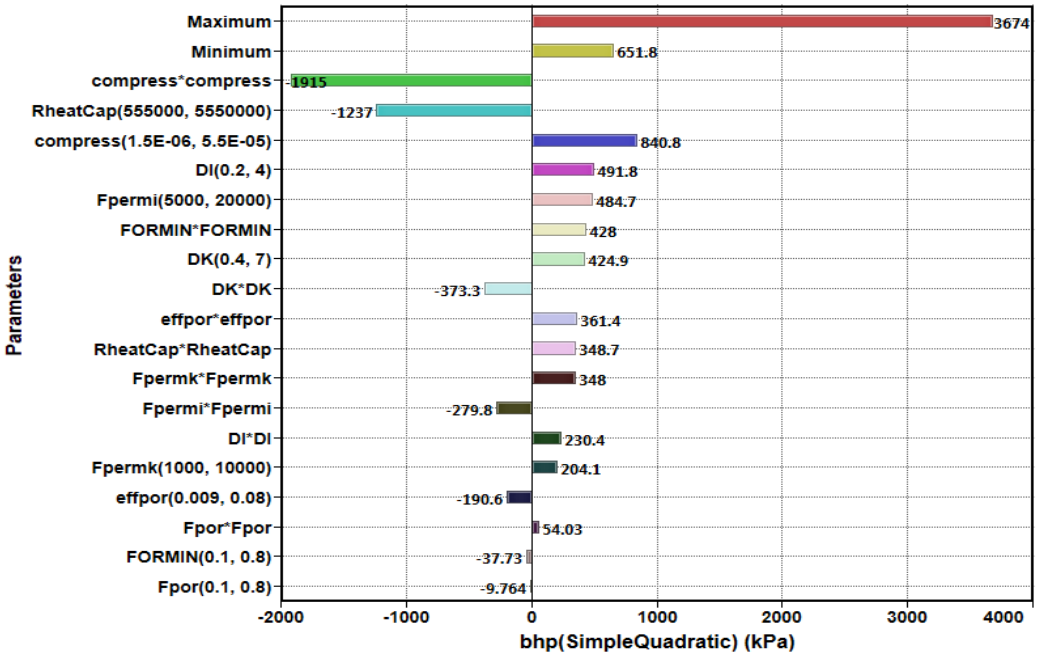

Figure 4-11 Tornado plot of bottom-hole pressure effect estimates (lower fracture permeability range)

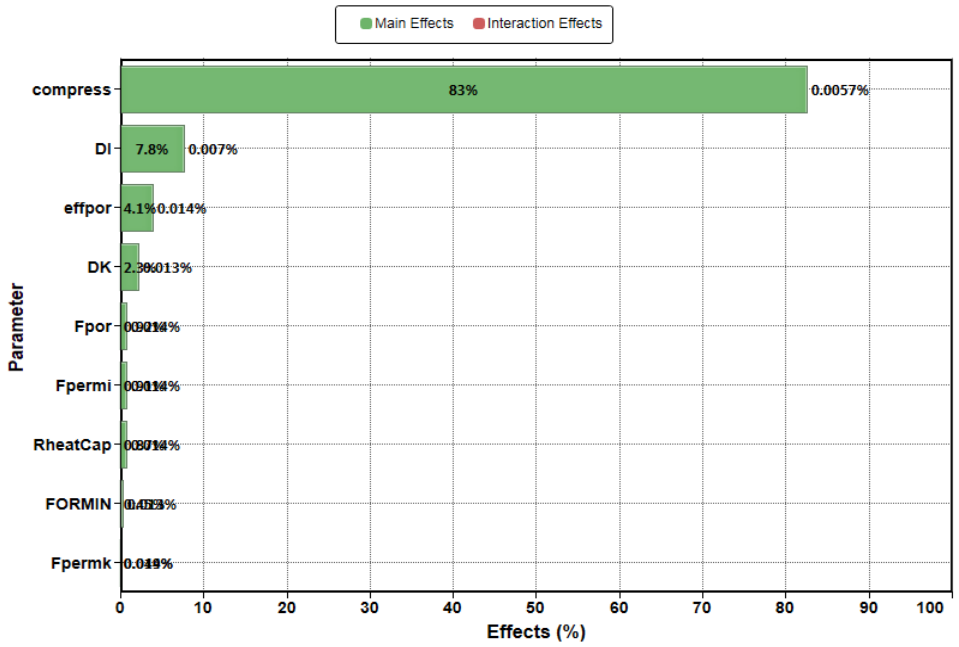

Figure 4-12 Sobol plot of cumulative oil production objective function (lower fracture permeability range)

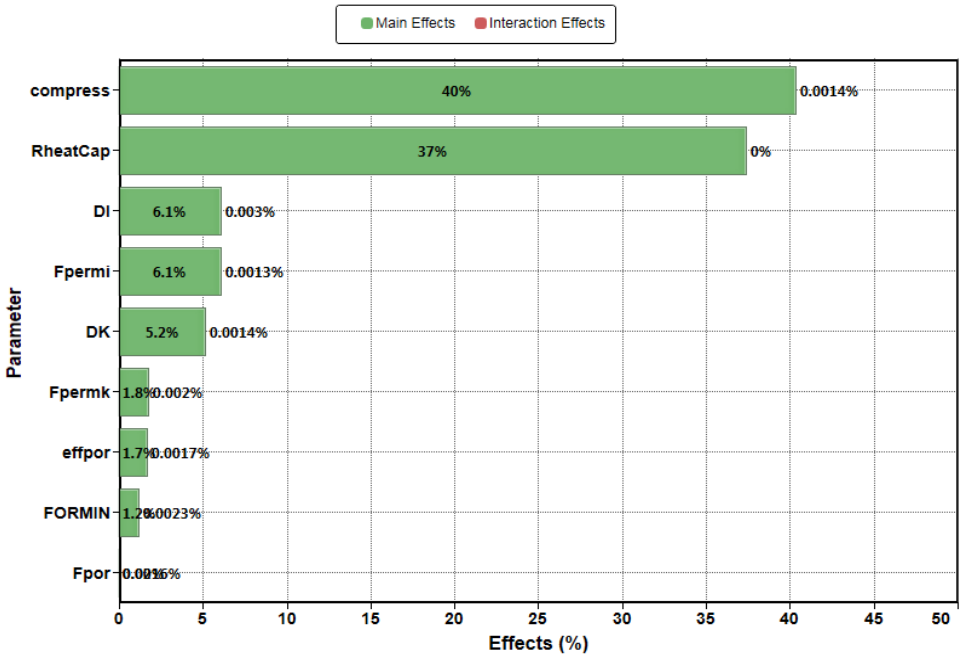

Figure 4-13 Sobol plot of bottom-hole pressure objective function (lower fracture permeability range)

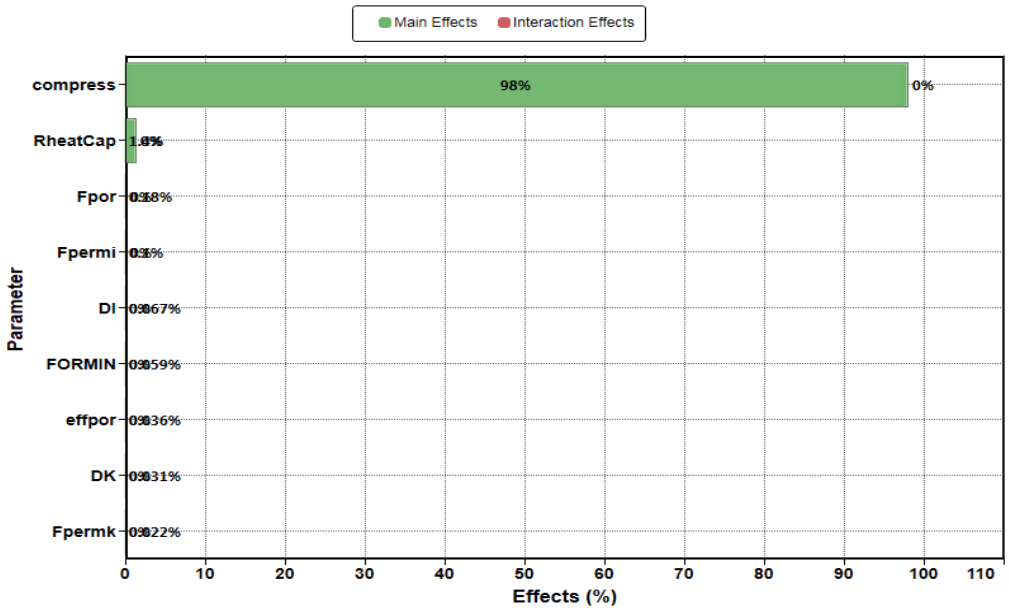

Figure 4-14 Sobol plots of cumulative steam injection objective function (lower fracture permeability range)

4.1.5 CSS History Matching Results

To check whether this numerical model truly represents the Grosmont carbonate, history matching should be completed, though it is much more difficult due to uncertainties of some input data. There is limited information about observation wells records, so it is impossible to catch and match temperature trends for the Mclean pilot. As mentioned in Section 4.1.2, inter-wells communications extensively exist in the Mclean pilot resulting in abnormal water production for some wells. Thus, it is meaningless to match water production if we focus only on the single well BD. After sensitivity analysis, the most sensitive parameters have significant impacts on the results so they should be adjusted first during the history matching. Slightly sensitive parameters are also

useful to fine tune the final match results. Adjusting relative permeability endpoints like connate water saturation, rock compressibility and heat capacity first, and then tuning some fractures properties, an oil production rate and bottom-hole pressure of well BD can be matched from the pre-casing leak to the controlled production period. The history matching results are displayed in Figures 4-15 to 4-17. The injection bottom-hole pressure cannot be matched accurately during the initial period. As we mentioned in field performance analysis, the main reason is because of inter-well communications. A large amount of steam is injected to well DB with less water production in cycles 1 and 3, and meanwhile, well BD produces numerous water which suggests a strong NE directional communication between wells. Therefore, well DB injection interferes the bottom-hole pressure matching result of well BD. Instead of matching all wells, which is not practical, only well BD is included in this model, so it is reasonable to see the deviation of injection pressure from March to June of 1983, but still with a consistent trend.

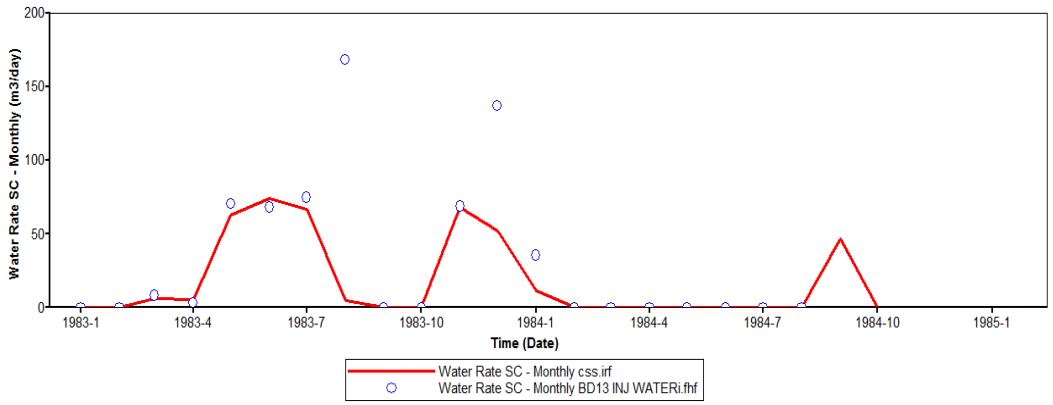

Figure 4-15 Field steam injection rate (monthly) as the constraints

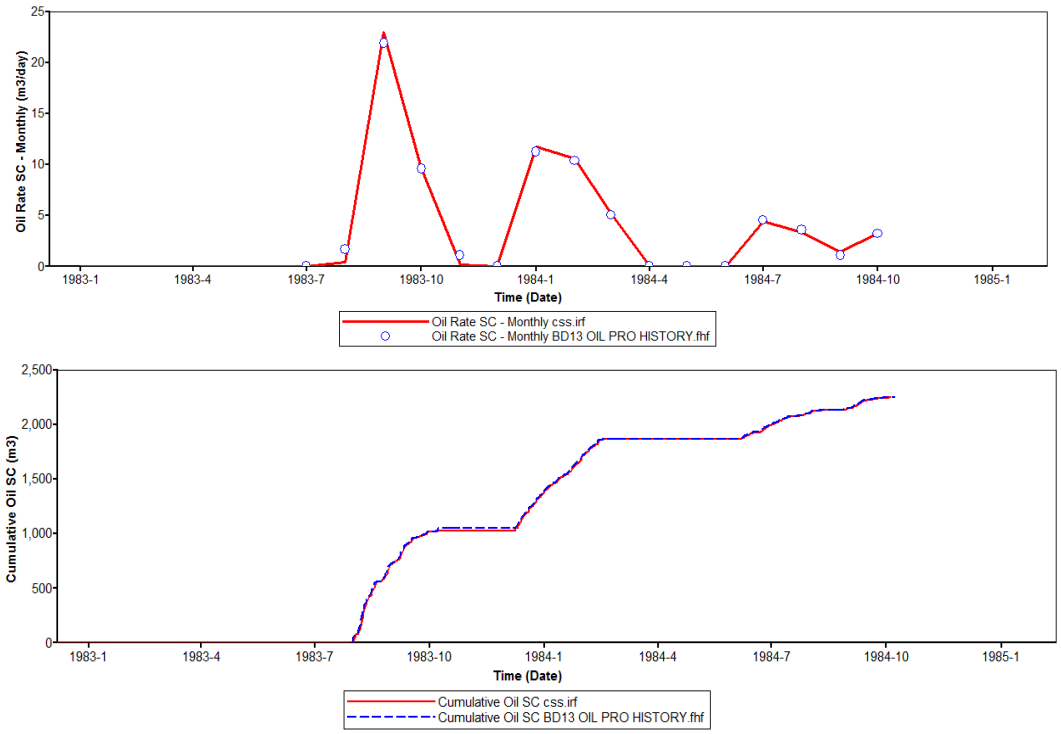

Figure 4-16 Oil production history matching result

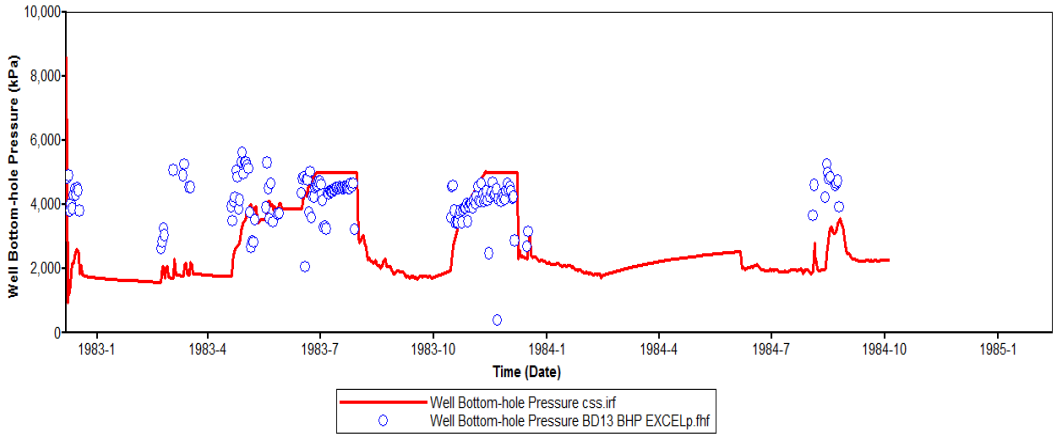

Figure 4-17 Well bottom-hole pressure history matching result

4.1.6 Results Discussion

From the simulation results in Table 4-2, the cyclic steam-oil ratio of well BD is almost up to 8 m^3/m^3 initially, because a large portion of steam condenses during the first cycle and the reservoir is not heated enough without abundant mobilized oil flowing to the wellbore. Also, the recovery factor of 2 years CSS is only 2.7% as a result of extreme heterogeneity in the Grosmont carbonate and limited sweep regions during the CSS process. Moreover, the oil recovery factor is declined with the cycle number resulting in rich oil remained in the formation.

A 230^oC iso-temperature surface is created and regarded as the steam chamber shape at the end of steam injection of the second and third cycles (Figure 4-18). An asymmetrical iso-temperature configuration reveals the heterogeneity of the Grosmont carbonate again, so the uniform steam chamber cannot be generated in this model. As discussed in Section 3.1, there are noticeable high permeability conduits ($K_{VERTICAL} \geq 3500mD$) existing mainly in the left part (J=1-3) of the upper model along the I direction. Vertical permeability larger than 3500mD is filtered as background in Figure 4-19. Steam prefers penetrating into the regions where permeability is high, so it is clear that the steam zone shape inclines to the high permeability part in this figure, making lower permeability regions less heated and swept. Furthermore, due to the existence of high vertical permeability fractures or karst related regions and the high-pressure injection condition, steam overriding or channeling phenomenon is evident during the CSS process, even when the wellbore is perforated beneath discontinuous marl layers. Severe steam overriding can be observed from the

mobile bitumen (μ≤150cp) distribution profile at the end of production (Figure 4-20) which demonstrates that steam channeling upward through the permeable regions heats and mobilizes the bitumen enough around the upper part of this model. Limited sweep and heat efficiency with much oil remaining between vertical wells is seen also. Therefore, well placements and operations should be noticed in later study in case of steam effectivity affected.

Table 4-2 CSS process simulation results (starting from 1982-12-08)

	Cycle 2	Cycle 3	Controlled Cycle (Partial)
End date	1983-10-07	1984 -02-18	1984-10-03
Cyclic SOR (m^3/m^3)	7.6	6.3	5.5
Recovery Factor (%)	1.2	1	0.5

(a) the second cycle **(b) the third cycle**

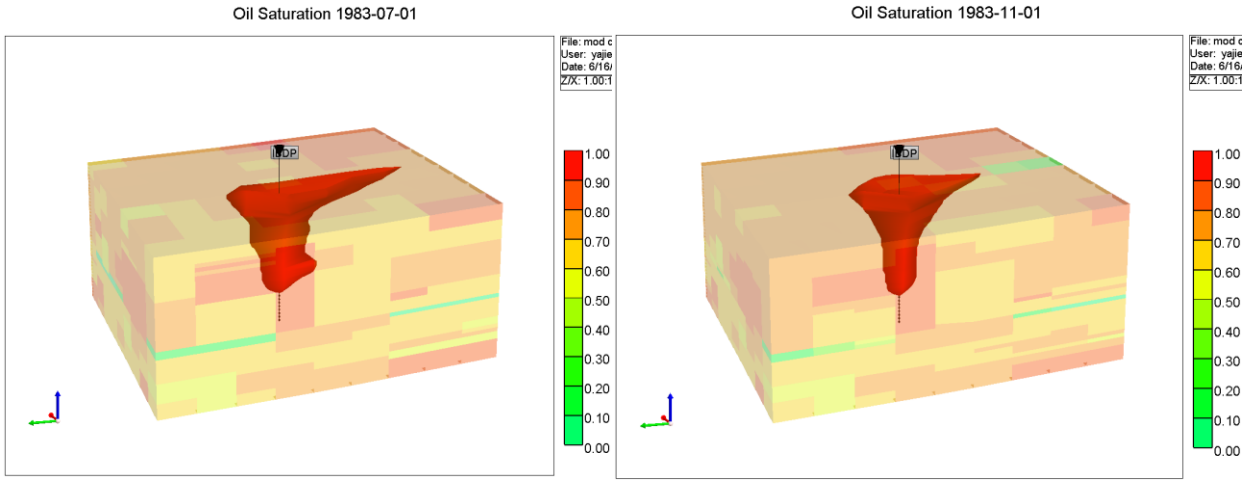

Figure 4-18 230ºC iso-temperature surface at the end of (a) the second cycle, (b) the third cycle

(a) the second cycle **(b) the third cycle**

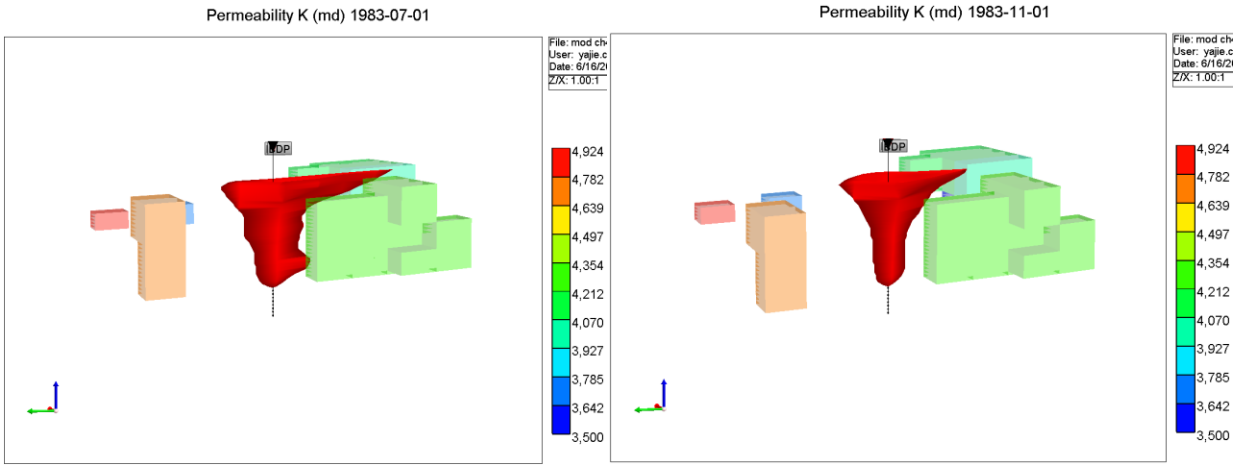

Figure 4-19 230ºC iso-temperature surface at the end of (a) the second cycle, (b) the third cycle with $K_{VERTICAL} \geq 3500$mD filtered as the background

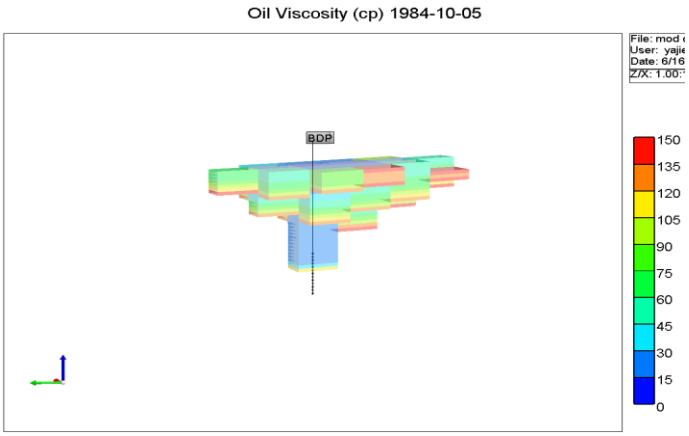

Figure 4-20 Mobile bitumen distribution at the end of production with μ≤150cp filtered as the background

4.2 Steam Assisted Gravity Drainage

4.2.1 Introduction

Sometimes the CSS method cannot work well to produce heavy oil from a deeper reservoir, so the steam assisted gravity drainage (SAGD) process is developed by Butler (1985) which has been applied to Alberta oil sands reservoirs widely and achieved encouraging results. For this operation, a pair of parallel horizontal wells are drilled with a certain distance apart. Continuous steam injection from the upper well reduces the viscosity of bitumen and makes it mobile, so oil and condensed water are drained to the lower producer well due to gravity effects. The key of SAGD process is thermal communication between wells so that an even steam chamber can be built. Steam and gas rise filling the void space hence forming a steam chamber, while oil flows down along the chamber side because of a density difference and interfacial tension.

However, SAGD which requires high vertical permeability and a relatively thick formation is sensitive to oil mobility, heterogeneity of the formation and other parameters. Especially for the Grosmont carbonate, an extremely heterogeneous reservoir, application of SAGD is unidentified and simulation or field studies published exhibit conflicting results in different research regions (Yuan, 2010; Song, 2015; Ezeuko, 2013; Yang, 2014; Hosseininejad, 2014).

4.2.2 Simulation Well Placements and Operation Constraints

For the Base-SAGD case, two parallel horizontal wells are placed in the middle of this model below the discontinuous marl layers which separate Grosmont C and D members. In this case, SAGD operation drains almost the same regions as the CSS method. Three months preheating since 1983-04-30 is applied before SAGD initialization to build sufficient heat communication between two wells. 80% quality steam is injected at 60 m^3/day with 3000 kPa maximum injection pressure. The producer in the I direction (I=1-9, J=5, K=39), 5 m apart below the injector, is constrained with a 100 m^3/day liquid rate and 10 ^{o}C steam trap control in case of live steam loss.

4.2.3 Results Discussion

4.2.3.1 Steam Profiles Analysis

Due to the heterogeneously distributed properties and various porosity types in the Grosmont carbonate, a typical steam chamber profile during the SAGD process is hardly formed and the conformance of steam is affected apparently. Figure 4-21 displays a cross-section of steam profile evolution every 4 months for the base case. An uneven steam drainage zone is generated and steam prefers flowing to the high permeability conduits as mentioned in Section 4.1. Limited lateral and downward expansion is observed in this carbonate model. On account of the barriers of mar layers between Grosmont C and D, the middle of the steam zone is obstructed resulting in a less oil rate in the early time (Figure 4-22). However, mar layers are not the real barriers and communication between C and D is existing proved by multiple field data. With more steam injection, more conductive heat will overcome the discontinuous mar layers and connect the steam zone. From

Figure 4-22, rate fluctuation indicates oil produced from various porosity regions. It can reach up to 41 m^3/day during the SAGD process in Grosmont and SAGD has a stable and longer production period.

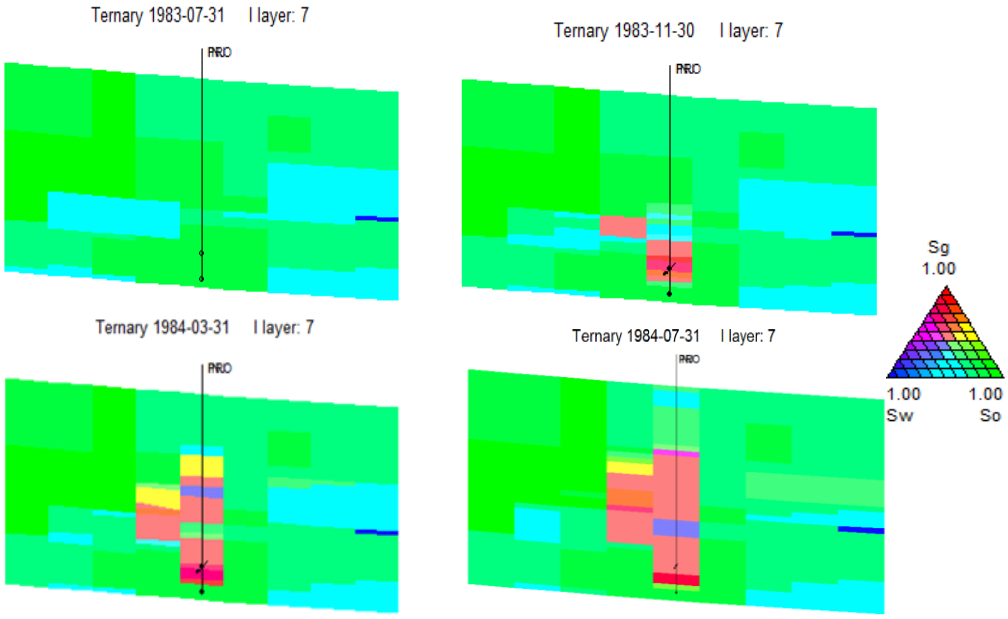

Figure 4-21 Ternary evolution plots every 4 months for the first year

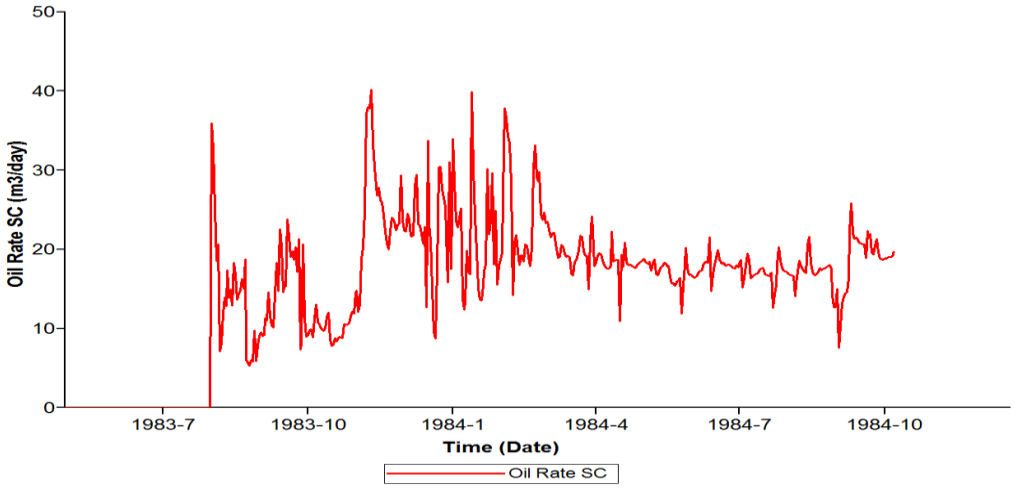

Figure 4-22 Oil production rate for the Base-SAGD case

4.2.3.2 Existing of High Permeability Conduits

From discussion in the last section of CSS results, steam channeling and override phenomenon is observable as a result of existing of regional high permeability conduits in the upper part of the model. It has been concluded that Grosmont holds heterogeneously distributed massive permeability due to various pore types of large vugs and fractures (Novak et al., 2007). Therefore, different well placements are designed to detect the effects of high permeability zones. For the SAGD-A case, an injector well is perforated in the J direction (I=5, J=1-9, K=34) making half of the well below high permeability regions. Figure 4-23 is the ternary development versus time plot of the top layer for both the Base-SAGD and the SAGD-A case. The first time that steam channels to the top layer along high permeability conduits for the SAGD-A case is around four months after steam injection at 1983-11-13 whereas steam appears in the top at 1984-07-06 for Base-SAGD. Earlier steam breakthrough will impact the steam effectivity and then make the final recovery factor reduced as Table 4-3 listed. For another case SAGD-B, an injector is placed right below high permeability conduits in I direction (I=1-9, J=3, K=34). Seen from the cross-section of steam profile comparison plots (Figure 4-24) at the time that steam appears to top for the Base-SAGD case (1984-07-06), a steam chamber which is vital to the SAGD process cannot be formed for the SAGD-B case when the high permeability regions exist just above the wells, because steam tends to escape through high permeability conduits leading to partially developed steam chambers. A 190^{o}C iso-temperature surface at 1984-07-06 (Figure 4-25) is generated to observe the steam chamber. It is noticeable that the reservoir cannot be heated evenly along the wells owing to severe

and fast steam override for the SAGD-B case. In a heterogeneous carbonate reservoir, a uniform steam chamber is hard to form actually. If the wells are drilled right below high permeability conduits, a steam chamber will be affected even more severely and hence oil production will decrease consequently. The base case has a higher recovery factor and a lower CSOR than other cases (Table 4-3). Therefore, well placements should be noticed and drilling should be avoided near severe vugs or karst related zones. Geological prospecting in advance is essential for Grosmont carbonate recovery.

(a) SAGD-A

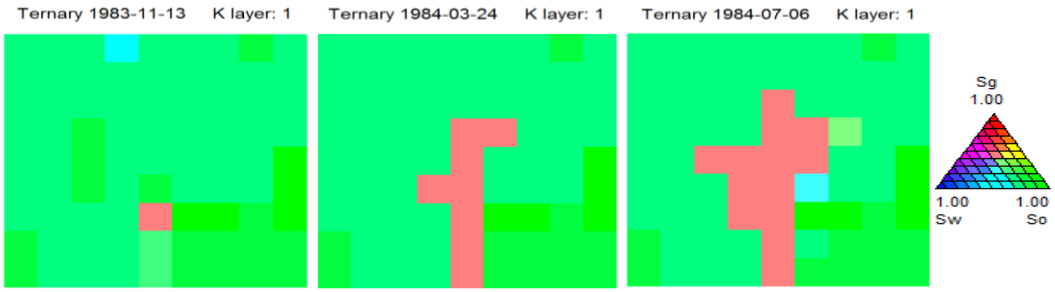

(b) Base-SAGD

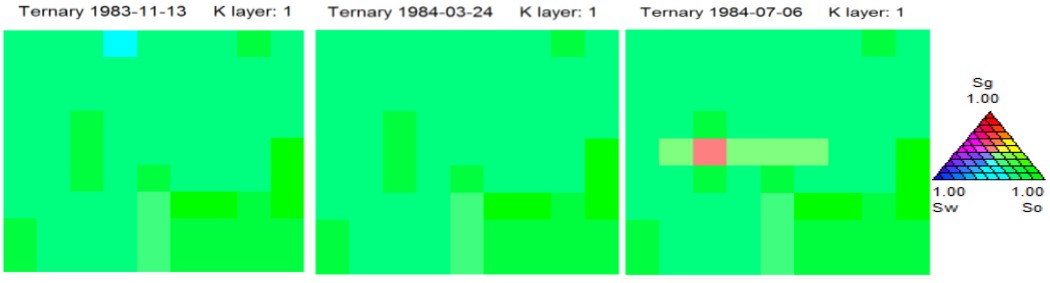

Figure 4-23 Ternary evolution plots to detect the first time of steam channeling to the top layer for (a) SAGD-A, (b) Base-SAGD case

Table 4-3 SAGD process simulation results for different well placement strategies

	Base-SAGD	SAGD-A	SAGD-B
Injector Position	I=1-9, J=5, K=34	I=5, J=1-9, K=34	I=1-9, J=3, K=34
Recovery Factor	9.6	8.3	7.8
CSOR (m^3/m^3)	3	3.8	4

(a) SAGD-B **(b) Base-SAGD**

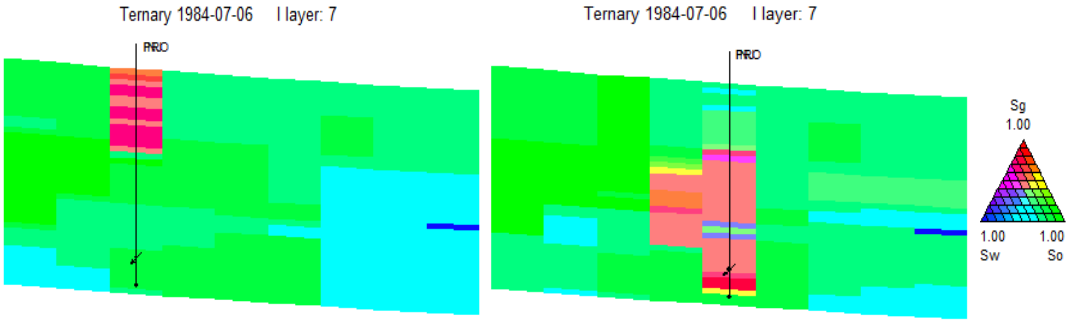

Figure 4-24 Ternary plots at 1984-07-06 for (a) SAGD-B, (b) Base-SAGD case

(a) SAGD-B **(b) Base-SAGD**

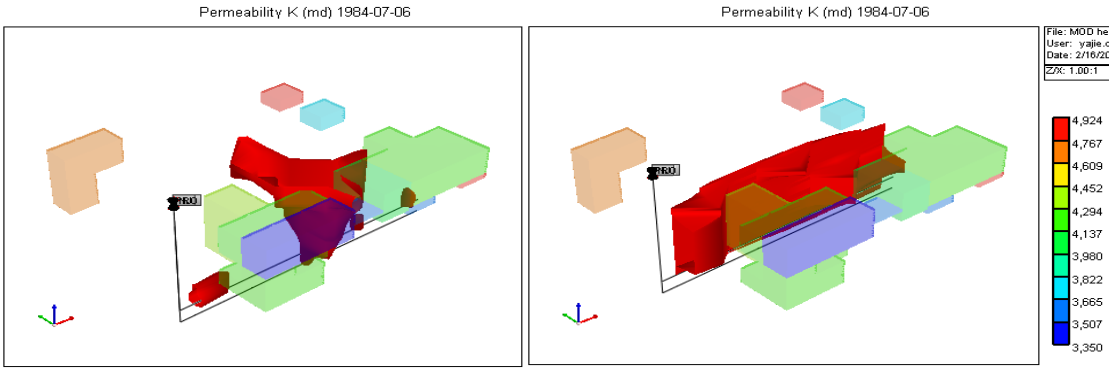

Figure 4-25 190°C iso-temperature surface at 1984-07-06 with $K_{VERTICAL} \geq$ 3500mD filtered as the background for (a) SAGD-B, (b) Base-SAGD case

4.2.3.3 Effects of Well Operations

When the operation constraints of wells change, reservoir performance will be modified accordingly. To understand the roles of BHP, an injection rate and steam trap control on performance, additional simulations are completed with step-wise increased parameter values. Effects of each factor on oil production and CSOR are depicted in Figures 4-26 to 4-28. Blue histograms represent the cumulative bitumen production while orange curves characterize the CSOR variation. Comparing all these parameters, it is obvious that a steam injection rate has the most significant influence on cumulative SOR and oil production in this carbonate model. With an increase in the injection rate from 40 m^3/day to 100 m^3/day, CSOR initially decreases to 3.37 and then increases to 11.4 sharply due to too much water injection and less oil production. Thus, a moderate steam injection rate should be chosen to obtain an optimal result. Figure 4-27 shows that steam trap at 10^{o}C yields the lowest CSOR and relatively high oil production. Overly high steam trap will not be economic if temperature continues increasing. When adjusting the maximum BHP at 2500 kPa, 3000 kPa and 3500 kPa, the difference of CSOR is relatively small, around 0.1. Higher injection pressure can promote the growth of the steam chamber, overcome the marl barriers initially, and then produce more oil. On the other side, higher pressure will also accelerate the steam breakthrough.

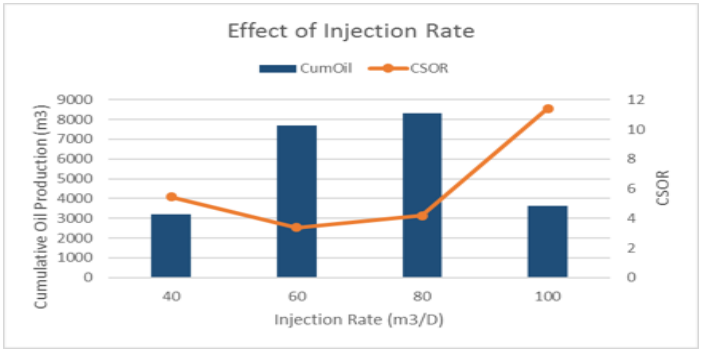

Figure 4-26 Effect of steam injection rate on oil production and CSOR

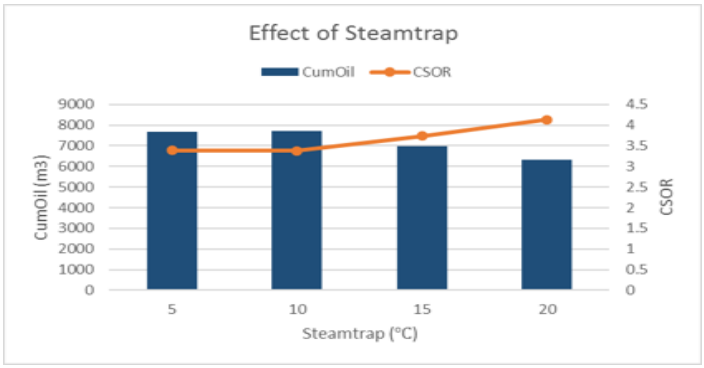

Figure 4-27 Effect of steam trap control on oil production and CSOR

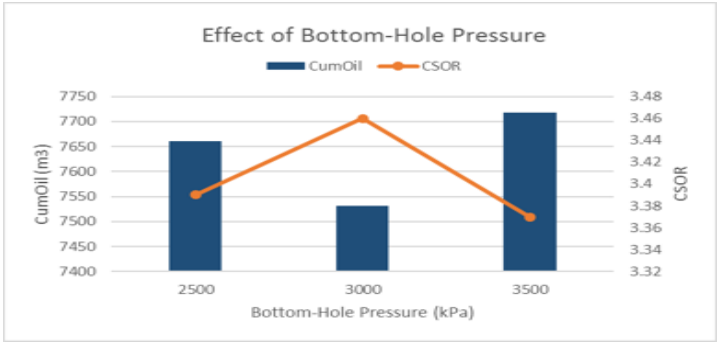

Figure 4-28 Effect of maximum BHP on oil production and CSOR

4.2.3.4 Comparison of CSS and SAGD in Grosmont Carbonate

From the oil production graph for both operations (Figure 4-29), the oil rate is declined with time during the CSS process whereas SAGD has a more stable and longer production period. Compared with CSS, the main strength of SAGD is two times more oil recovery in 169 days earlier with the same amounts of steam injection (Table 4-4), because gravity drainage plays as an additional drive mechanism owing to extensively distributed sub-vertical fractures and high vertical permeability in Grosmont. in the reservoir by dilating the porous media resulting in higher production than SAGD during the early time. On the other hand, however, the much higher pressure will cause well damages and accelerate steam channeling prematurely, especially in this high permeability carbonate system. Lower well positions for SAGD will relieve the steam channeling phenomenon. Initial cyclic SOR is high for the CSS operation as a large portion of steam condenses during the first cycle and no much oil can be mobilized enough flowing to the wellbore. Moreover, limited sweep efficiency between vertical wells of CSS is observed. However, the greatest challenge for SAGD in Grosmont is that a steam chamber is hardly formed in such a heterogeneous reservoir with various porosity types. Although the production of Base-SAGD in this model is encouraging, reservoir heterogeneities in the Grosmont will make a steam shape uncontrolled and unknown such as in the SAGD-A and SAGD-B cases. Furthermore, the preheating period is vital for later production and steam chamber evolution as well. Without enough preheating, there is no uniform thermal distribution along the wells leading to steam breakthrough rapidly.

All of these features make a gravity drainage process not suitable as an initial operation and the heterogeneity of the Grosmont carbonate impacts steam chamber evolution which is the key to the SAGD process. Therefore, new strategies should be designed and investigated to combine the both advantages of cyclic and gravity mechanisms for Grosmont in the later study.

Table 4-4 Results comparison with the same amounts of steam injection

	Injection (m^3)	Time (D)	CSOR (m^3/ m^3)	Recovery Factor (%)
CSS	21901	627	5.5	2.7
Base-SAGD	21901	458	3.2	8.0

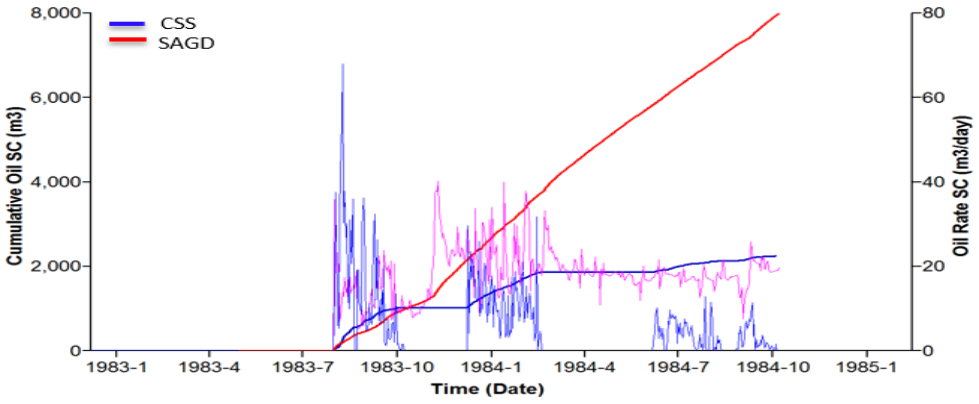

Figure 4-29 Oil production curves for CSS and Base-SAGD

4.3 Improved Hybrid SAGD

4.3.1 Regular Hybrid SAGD

A novel hybrid SAGD (HSAGD) is first introduced by Coskuner in 2009 whose well pattern is derived from the Fast-SAGD, but with a different operation strategy. In the beginning, CSS is performed in both SAGD injectors and offset horizontal wells until steam chambers contact each other. Then SAGD injectors keep injecting steam but continuously producing from both SAGD producers and offset wells. Analysis of the numerical results in Clearwater, a complex oil sand reservoir with marine shales, suggests that this proposed hybrid method has more oil production and less steam injection within a shorter period compared with the traditional CSS or SAGD process. However, the viability of H-SAGD in the Grosmont carbonate has not been investigated in previous studies.

4.3.2 Improved Hybrid SAGD Well Configurations in Grosmont

Gravity drainage is favorably applied to a high vertical permeability reservoir and there are several vertical wells remaining in the Grosmont pilot. Vertical wells are cheaper and easier in drilling and completion. Thus, a single horizontal SAGD well and a vertical well are utilized in this thesis. For the improved hybrid SAGD process, CSS is conducted in a staggered pattern initially for both lower horizontal SAGD and upper vertical wells and operated at the same pressure. Once the steam chambers of individual wells contact with each other, continuous injection from the upper vertical

well and production to the lower horizontal well will start. Well configurations are shown in Figure 4-30. Because severe steam override exists in the vertical well CSS, the 10m vertical well (I=5, J=5, K=25-35) is placed in the middle of the model away from the high permeability regions and 5m upon the horizontal SAGD well (I=2, J=1-9, K=39) with 30m spacing distance in the Grosmont C zone. Operation starts at 1983-06-21 and well constraints for different stages are set the same as the pure SAGD and pure CSS processes. During the initial CSS period, two wells should be controlled at the same pressure, because different pressure will make steam to arrive prematurely at another one's steam chamber, then exacerbating the reservoir conformance.

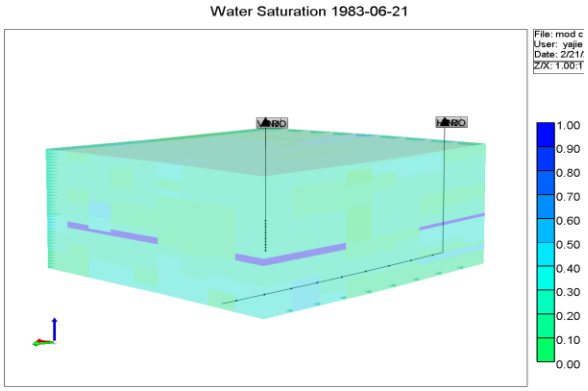

Figure 4-30 Well configurations for Hybrid SAGD operation

4.3.3 Results Discussion

4.3.3.1 Improved Sweep Efficiency

Compared with vertical well CSS and horizontal SAGD, Hybrid SAGD improves the sweep efficiency and provides more producible reserves. As shown in the ternary plots of improved hybrid SAGD and Base-SAGD (Figure 4-31), improved hybrid SAGD explores the oil retained in

the lower base of the model among wells after 3 years production, though with the same number of wells. Note that the SAGD results we use for comparison are from the Base-SAGD case which achieves the best performance and has a more conformed steam shape. In a real carbonate formation with fractures, heterogeneity may impact the steam chamber evolution, leading to worse results during the SAGD process. At first, CSS in a staggered pattern operated at the same pressure can make heat distribution widely and relieve the steam channeling to the top quickly, then promoting the lateral and downward growth. Furthermore, half of the reservoir is heated with mobile oil less than 150cp around the wells for Hybrid SAGD whereas steam flow downward is quite difficult during the vertical well CSS making mobile oil mainly to accumulate around the top of the reservoir after 2 years production (Figure 4-32). Thus, the improved hybrid SAGD provides further sweep regions and retains more heat in the formation due to slower breakthrough and gravity mechanisms.

(a) Hybrid SAGD **(b) Base-SAGD**

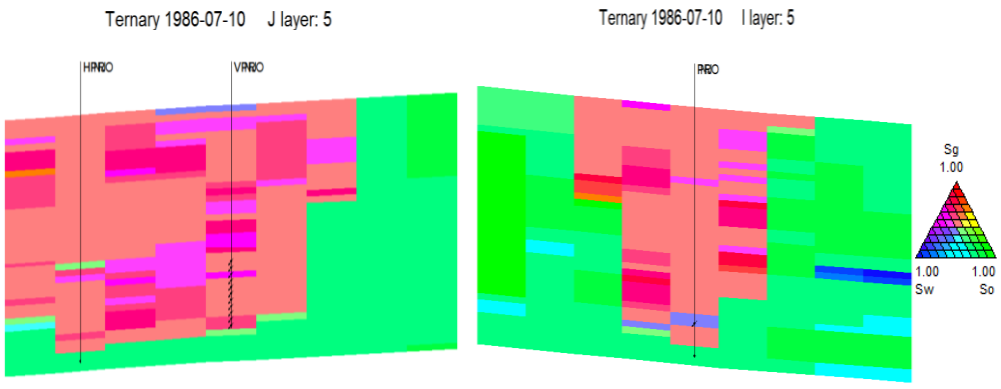

Figure 4-31 Ternary plots for (a) Hybrid SAGD, (b) Base-SAGD after 3 years production

(a) Hybrid SAGD **(b) Vertical Well CSS**

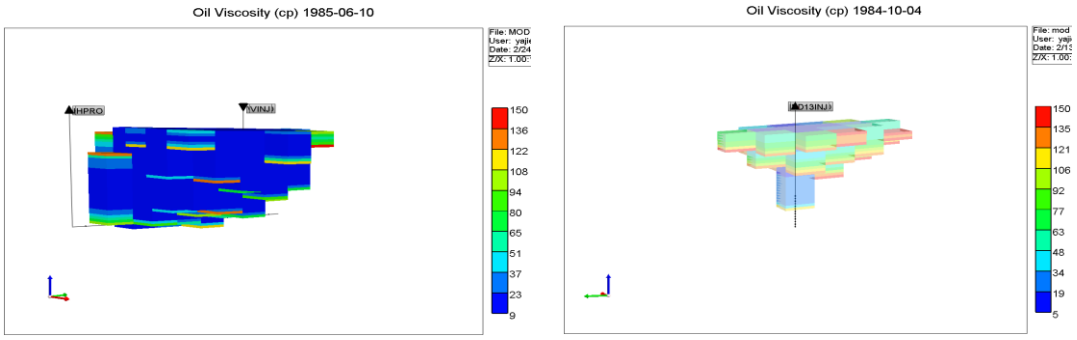

Figure 4-32 Mobile bitumen distribution after 2 years production for (a) Hybrid SAGD, (b) Vertical Well CSS with μ≤150cp filtered as the background

4.3.3.2 Performance Analysis Compared with CSS and SAGD

During the initial stage of CSS in both the upper vertical well and the lower horizontal well (Hybrid SAGD), the same steam injection rate of 70 m^3/day leads to distinct amounts of oil production for two wells (Figure 4-33). The horizontal well has an augmented recovery than the vertical well due to the additional mechanism of gravity drainage and more sweep regions along the horizontal well. Also, the lower horizontal well will relieve steam override and improve steam efficiency as stated in the last section. Comparing the bitumen production curves for all three operations (Figure 4-34), Hybrid SAGD reverses the obvious cycle decline of the conventional CSS. Furthermore, it compensates a weak production during the earlier time of SAGD, because initial high-pressure CSS will heat large amounts of a reservoir volume in a shorter time and overcome the shale barriers separated Grosmont C&D members to some extent. There is an increased slope of the production curve during the continuous production period of hybrid SAGD though with the same steam

injection rate of 60 m^3/day as the conventional SAGD. It indicates that more heat including the remained energy from previous cyclic periods promotes a sweep region, and enough preheating improves the thermal efficiency compared with other operations.

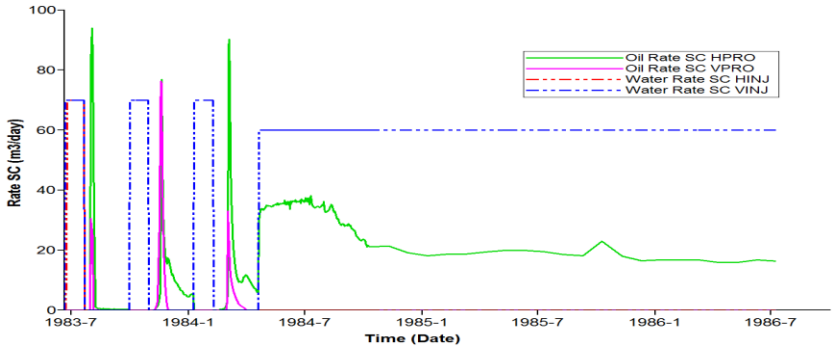

Figure 4-33 Steam injection and oil production rate curves for both wells (Hybrid SAGD)

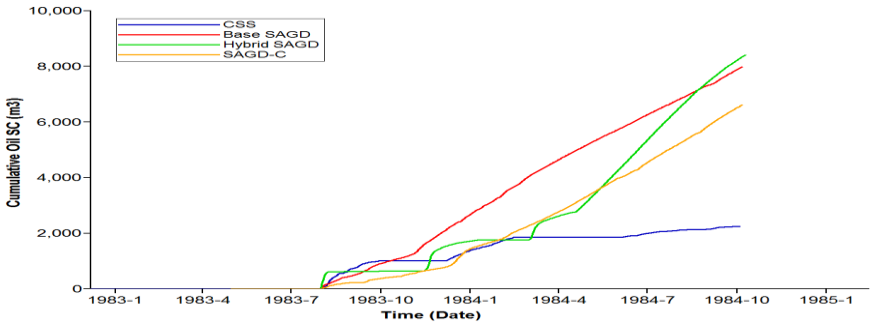

Figure 4-34 Comparison of the bitumen production curves for all three operations

Hybrid SAGD can reach a higher recovery factor for a sustained period (Tables 4-5 and 4-6). Since the start time for each operation is different, we set the same steam injection as an evaluation standard. For Hybrid SAGD, 21901m^3 steam can be used for a longer time with the highest recovery factor of 10% and the lowest cumulative SOR of 2.7 compared with CSS and SAGD.

Although performance after 2 years with 41000m^3 injection for the hybrid process is slightly better than Base-SAGD, we should notice that the Base-SAGD we choose for comparison has the best results and a more conformed steam shape. The SAGD process is extremely sensitive to steam chamber evolution which is detrimentally influenced by the heterogeneity of the Grosmont carbonate with fractures, whereas Hybrid SAGD production in this well configuration is favorable to promote lateral and downward flow and not constricted with a complete steam chamber shape. For instance, the producer of the SAGD-C case is placed in the same position (I=2, J=1-9, K=39) as the horizontal well of Hybrid SAGD, partially below high permeability regions which impair the steam shape evolution. After 2 years with 41000 m^3 injection, it achieves a 14% recovery factor lower than Base-SAGD (15%) and Hybrid SAGD (17%). The SAGD-C case performs even worse during the initial time (21901m^3 steam injection) with a 6% recovery factor while 8% for Base-SAGD and 10% for Hybrid SAGD. Moreover, the hybrid well placements can be patterned by drilling additional vertical wells along the horizontal well to expand heat distribution and oil production.

Table 4-5 Results comparison for different operations with 21901m^3 steam injection

	Injection (m3)	Time (D)	CSOR (m3/ m3)	Recovery Factor (%)
CSS	21901	627	5.5	2.7
Base SAGD	21901	457	3.2	8.0
SAGD-C	21901	457	4.3	6.1
Hybrid SAGD	21901	462	2.7	10

Table 4-6 Results comparison for different operations with 41000m^3 steam injection

	Injection (m^3)	Time (D)	CSOR (m^3/ m^3)	Recovery Factor (%)
Base SAGD	41000	772	3.2	15
SAGD-C	41000	772	3.5	14
Hybrid SAGD	41000	781	2.8	17

4.3.3.3 Influence of Cycle Numbers and Cycle Length

Enough thermal communication between wells is essential for later production during the Hybrid SAGD process. Otherwise, it will have detrimental effects on the whole recovery process. Three cycles are set before a continuous injection/production period in the previous study. Seen from Table 4-7, more cycle numbers will hardly change oil production and steam injection amounts in each cycle; however, it enhances the bitumen recovery gradually with slightly reduced steam injection during the 2 years continuous stage for the reason that enough preheating is favorable to the later continuous production period. Then, a lower CSOR for the later 2 years continuous stage or the whole recovery process is acquired through more cycle numbers (Figure 4-35). Therefore, enough cycle numbers provide more thermal communication between the wells which improve the whole recovery process. However, the growth of oil production and the fall of CSOR than its previous cycle during the cyclic process is less and less when cycle numbers continue increasing. Thus, the optimal cycle numbers when switching to a continuous production period is the time that cyclic production become declined.

Table 4-7 Steam injection, oil production data in the cyclic and continuous periods for different cycle numbers

Cycle Period		1st	2nd	3rd	4th	5th	6th	Continuous (2 years)
Steam Injection (m3)	2 Cycles	3968	4200	Null				43919
	3 Cycles	3992	4200	4200	Null			43793
	4 Cycles	3968	4200	4142	4173	Null		43784
	5 Cycles	3968	4200	4142	4173	4197	Null	43788
	6 Cycles	3968	4200	4142	4173	4197	4198	43787
Oil Production (m3)	2 Cycles	385	1027	Null				15097
	3 Cycles	636	1122	1018	Null			16057
	4 Cycles	385	1027	1130	1141	Null		19880
	5 Cycles	385	1027	1130	1141	1436	Null	21065
	6 Cycles	385	1027	1130	1141	1436	1441	22021

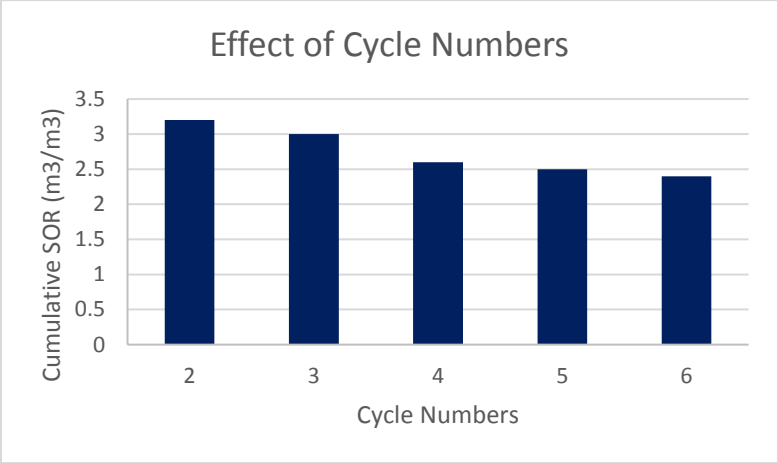

Figure 4-35 Cumulative SOR after 2 years continuous process for different cycle numbers

In this thesis, 30 days steam injection, 10 days soak and 60 days production for each cycle repeat for three cycles during the cyclic operation. CSS operation is required to establish and achieve heat

communication along the entire wells. If the steam injection time extends to 55 days, both of the longer and shorter cycles display improved cyclic SOR as time progresses during the cyclic operation (Figure 4-36). For a 30D injection length, less steam injected to the reservoir leading less oil heated to being mobile for production results in higher SOR initially. During the third cycle, oil from fractures or high permeability karst related vugs has been explored easily in the earlier time, so a shorter cycle is hard to exploit the oil from matrix. Therefore, a shorter cycle length initially may be economic to save the steam injection and a longer cycle later may be effective for the whole hybrid SAGD operation.

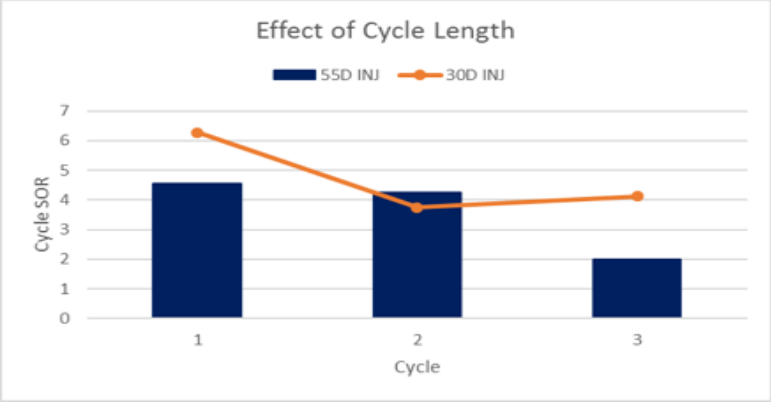

Figure 4-36 Cyclic SOR in each cycle for different cycle length

4.3.3.4 Effects of Well Distance

Changing the well spacing between the vertical well and the horizontal well, there is a slight difference on recovery performance (Table 4-8). 20m, 30m and 40m are tested, and the vertical

well is placed in the middle all the time. An effect of well distance is more significant for the cyclic periods than a continuous process. In Figure 4-37, 30m distance has a relatively high production in the first two cycles for both the horizontal and vertical wells. The reason for higher production during the third cycle for 20m or 40m distance is the model boundary effects. When the horizontal well is placed near a boundary of the model, steam chambers touch the boundary earlier which accelerate the lateral expansion and hence more production during the third cycle. In fact, a moderate well spacing distance will be positive for thermal communication and heat distribution.

Table 4-8 Simulation results at 85-10-01 for different well distances

Well Distance (m)	20	30	40
Recovery Factor (%)	18.6	16.3	17.9
CSOR (m3/ m3)	2.4	2.8	2.6

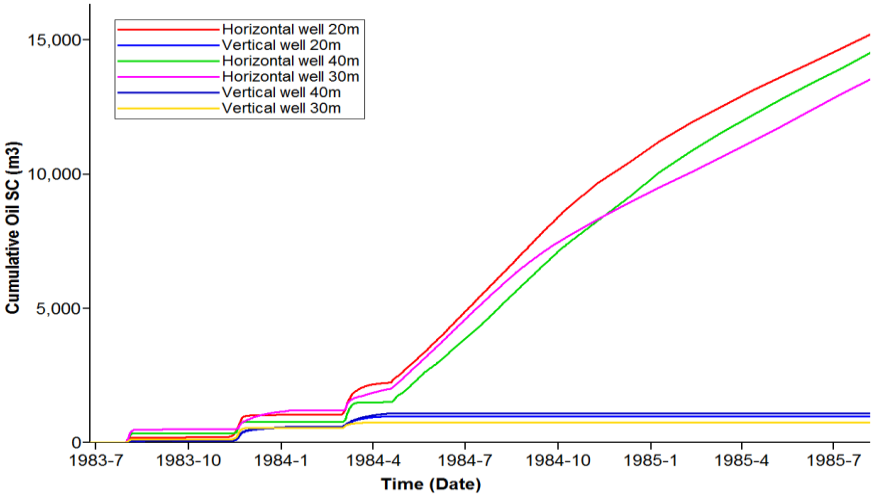

Figure 4-37 Cumulative oil production curves for different well distances

4.4 Conclusions

In this chapter, a heterogeneous carbonate model is built and validated by the history matching of the Mclean pilot in Grosmont at first. Sensitivity assessments detect that parameters like fracture spacing, rock compressibility, rock heat capability and a rock-in-fracture fraction have relatively large influences on the production and BHP simulation results. Also, fracture related properties are more sensitive in a higher fracture permeability reservoir. Severe inter-well communications impact the history matching results. Due to the existence of high permeability fractures and high-pressure injection condition, steam override and limited sweep efficiency are evident during the CSS process while SAGD has a stable and longer production period. However, the performance of SAGD varies dramatically when well placements or operations change. A steam chamber which is extremely sensitive to the SAGD process is hardly formed in such a heterogeneous reservoir with various porosity types. Furthermore, the improved hybrid SAGD in a staggered pattern promotes lateral and downward growth and retains more heat regardless of the steam chamber shape. Also, when the total injected steam is the same, hybrid SAGD achieves a higher recovery factor faster than other operations. c. The optimal cycle numbers when switching to a continuous production period are the time that cyclic production become declined. Moreover, a shorter cycle initially and a longer cycle later may be more economic and effective. Also, a moderate well spacing distance will be positive for thermal communication and heat distribution.

CHAPTER 5 : SOLVENT-AIDED RECOVERY IN GROSMONT CARBONATE

Steam-based thermal recovery methods require tons of energy and water resources accompanied with GHG emissions and produced water treatment problems. Moreover, a heterogeneous carbonate with high permeability conduits adversely influences the efficiency of conventional SAGD. Recently, people are trying to utilize solvent and thermal together to enhance the bitumen recovery. Simple experiments have been tested to show the viability of solvent-aided methods in the Grosmont carbonate. Therefore, numerical simulation of solvent additives for the heterogeneous carbonate will be investigated comprehensively to detect the recovery mechanisms, phase behavior, and optimal solvents or conditions in this chapter.

5.1 Solvent Properties

A solvent viscosity function is:

$$\mu_s = a * e^{b/T} \tag{5-1}$$

where a and b are the viscosity coefficients corresponding to the unit of viscosity or absolute temperature. Some of the solvent viscosity-temperature curves are shown in Figure 5-1.

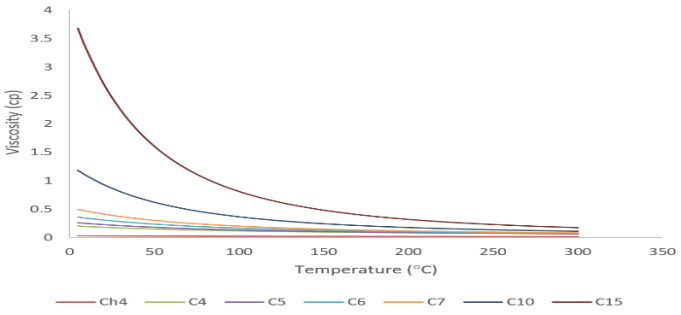

Figure 5-1 Solvent viscosity-temperature curves

Liquid mixture viscosity is obtained by the linear mixing rule:

$$In\mu = \sum_{i=1}^{n} n_i \, In\mu_i \tag{5-2}$$

where n_i is the mole fraction of component i.

A gas-liquid K-value of solvent is decided by the function below:

$$K = \left(\frac{K_{V1}}{P}\right) * e^{K_{V4}/(T-K_{V5})} \tag{5-3}$$

where K_{V1}, K_{V4} and K_{V5} are the coefficients corresponding to the unit of pressure and temperature.

A liquid-liquid K-value is not considered in this simulation due to no liquid-liquid solubility. All correlation coefficients and critical properties for the solvents are from CMG STARS manual (2015). Steam and solvent saturation temperature and pressure are cited from the database of National Institute of Standard and Technology (NIST) website. The curves are depicted in Figure 5-2.

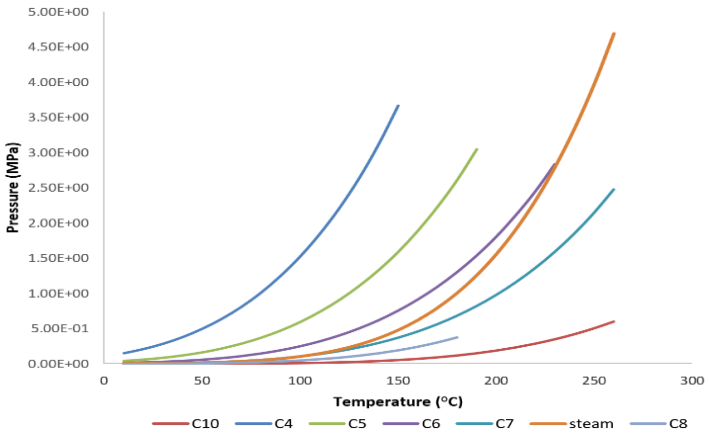

Figure 5-2 Steam and solvent saturation temperature-pressure curves

5.2 Well Operation conditions

A well configuration for the solvent-aided process is the same as the Base-SAGD case. Two parallel wells are placed below discontinuous marl barriers (I=1-9, J=5, K=34 or 39) in the middle of the model. 20% volume fraction pure solvent is injected with 80% quality steam at 60 m^3/day and constrained at 3000 kPa maximum pressure. Steam saturation temperature at 3000 kPa is 230°C. A minimum steam trap control of 10°C is set to limit live vapor production for the producer. The mole fraction of methane in live oil is 0.05, so the initial solution gas is included in this model. A diffusion coefficient of solvent is not considered at this moment, because the diffusion difference can be seen only in a finer grid model.

5.3 Heterogeneously Distributed Properties

In a simulation model with heterogeneously distributed permeability, porosity and oil saturation, an irregular steam chamber shape is formed resulting in various performance between solvents C_5-C_{10} compared with that in a homogeneous model. At this moment, if the properties of carbonate are simplified to homogeneous average values (Table 5-1) but still using a dual permeability/dual porosity model, cumulative oil production curves for different solvents are displayed in Figure 5-3. In this homogeneous model, the difference of bitumen production between solvents C_5-C_{10} is not obvious. Also, heavy solvent like C_{10} displays slightly better production than other solvents owing to its higher saturation temperature. From the saturation pressure-temperature curves (Figure 5-2), solvents heavier than C_7 can condense before steam so that they diffuse into bitumen

quickly. Nevertheless, in a heterogeneous carbonate model, C_5 performance exceeds other solvents evidently which coincides with some previous reports (Li, 2010; Keshavarz, 2015). Since a light solvent with a lower density and saturation temperature is carried to high permeability conduits and large-scale karst or vug related regions easily and hence condenses in these regions to push more oil out, whereas a heavy solvent like C_{10} may condense earlier before it contacts with oil in the high permeability conduits and hence impairs the mixture efficiency. That explains why heavy solvents lead to a worse result than lighter solvents in the heterogeneous Grosmont carbonate. Therefore, pentane which has a better ability to mix with bitumen acquires the highest cumulative oil production in a heterogeneous model.

Furthermore, the solvent-aided process in this heterogeneous carbonate model exhibits higher cumulative oil production despite of solvent types compared with that in a homogeneous model. An actual carbonate reservoir is always heterogeneous because of complicated digenesis evolutions. The existence of various porosity types and high permeability conduits play significant roles in the oil recovery, so an average value of each property is not viable to represent the real Grosmont carbonate. Therefore, a heterogeneous model is essential for later study and the choice of an optimal solvent is especially crucial to this heterogeneous carbonate reservoir.

Table 5-1 Average values of carbonate properties

Parameter	Average Value
Matrix Porosity	0.22
Matrix Permeability I & J, mD	1100
Matrix Permeability K, mD	200
Fracture Permeability I & J& K, mD	16000
Fracture Volume Fraction	0.06
Oil Saturation	0.8

(a) Homogeneous model **(b) Heterogeneous model**

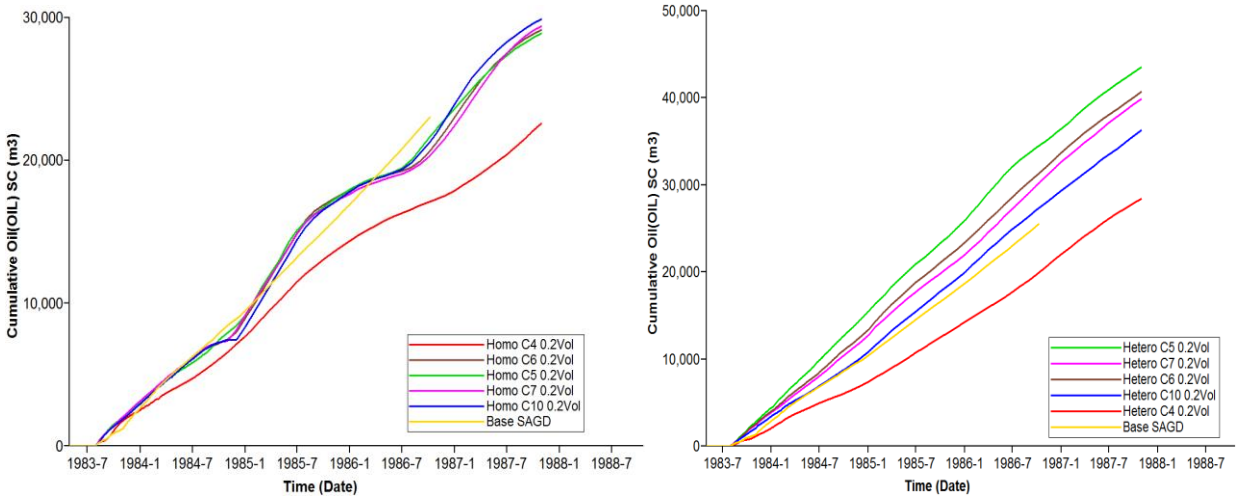

Figure 5-3 Cumulative oil production curves of different solvents for a (a) Homogeneous model, (b) Heterogeneous model

5.4 Initial Solution Gas

Usually, solution gas is present in a real reservoir and it has detrimental effects on the solvent-aided process. Even small amounts of solution gas may impact the operation performance

evidently. Thus, several previous numerical studies neglecting the initial solution gas are impractical and meaningless. Influence of solution gas on the solvent-aided process in this heterogeneous model will be discussed here and the main composition of solution gas for Athabasca bitumen is methane. The original mole fraction of methane in bitumen is set to 0.05. Comparing the Figure 5-3(b) with Figure 5-4, oil production is apparently decreased for all cases with the solution gas regardless of solvent types, because even small amounts of solution gas accumulated at the chamber edge will impede heat transferring and solvent mixing with bitumen seriously. Owing to the obstacle of solution gas films, heavy solvent with a higher saturation temperature like C_{10} may condense earlier before it contacts with bitumen. Consequently, it influences the mixture efficiency and leads to a worse performance for heavier solvents. Therefore, the difference of cumulative oil production between C_5-C_{10} is more evident in the simulation cases with solution gas.

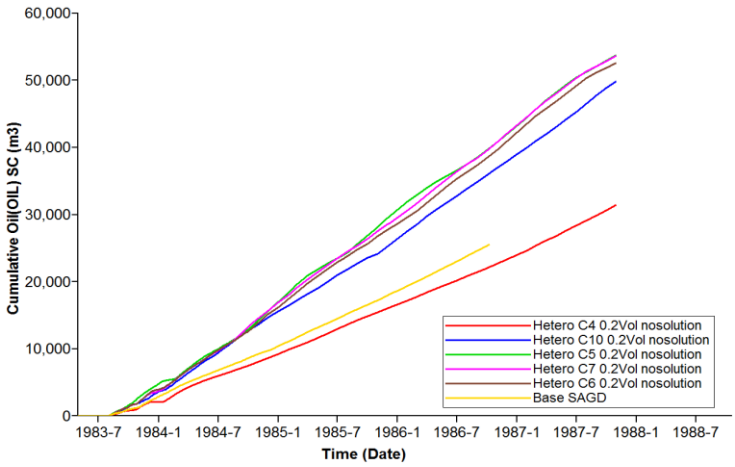

Figure 5-4 Cumulative oil production for the heterogeneous model without solution gas

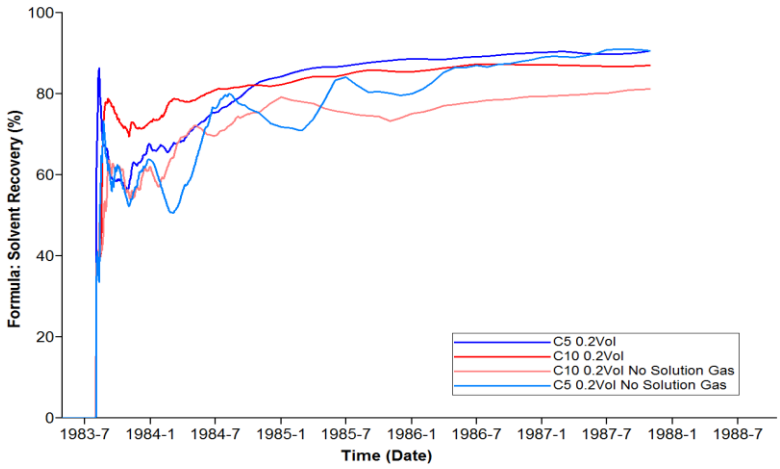

Figure 5-5 Solvent recovery factor curves comparison

On the other hand, the solvent recovery factor is enhanced with only a small amount of solution gas as depicted in Figure 5-5. Especially for heavier solvent like C_{10}, more than 80% of decane can be recovered for recycle when solution gas exists in the model. Without the initial solution gas, a large mole fraction of C_{10} in oil prefers to flow along the high permeability conduits and accumulates at the top layers after 3 years production (Fig. 5-6(a)). Due to the existing of large fractures and vugs in the Grosmont carbonate, without the separation of solution gas films, high permeability conduits will make steam or solvents channeling to the top layers quickly. It can be proved in Fig. 5-6(b) as well that the main condensation zone is surrounded by CH_4 gas films and hence solvents channeling or flowing to the top layers phenomenon is improved apparently. In conclusion, the existing of insulation gas films prevent solvents losing to top quickly and hence present a higher solvent recovery factor (namely lower solvent retention) in this carbonate

reservoir (Figure 5-5), although the methane layers impede thermal sweep efficiency to some extent.

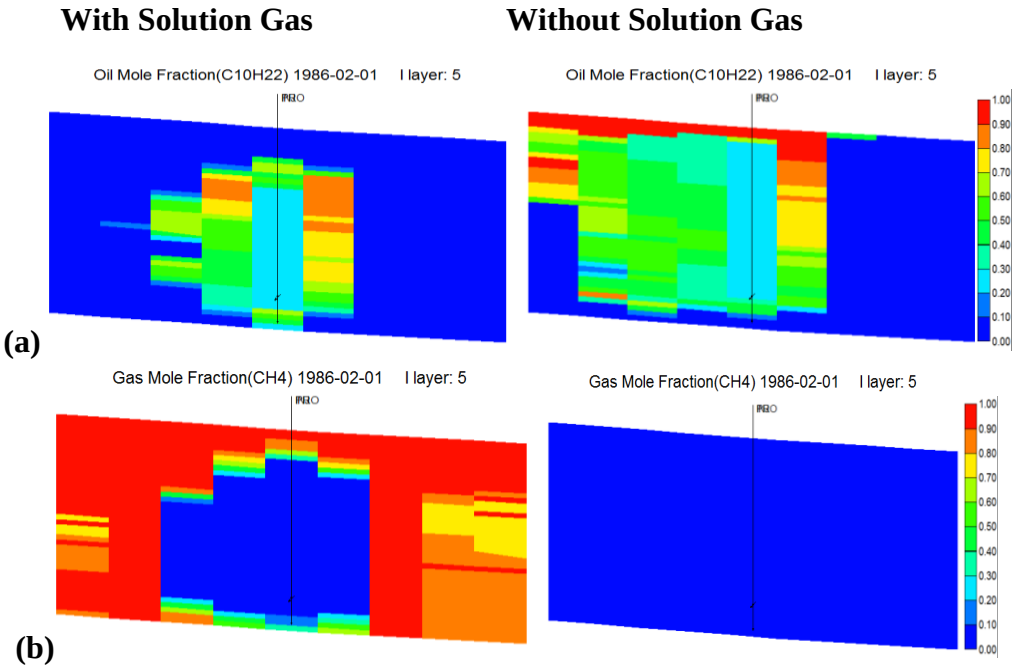

Figure 5-6 comparison profiles of (a) Decane mole fraction in oil phase and (b) methane mole fraction in gas phase

5.5 Phase Behavior and Mechanism Analysis

Mechanisms of the solvent-aided process in this heterogeneous carbonate with initial solution gas are complex due to various componential zones. C_7 as a solvent in the co-injection process is analyzed at this moment, because it has a similar saturation temperature with steam and achieves a better production in a homogeneous model. Property evolution curves along the observation line 1 (Fig. 5-7) in Grosmont C member (I=5, J=1-9, K=31) are depicted in Figure 5-8. The asymmetric

and inclined to left chamber shape demonstrates that fluid prefer flowing to the high permeability regions. Considering these situations, we only analyze the right-hand side of the chamber in this part for simplification.

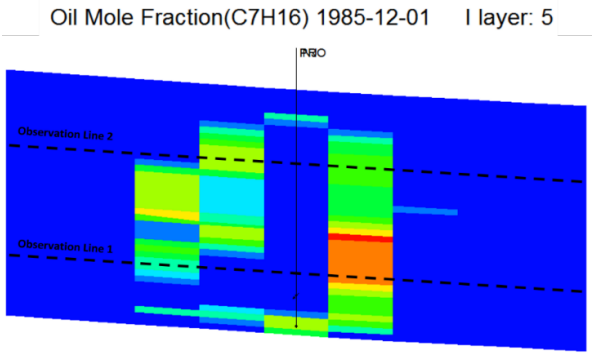

Figure 5-7 Observation line positions in this model

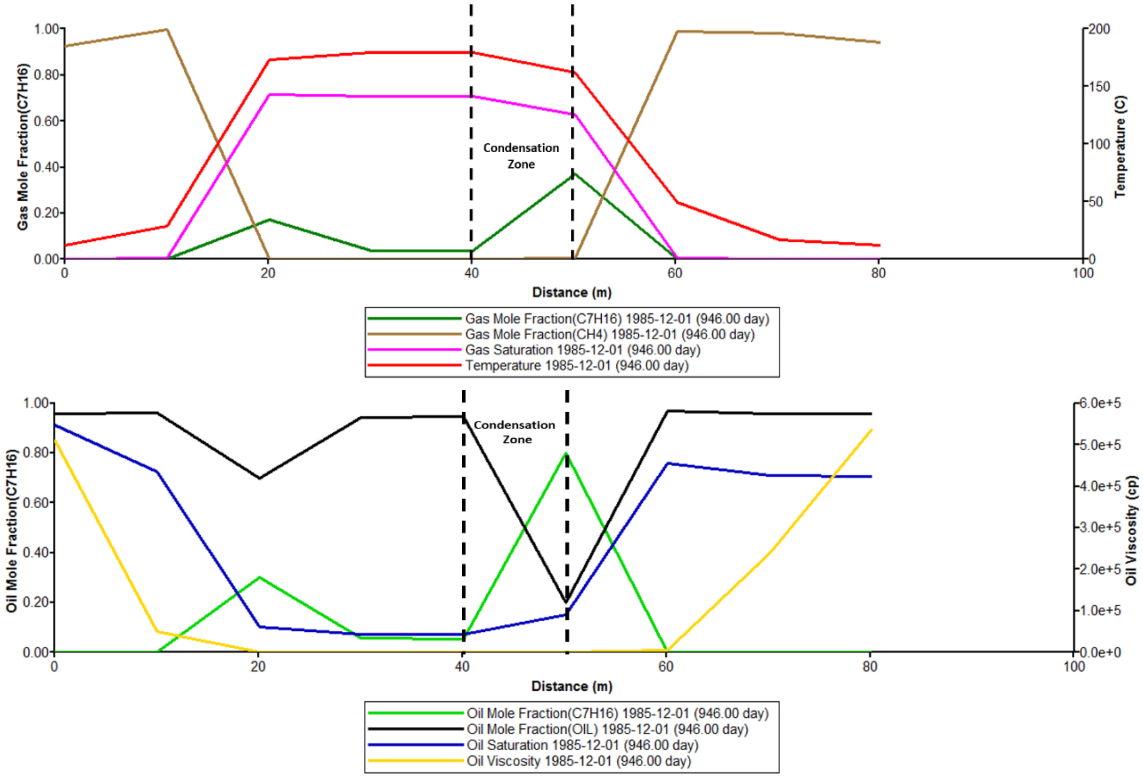

Figure 5-8 Property evolution curves along the observation line 1 at 946 days

As we can see from the property evolution curves along the observation line 1 at 946 days (Figure 5-8), less oil is remained and temperature and pressure keep almost constant inside the non-condensing zone (35m-40m). With a decrease of temperature along the horizontal distance, steam and solvent mixtures begin to condense in the condensation zone (40m-50m). Steam condensation to water phase enhances the C_7 mole fraction in vapor phase, and then the C_7 in vapor phase condenses resulting in more C_7 mole fraction in oil phase up to 0.8 at the chamber edge of 50m. This maximum C_7 mole fraction in oil phase is decided by the gas-liquid K-value. Therefore, C_7 in both the vapor and oil phases accumulate around the chamber boundary. Also, the increasing dissolution of C_7 in the oil phase promotes a growth of oil saturation in the main condensing zone. Furthermore, solvent and heat combine to reduce the bitumen viscosity, though temperature is decreased in this condensation zone (40m-50m). Condensed water and solvents will move downwards due to the gravity effects. Beyond the chamber edge of 50m, C_7 mole fraction in the oil and vapor phase start decreasing gradually and temperature of the reservoir continues falling, so the oil viscosity increases consequently. Nevertheless, C_7 can be further transferred to oil beyond the condensation zone which is observed from the continuously increased oil saturation along the horizontal distance in this drainage region (50m-60m). We should notice that fluid can flow in both the main condensation zone and drainage region. From the oil flux vector profile for layer I=7 at 946 days (Fig. 5-9), it is clearly shown that oil flow towards various directions at the C_7 accumulation zone, which means that gravity gives two component forces on the solvent: a

parallel to the sloped chamber boundary force and a vertical to the boundary force. This explains why solvent is further transferred to bitumen beyond the main condensation zone.

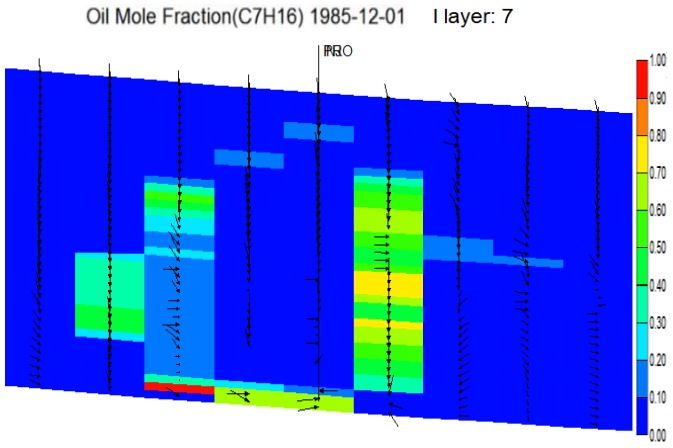

Figure 5-9 Oil flow flux vector profile (layer I=7) at 946 days for C_7-aided process

The initial solution gas is included in this heterogeneous model, so methane in the oil phase becomes a free gas when pressure and temperature change. From the methane mole fraction in the gas phase evolution curve in Fig. 5-8, CH_4 gas zones that occupy a wide range of the reservoir will impede heat transferring and solvent mixing into bitumen. On the other hand, since most of these gas films surround the main condensation zone, they can prevent steam or solvents channeling to the high permeability conduits. Comparing Figure 5-8 with the property variation curves along horizontal observation line 2 (Figure 5-10) in the upper Grosmont D (I=5, J=1-9, K=13), the thickness of gas zone expands around the upper parts of this model which impedes solvent contacting with bitumen more seriously.

Above all, the complicated phase behavior variation along different horizontal observation lines is described. Several drainage mechanisms including heat transfer, gravity effects, solvent dilution and solvent accumulation around the chamber boundary, gas films separation are utilized to decrease bitumen viscosity and increase bitumen recovery during the solvent-aided process.

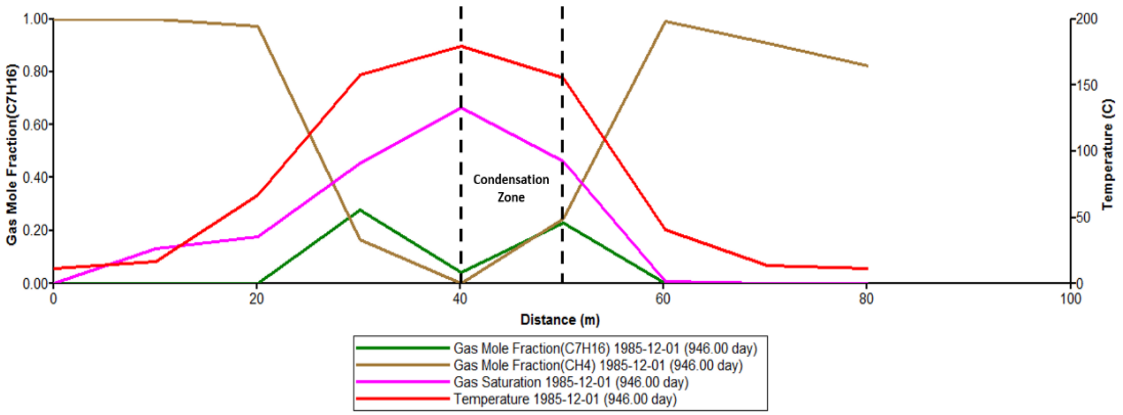

Figure 5-10 Property evolution curves along the observation line 2 at 946 days

5.6 Results Discussion Compared with Conventional SAGD

From the cumulative steam oil ratio and recovery factor curves of Base-SAGD and C_7-aided process (Figure 5-11), C_7 at a 20% volume fraction has a higher recovery factor and a lower CSOR in the Grosmont carbonate though the liquid injection rate is the same for both operations. Heptane has a 34% oil recovery factor around 3 year's production (1986-10-01). In the meanwhile, pentane enhances the recovery factor to 39% compared with that of 27% for the Base-SAGD process. CSOR for the Base-SAGD up to 4.55 is larger than that for the solvent-aided operation, especially

during the initial period. Also, it is observed in the oil production rate plot (Fig. 5-12) that a lower production occurs during the earlier time for Base-SAGD due to uneven preheating. After more than 3 years production in 1987, the oil production rate starts decreasing for the solvent-aided operation because less oil is left in the model. However, the oil rate in the C_4-aided process in which solvent remains mostly in the gas phase is slightly increased before the decline stage (1987) owing to quite small production initially. The reason of more bitumen recovery within the same time for the solvent-aided process is that solvent accelerates the lateral chamber propagation and expands the sweep region. It can be observed from the oil saturation comparison profiles of both operations (Fig.5-13) that the heptane-aided process has a larger drainage region. Also, the residual oil saturation (s_{or}) inside chamber for heptane-aided process is only 0.07 which is apparently lower than the value of 0.32 for Base-SAGD at the same position (I=5, J=5, K=31), because various drainage mechanisms are utilized to decrease bitumen viscosity and increase oil recovery further during the solvent-aided process which will be elaborated in next paragraph.

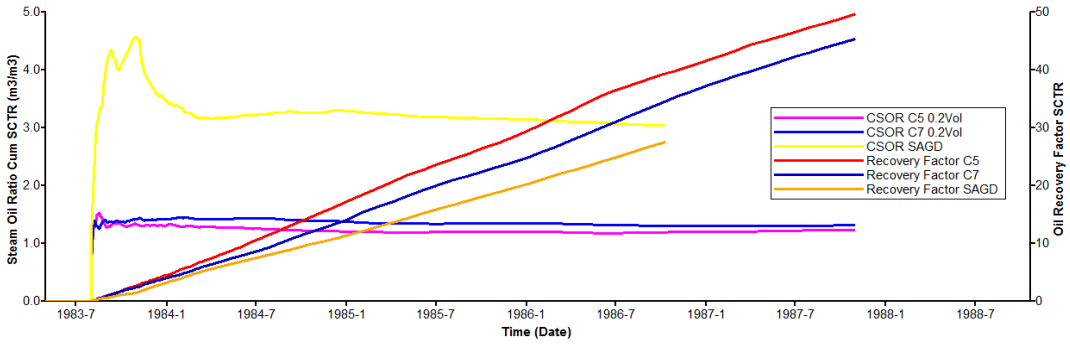

Figure 5-11 CSOR, recovery factor curves for the Base-SAGD and C_5, C_7-aided process

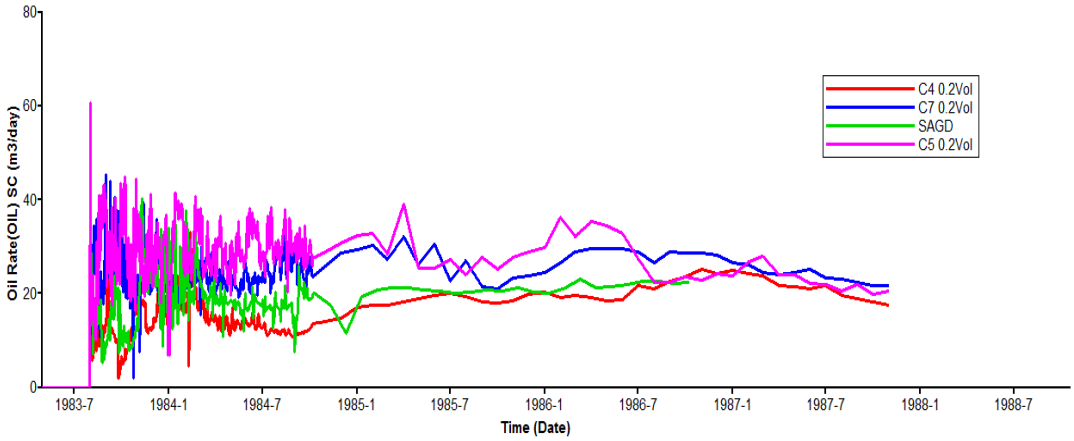

Figure 5-12 Bitumen production rate for the Base-SAGD and solvent-aided process

(a) Base-SAGD

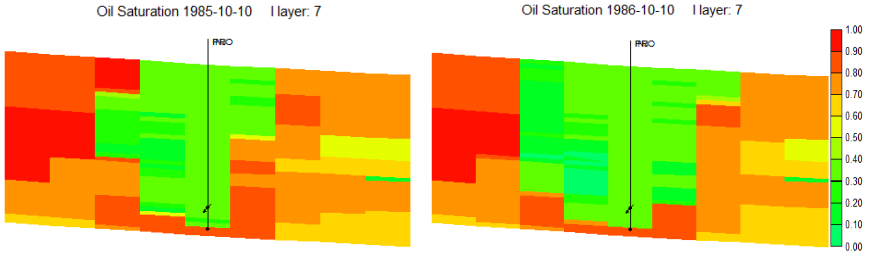

(b) Heptane-aided

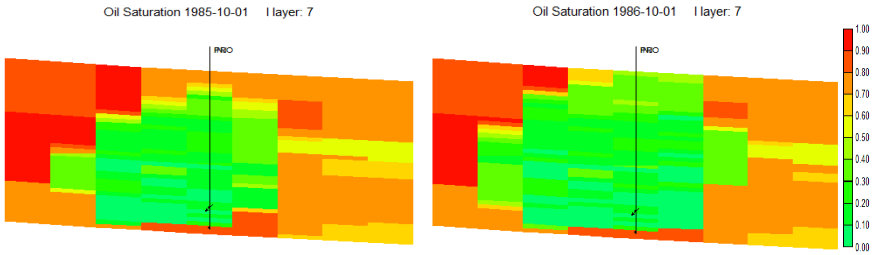

Figure 5-13 Oil saturation profiles after 2 and 3 years production for (a) Base-SAGD, (b) Heptane-aided process

As discussed in Section 5.5, the C_7 mole fraction in the gas or oil phase starts increasing around the chamber boundary in the main condensation zone. Also, it is observed in Figure 5-14 that C_7

accumulates in the vapor and oil phase around the chamber edge. Solvent and thermal combine together to reduce the viscosity of bitumen during the solvent-aided process. Additionally, solvent can be further transferred to oil beyond the chamber boundary as shown in the solvent mole fraction and oil saturation evolution curves along the horizontal observation line 1 or 2. Comparing the oil flow flux vector profiles between Base-SAGD and heptane-aided process (Fig. 5-15), there is a vertical to chamber boundary outward force on the C_7 accumulation zones which explains why solvent further transits to oil and dilutes bitumen beyond the condensation zone. Oil flux vectors alteration around the chamber boundary between two operations associated with the gravity effects on solvent will accelerate a lateral expansion of condensation zone. Also, both gas films and solvent rich zones relieve the steam channeling or override phenomenon. Therefore, the solvent-aided process improves sweep efficiency apparently than the conventional SAGD. Furthermore, from temperature and viscosity evolution data along the horizontal observation line 1 and 2 of the right-hand side chamber (Table 5-2), temperature inside chamber (0-10m) during the solvent-aided process is lower than that in the Base-SAGD case due to a lower steam partial pressure with the existing of solvents. Steam condensation which releases its latent heat to mobilize the bitumen induces a further decline of temperature and an increase of viscosity along the horizontal distance for the Base-SAGD case. On the contrary, bitumen viscosity during the solvent-aided process is reduced to an even smaller value as a result of solvent accumulation and dilution around the chamber boundary (10-20m), though the reservoir temperature is decreased.

In conclusion, the solvent-aided process has an improved RF and CSOR, a lower s_{or} and μ_o inside chamber, an enlarged sweep region compared with the conventional SAGD, because various drainage mechanisms including heat transfer, gravity effects, solvent accumulation and solvent transit beyond the chamber boundary for bitumen dilution combine together to reduce bitumen viscosity and enhance oil recovery during the solvent-aided process.

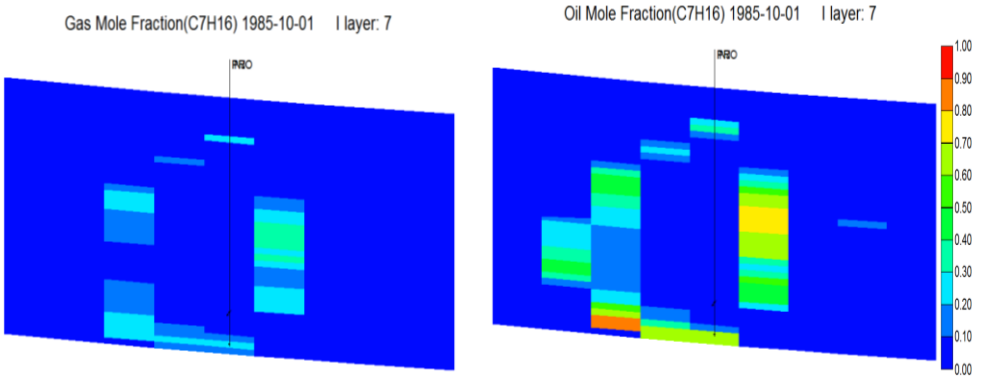

Figure 5-14 C_7 accumulation in gas or oil phase at the chamber edges around 2 years

(a) Base-SAGD **(b) Heptane-aided**

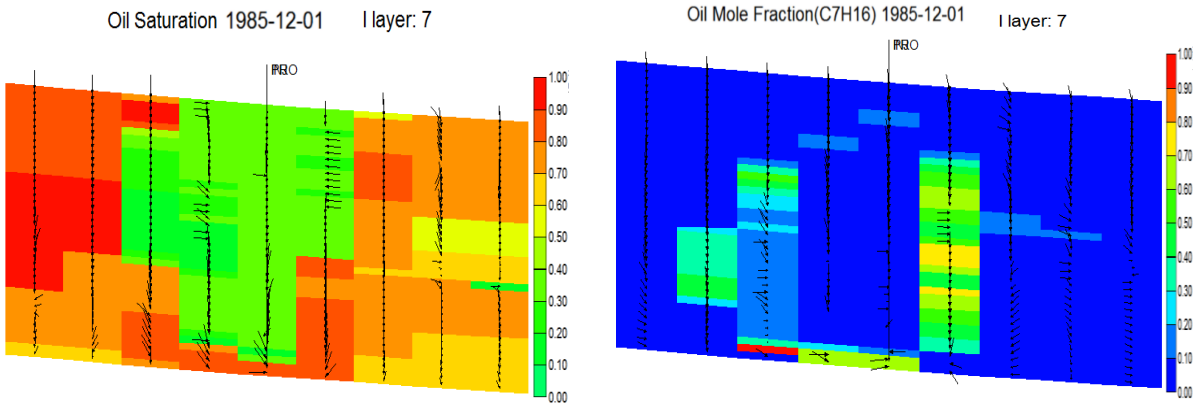

Figure 5-15 Oil flow flux vector profiles (layer I=7) at 946 days for (a) Base-SAGD, (b) C_7-aided process

Table 5-2 Temperature and viscosity evolution data for the right-side chamber along horizontal observation lines at 946 days

(5,4,31) - (5,9,31), (m)		0	10	20	30	40	50
T (°C)	SAGD	192.4	194.5	65.0	22.0	12.5	11.3
	C_7	179.9	180.1	162.2	49.3	16.8	11.8
μ (cp)	SAGD	11.1	10.7	1283.4	110882	476645	579825
	C_7	10.8	10.9	0.4	5230.7	239873	537873
(5,4,13) - (5,9,13), (m)		0	10	20	30	40	50
T (°C)	SAGD	194.3	194.4	194.1	30.9	12.8	11.2
	C_7	157.5	179.7	155.1	40.7	13.4	11.2
μ (cp)	SAGD	10.8	10.8	10.8	33545	335522	638489
	C_7	0.8	10.6	1.21	11359	440748	664405

5.7 Parameters Optimization for Solvent-aided Process in the Grosmont Carbonate

5.7.1 Solvent Concentration

The optimal solvent concentration is a crucial parameter which decides the overall bitumen production and solvent retention. 1%, 5%, 10%, 15% and 20% volume fractions of heptane injection are investigated in this section. Oil recovery factor curves at the end of production (Figure 5-16) reveal that more solvent concentration in the volume fraction range of 1%-10% presents a higher oil recovery factor. From the comparison profiles of oil saturation and the C_7 mole fraction in the oil phase at 946 days (Fig. 5-17), more solvent accumulation and higher solvent solubility into bitumen around the chamber boundary lead to a larger sweep region and a higher recovery factor in the solvent volume fraction range of 1%-10%. However, when the solvent concentration

is larger than 10%, both the ultimate bitumen recovery and solvent accumulation around the chamber boundary are slightly decreased. Moreover, properties at the left chamber edge (5, 3, 31) for different concentration of 1%-20% are displayed in Table 5-3. When the solvent concentration is less than 10%, temperature of the left-side chamber boundary is lower at a higher concentration owing to a reduced steam partial pressure. However, temperature will not continue decreasing with a higher solvent injection fraction. In addition, the most solvent mole fraction in the oil phase (0.51) and the lowest oil viscosity (1.44 cP) around the chamber edge make it possible to achieve the lowest residual oil saturation (0.09) at 10% injection concentration. Therefore, the improved trend is reversed if the solvent concentration continues increasing. Bitumen recovery is not proportional to a solvent volume fraction, because the ultimate recovery is influenced by bitumen viscosity improvements which are decided by the combination effects of solvent accumulation and thermal transfer.

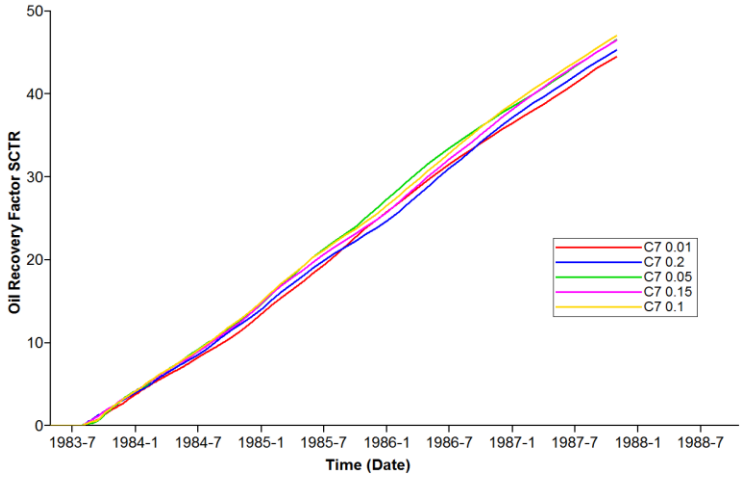

Figure 5-16 Oil recovery factor curves for different C_7 injection volume fraction

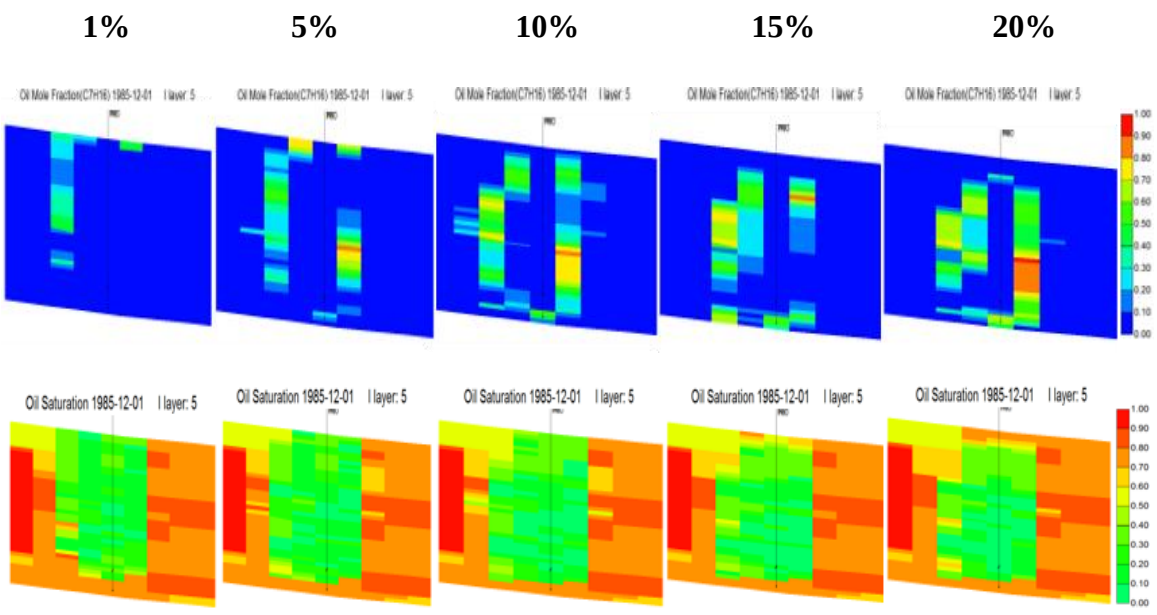

Figure 5-17 Oil saturation and C_7 mole fraction in oil phase comparison at 946 days

Table 5-3 Properties at (5, 3, 31) for different C_7 injection volume fraction at 946 days

Properties at the left chamber edge (5, 3, 31)	1%	5%	10%	15%	20%
Temperature (°C)	185.2	172.8	170.2	175.1	172.3
Viscosity (cp)	25.17	2.44	1.44	4.9	3.78
Solvent mole fraction in oil	0.13	0.39	0.51	0.21	0.30
Residual oil saturation	0.51	0.13	0.09	0.10	0.10

Furthermore, CSOR is reduced gradually with a continuously increasing of solvent concentration due to less steam injection (Figure 5-18). Considering the solvent retention in terms of bitumen production (Fig. 5-19), more C_7 is retained in the reservoir with a unit of bitumen production when the solvent injection concentration is gradually increased. Solvent is very expensive, so the recycle process which impacts economic viability of the whole recovery is extremely important. Thus, a higher concentration is not favorable to the solvent recycle. Above all, there is a balance between

the effects of thermal transfer and solvents, so C_7 concentration around 10% will provide the highest bitumen production and a moderate solvent retention in this carbonate reservoir.

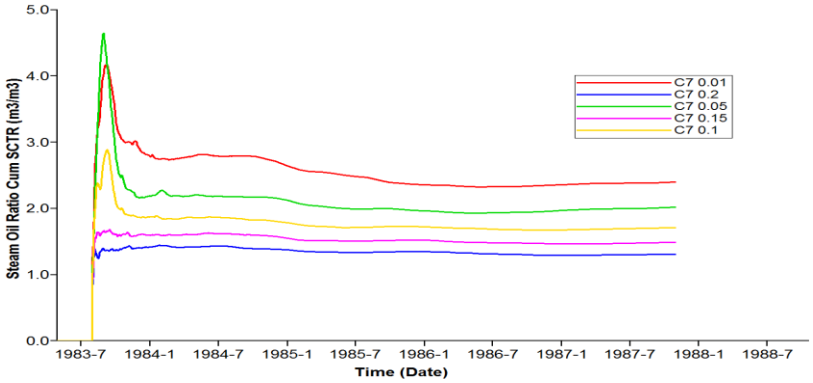

Figure 5-18 CSOR curves for different C_7 injection volume fraction

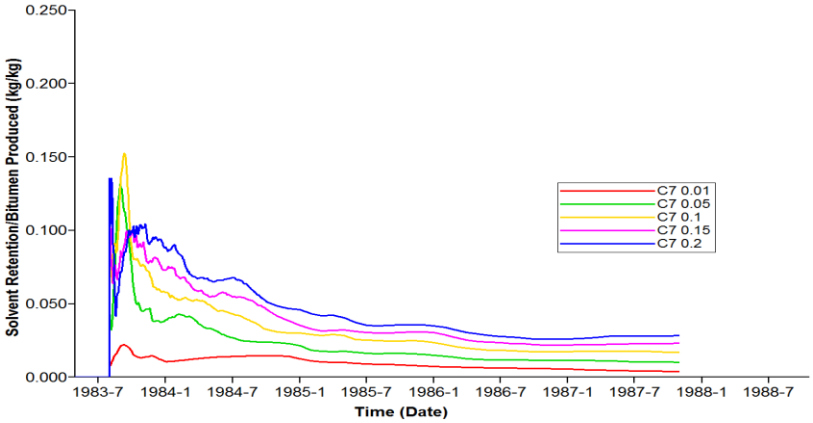

Figure 5-19 Solvent retention in terms of bitumen production for different C_7 concentration

5.7.2 Solvent Types Selection

As mentioned in Sections 5.3 and 5.4, performance of different solvent varies under the consideration of several factors, especially in a heterogeneous carbonate with solution gas. Therefore, the optimal solvent type for Grosmont will be discussed in this section, not only depending on the phase behavior evolution, but also the geological environment.

Oil recovery factor and cumulative steam-oil ratio curves for different solvents are depicted in Figures 5-20 and 5-21. They display that lighter solvents like C_5-C_7 have a higher bitumen recovery factor and a lower CSOR in this carbonate reservoir compared with Base-SAGD. C_4 co-injection with steam significantly decreases the bitumen recovery factor to 23.5% after 3 years production at 1986-10-01 in the Grosmont model whereas 27.6% for Base-SAGD. From Figure 5-2, butane has an obviously lower saturation temperature whereas C_5-C_7 have a closer condensation temperature with respect to steam. The boiling point of C_4 is lower so that it mainly remains in the gas phase which is decided by the K-value. The gas phase of lighter C_4 flows upward easily and obstructs the formation of a steam chamber, especially for the reservoir with high permeability conduits. Accumulation of gas phase C_4 around the top large porosity regions also impedes heat transfer. Thus, volatile solvents less than butane have worse recovery than the conventional SAGD so that they are not suitable in the Grosmont reservoir and will not be considered in later discussion.

Generally, the lighter solvent (C_5-C_7) co-injection process provides a lower chamber temperature, because the lighter solvent which has a larger K-value and hence a higher mole fraction in the vapor phase reduces the steam partial pressure. It can be observed in temperature profiles at 946 days (Fig. 5-22) that the chamber boundary temperature is higher for a heavier solvent. However, oil viscosity at the chamber edge for a heavier solvent will be higher even though the temperature is increased. It is because of the less effects of solvents which can be seen from the solvent mole fraction in the oil phase profiles at the chamber edge (Fig. 5-22). Moreover, the thickness of the

solvent rich zone is getting thinner for a heavier solvent compared with a lighter solvent like C_5. It is also visible from the data of properties at the chamber boundary in Grosmont C (5, 3, 31) for different solvent types (Table 5-4) that solvent and thermal effects combine to decide the bitumen viscosity. Furthermore, since the ultimate recovery is influenced by bitumen viscosity improvements, a lighter solvent like C_5 which presents the most solvent mole fraction in oil phase (0.68) and the lowest oil viscosity (0.96 cP) at the chamber edge makes it possible to achieve the lowest residual oil saturation (0.08) and hence the most ultimate bitumen recovery in Grosmont.

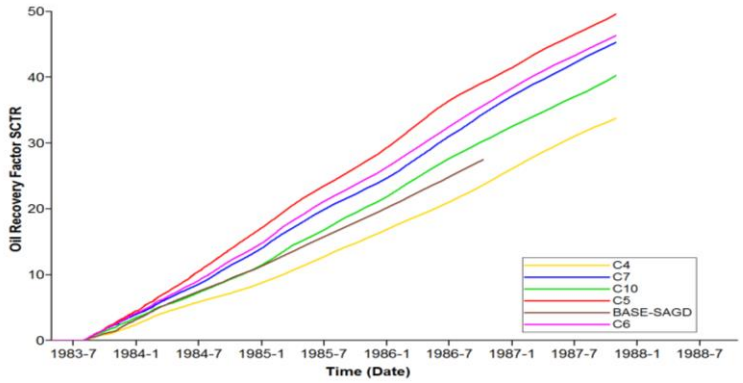

Figure 5-20 Oil recovery factor curves for different solvents

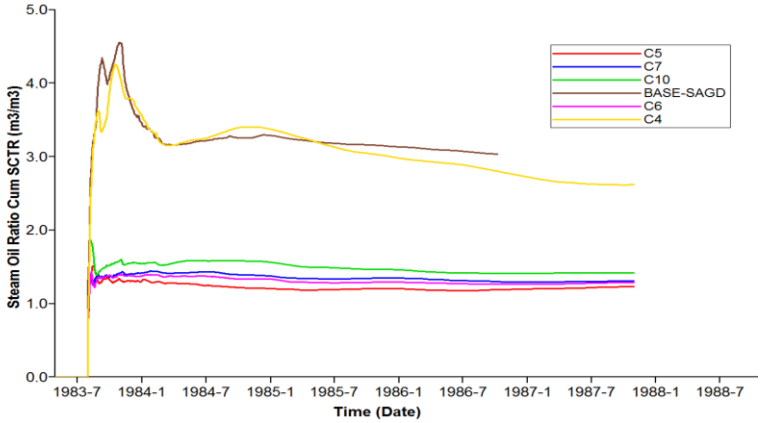

Figure 5-21 Cumulative steam oil ratio curves for different solvents

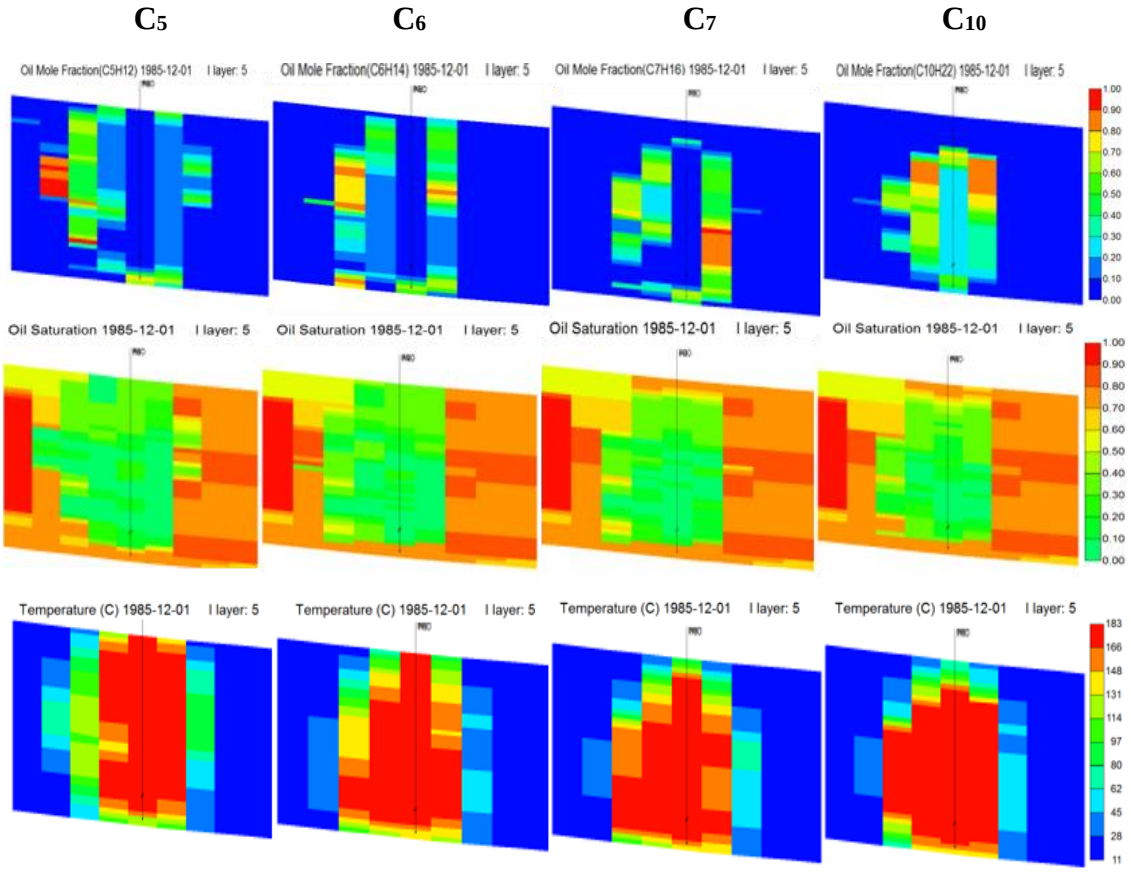

Figure 5-22 Solvent mole fraction, oil saturation and temperature profiles for different solvent types at 946 days

Table 5-4 Properties at the left chamber edge (5, 3, 31) for different solvents at 946 days

Properties at the left chamber edge (5, 3, 31)	C5	C6	C7	C10
Temperature (°C)	120.64	166.38	173.33	180.26
Viscosity (cp)	0.96	4.85	3.78	3.27
Solvent mole fraction in oil	0.68	0.27	0.30	0.34
Residual oil saturation	0.08	0.09	0.10	0.16

Next from a geological aspect, for a homogeneous model where vertical permeability is not too high as discussed in section 5.3, all solvents show similar cumulative bitumen production and

heavier solvents perform slightly better than lighter ones due to higher saturation temperature. Nevertheless, in this heterogeneously distributed thick Grosmont carbonate model with high permeability conduits or large porosity types, the lighter solvent like C_5 noticeably performs better than the others, because lower density and saturation temperature make it volatile and easily carried to high permeability conduits or large-scale karst related vug regions and then condense to push more oil out. Also, heavier solvents are not able to fully mix with bitumen, because they will condensate earlier before contacting with bitumen due to the heterogeneity of the reservoir and the existing of solution gas. Moreover, with the expansion of the chamber, some condensed solvents in these regions may be vaporized again due to the increasing temperature inside chamber (Jha, 2013).

All the above are the reasons that lighter solvent (C_5) expands a sweep area and achieves a lower residual oil saturation as seen from oil saturation and solvent mole fraction in oil phase profiles at 946 days on 1985-12-01 (Figure 5-22). In addition, in Figure 5-24 at 581 days on 1984-12-01, C_5 still appears the best propagation when the chamber has not contacted with a model boundary so that the boundary effects on sweep efficiency are eliminated. Furthermore, considering the important solvent retention problems, gas phase C_4 has a bad ultimate recycle compared with other solvents (Fig. 5-23). Initially, lower boiling point solvents like C_4 mainly remain in the gas phase which can be produced quickly. However, lighter C_4 flows override easily through high permeability conduits and accumulates around the top large porosity regions making C_4 recycle

difficult later. The solvent recovery percentage for C_5-C_7 is similarly more than 90% at the end of production which saves the economic cost. Heavier solvent like C_{10} has a higher recycle rate earlier and a lower solvent recovery factor later due to its high saturation temperature, which makes the blowdown recycle process more difficult.

In conclusion, volatile solvents like C_4 are detrimental to the whole solvent-aided process. Also, a lighter solvent like C_5 may be more suitable in an actual Grosmont carbonate no matter in terms of phase behavior evolution or geological environment, which is conflicting with an opinion previously that the solvents having a closer saturation temperature with respect to steam achieve the best results (Nasr, 2003). It is noteworthy that the diffusion coefficients are neglected in this chapter, the optimal solvent type may change when considering the effects of diffusion. However, some people insist that the diffusion difference to production can be seen only in a finer grid system (Ji, 2014; Mohebati, 2010).

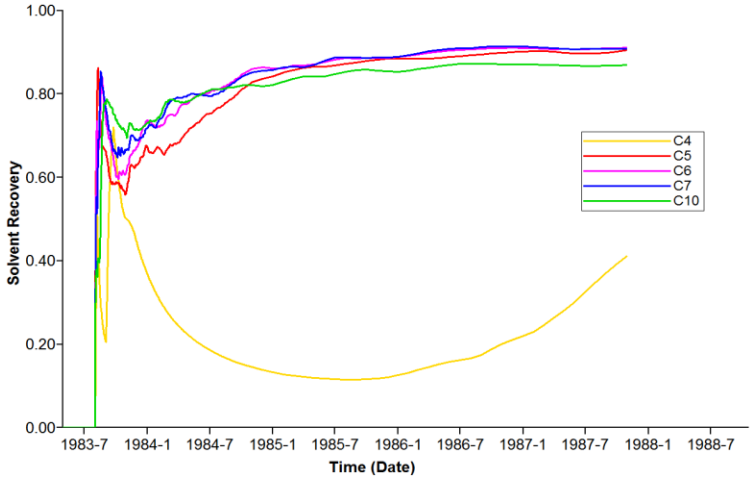

Figure 5-23 Solvent recovery curves comparison for different solvent types

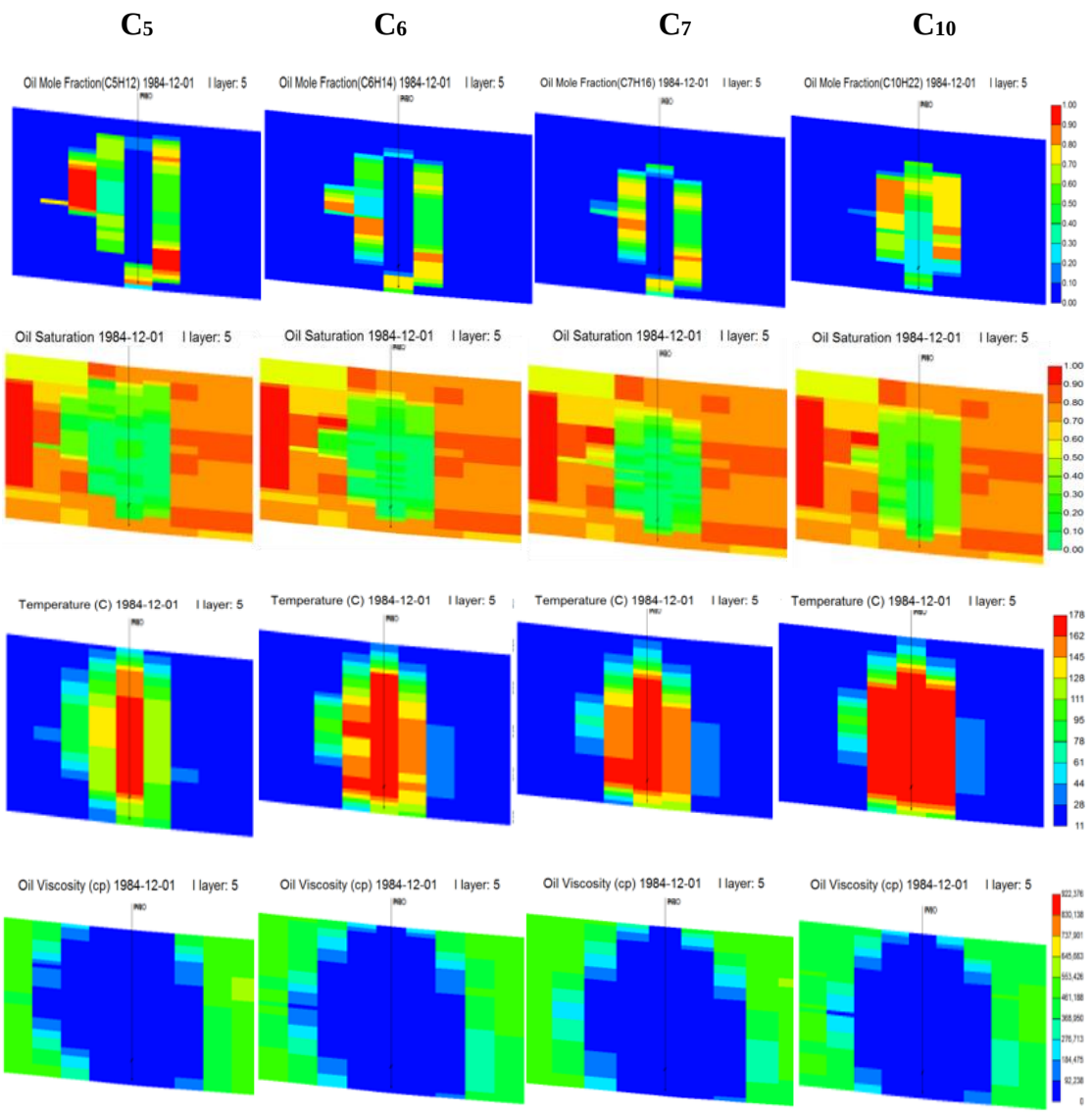

Figure 5-24 Solvent mole fraction, oil saturation, temperature and oil viscosity profiles for different solvent types at 581 days (Model boundary effects excluded)

5.7.3 Recycle of Solvents

A main economic problem during the solvent-aided process is that expensive solvents retained in the reservoir seems difficult for recycling. However, this method will be efficient if most of the

injected solvent can be recycled. Retention of solvent is mainly trapped in the vapor phase and dissolution in the oil phase (Ji, 2014). Thus, a part of solvent that is recovered with oil can be increased through oil production maximum strategies. Usually, the retained solvent will be recovered by a pressure blowdown process after the whole bitumen production. If the solvent co-injection is changed to pure steam injection during the last year of production with just 7 m^3/day, it can be seen in Figure 5-25 that up to 96% of C_7 injection is recovered in the end. The reason for an enhanced C_7 recycle factor is pressure blowdown which makes condensed solvent flashing again and producing in the vapor phase. From Figure 5-26, average pressure in the reservoir is dramatically decreased when the operation switches to a lower pure steam injection rate. In the meantime, C_7 production in the vapor phase is increased accordingly. It is predictable that heavier solvents larger than C_{10} may not have a satisfied recycle result during the blowdown process due to their higher boiling points.

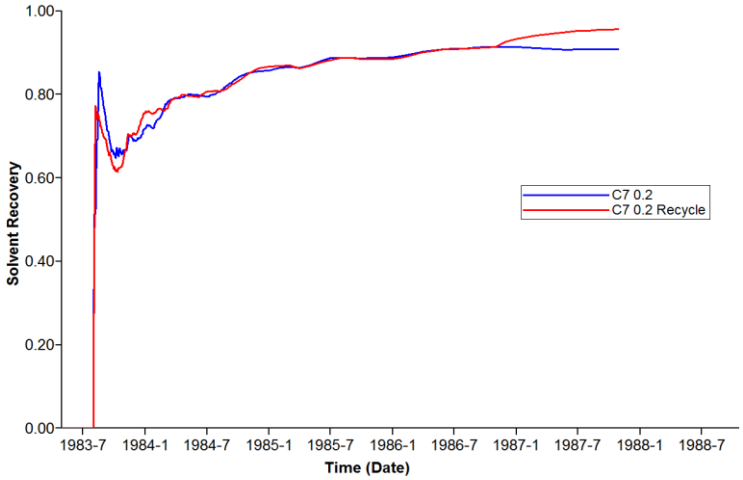

Figure 5-23 C_7 recovery curves comparison for pressure blowdown process

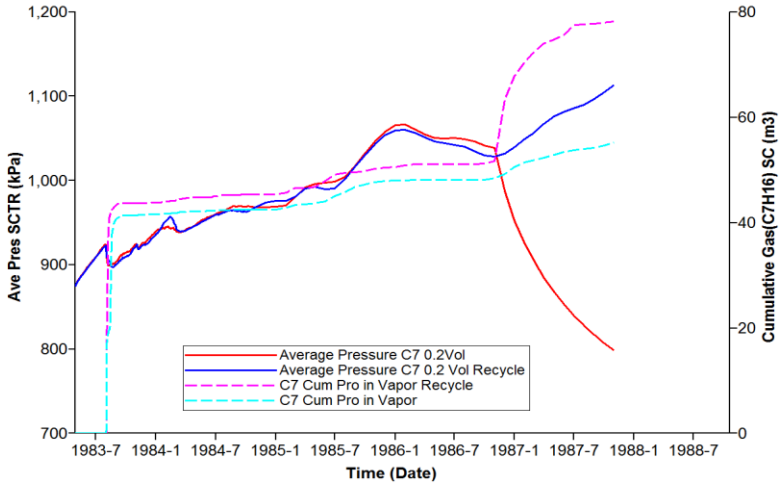

Figure 5-24 Average pressure and cumulative C_7 recovery in gas phase comparison

5.8 Conclusions

In this chapter, a detailed numerical simulation study of the solvent-aided process in the Grosmont carbonate has been discussed. Results show that carbonate reservoir heterogeneity and initial solution gas have significant effects on the ultimate bitumen recovery, and thus previous numerical studies of solvent-aided processes assuming a homogeneous model or neglecting the solution gas may not evaluate and predict the operation performance accurately in the carbonate reservoir. Existing of initial solution gas in the heterogeneous carbonate impedes bitumen production dramatically due to weakened heat transfer. Nevertheless, insulation gas films prevent steam or solvent channeling to the high permeability conduits like fractures and vugs leading to a lower solvent retention factor. Property evolution curves along the horizontal observation lines are analyzed to detect phase behaviors and mechanisms during the C_7-aided process. Solvent

accelerates the lateral chamber propagation and sweep regions. Furthermore, lower oil saturation less than the residual oil saturation inside chamber is observed, because several drainage mechanisms including heat transfer, gravity effects, solvent dilution and accumulation, steam channeling relieved by gas films and solvent rich zones combine together to reduce bitumen viscosity and enhance oil recovery during the solvent-aided process. Also, gas films and solvent rich zones relieve the steam channeling and overriding phenomenon. All of these explain why a solvent-aided process improves oil recovery and sweep efficiency compared with the conventional SAGD.

It is found that bitumen recovery is not proportional with a solvent volume fraction, because the ultimate recovery is influenced by bitumen viscosity improvements which are decided by the combination effects of solvent accumulation and thermal transfer. Also, a higher concentration is not favorable to the solvent recycle. Volatile solvents like C_4 are detrimental to the whole solvent-aided process. A lighter solvent with lower density and saturation temperature like C_5 is thought to be more suitable in an actual Grosmont carbonate with high permeability no matter in terms of phase behavior evolution or geological environment, if the effects of diffusion coefficients are negligible. A pressure blowdown process after the whole bitumen production will relieve the solvent retention and improve economic efficiency. Heavier solvents larger than C_{10} will not have a satisfied recycle result during the blowdown process due to their higher saturation temperature.

CHAPTER 6 : MULTI-PHYSICAL FLOW IN KARSTIFIED CARBONATE

6.1 Introduction

As discussed before, severe karstification forms the complex carbonate formation including various porosity types of fractures, vugs, matrix, breccia and karst. From the tomographic study, centimeter-scale vugs and large fractures embedded in the matrix are observed in Grosmont and half of the pore diameter is larger than 0.5mm (Edmunds, 2009). High permeability conduits existing in the Grosmont carbonate present a great challenge in modeling the intricated fluid flow process, especially for large-scale fractures or vugs. In the previous dual permeability/dual porosity (DK/DP) numerical simulation by CMG software, vugs are considered as a part of matrix to acquire reasonable history match results. A DK/DP model (Warren and Root, 1963) based on the dual continua theory divides a reservoir into matrix and fractures within an overlapping orthogonal grid. Then conservation and constraint equations are applied in the continua and Darcy's law is utilized to describe the liquid flow in both fractures and matrix. The dual continua method has been widely developed in the numerical simulation of naturally fractured reservoirs. However, in a carbonate reservoir with large-scale fractures or vugs, fluid prefer flowing mainly through these high permeability conduits. Considering that these regions have a significant effect on the whole flow field, isolated large fractures or vugs may not be treated as the traditional continua in a DK/DP model anymore and flow in large fractures or vugs may no longer be captured as a linear function of a pressure gradient by Darcy's law due to occurring free flow.

The study of fluid flow mechanisms is essential and necessary for reservoir numerical simulation. Recently, more accurate characterizations of multi-physical flow in the karstified carbonates have been studied. The Stokes equation can be employed to describe the free flow in large fractures or vugs while Darcy's law is still applicable in the porous matrix (Arbogast, 2006; Peng, 2009). However, complicated interface problems are proposed and precise information about boundary conditions should be required during the traditional Darcy-Stokes approach (Beavers and Joseph, 1967; Laptev, 2003), because Darcy's equation is a first-order partial differential equation while Stokes is a second-order one resulting in inconsistent interface problems. Brinkman modified Darcy's equation in order to use the no-slip boundary condition in porous regions. Thus, the Brinkman-Stokes approach, a unified equation combining both Darcy and Stokes flow, avoids additional slip boundary problems as in the Darcy-Stokes coupling (Brinkman, 1947; Neale, 1974; Salinger, 1994). Also, the transmissibility factor between fractures and matrix which should be set in Darcy's law is no longer specified during this multi-physical flow process (Saghir, 2001). Therefore, the Brinkman-Stokes model is more convenient especially for partially filled fractures, or if complicated boundary conditions of vugs are uncertain. Recently, it is being utilized to characterize the multiple physical flow regime between large-scale fractures or vugs and porous regions with a seamless transition boundary (Laptev, 2003; Popov, 2009; Gulbransen, 2009).

6.2 Brinkman-Stokes Model

6.2.1 Mathematical Equations

Incompressible steady fluid flow in the free flow region of large fractures or vugs can be described by the simplification of the Navier-Stokes equation neglecting the inertial force. The form of the Stokes equation together with mass conservation is:

$$\mu\nabla^2 u_F + \nabla p_F = 0$$

$$\nabla \cdot u_F = 0 \tag{6-1}$$

where μ is the fluid viscosity and the body force is negligible here.

Darcy's law is extensively used to define incompressible fluid flow in porous media:

$$u_M + \frac{k}{\mu}\nabla p_M = 0 \tag{6-2}$$

The Brinkman equation, namely the Brinkman-Stokes equation together with mass conservation, can describe fluid flow and capture the seamless transitional boundary layer effects between the free-flow fractures and porous regions:

$$\nabla p + \frac{\mu}{K}u - \mu_e\nabla^2 u = 0$$

$$\nabla \cdot u = 0 \tag{6-3}$$

where μ_e is the effective viscosity and K is the permeability tenser. This unified equation can be reduced to either the Stokes equation in free flow large-scale fractures if K is supposed to

infinity, or Darcy's equation in porous regions if μ_e equals zero. Usually, it is assumed that $\mu_e = \mu$, because the order of magnitude for $\mu_e \nabla^2 u_M$ is much smaller than other terms in equation (6-3). In other words, equation (6-3) is Darcy's equation with a small perturbation term.

Specific internal interface conditions are not required because this unified equation can change to the Darcy or Stokes form by varying parameters of the partial differential equation. Moreover, Stokes-Brinkman has a second-order partial differential equation form in both free flow and porous regions. Therefore, numerical calculations of the Stokes-Brinkman equation are easier without additional complex interface conditions compared with the traditional Darcy-Stokes coupling method. It acquires the velocity and stress continuity over an interface automatically through continuous spatial property variations. Therefore, the Brinkman-Stokes model is applied to describe multi-physical flow in a carbonate reservoir with large-scale fractures or vugs. Also, we should notice that a series of assumptions are made for simplification during simulation including incompressible steady single-phase flow and negligible inertial terms. In a 2D incompressible steady flow model, there are three unknown variables including p, u_x, u_y and three equations which can be solved through the finite element method. All of the multi-physical flow models in this chapter are finished by COMSOL finite element software. Velocity and pressure properties vary apparently in fractures and their boundaries, so finer grids should be created around fractures to capture the comparable grid resolution in free flow fractures and porous regions.

6.2.2 Model Validation

As mentioned, Brinkman-Stokes reduces to either the Stokes equation or Darcy's equation when some parameters change. A simple 2D smooth parallel plate model for simplification is utilized to represent flowing through a single 2 mm fracture (b) surrounded by porous media (a) in this part (Figure 6-1). Pressure difference (3000 kPa) is applied in the vertical direction. At first, if the permeability of porous regions is equal to that of the fracture representing an entire free flow region, observation line AB velocity comparison plots between the Brinkman-Stokes and Stokes equations applied in the whole region for different permeability values are depicted in Figure 6-2. It is verified that the gradually increased permeability values in porous regions make the Brinkman-Stokes velocity tending towards the Stokes velocity. That is to say, $\frac{\mu}{K}u$ term influence in the Brinkman-Stokes equation becomes negligible and can be reduced to the Stokes equation when the permeability in porous regions is relatively large.

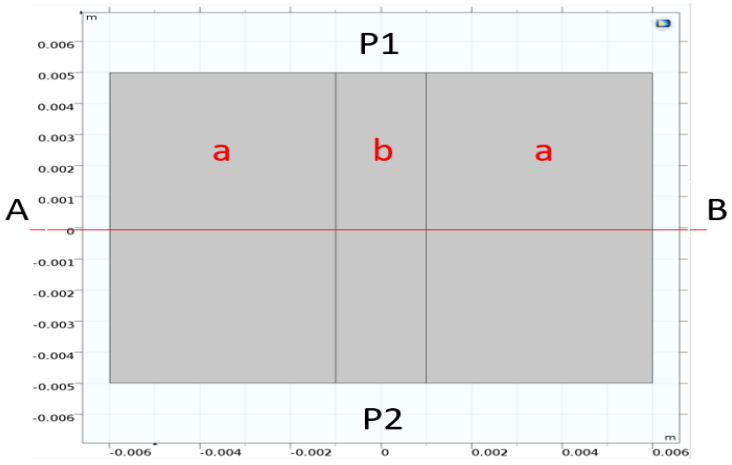

Figure 6-1 2D smooth parallel plate model with a single fracture

(a) K=10E+6 Darcy **(b) K=10E+8 Darcy**

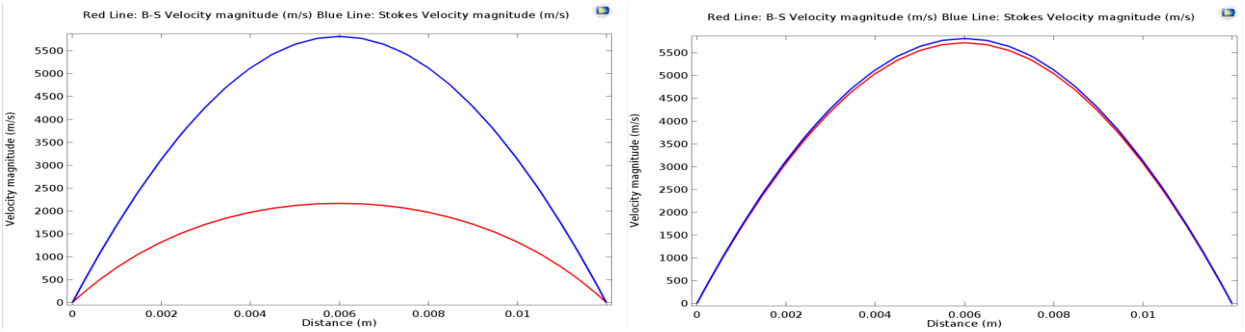

Figure 6-2 Observation line AB velocity comparison between Brinkman-Stokes model and Stokes model for (a) K=10E+6 Darcy, (b) K=10E+8 Darcy

The Brinkman equation contains an additional macroscopic shear term $\mu_e \nabla^2 u$ compared with the Darcy's law, and thus it can be reduced to Darcy's equation if μ_e equals zero. Furthermore, this additional term $\mu_e \nabla^2 u$ is preferable to describe the boundary layer effects in porous regions (Brinkman, 1947; Neale, 1974). At this time, Brinkman-Stokes and Darcy-Stokes coupling are investigated in this simple 2D smooth parallel plate model. Pressure difference (3000 kPa) is also applied in the vertical direction and classic interface conditions including velocity and pressure continuity are set between the free-flow fracture and the porous regions. In order to have a clear comparison plot of the boundary layer effects, permeability in porous regions is specified at a larger value (20D). Oil velocity results along the observation line AB for the Brinkman-Stokes and the Darcy-Stokes coupling are showed in Figure 6-3. The existence of boundary layer regions between the free flow fracture and the porous regions is verified during the Brinkman-Stokes

coupling. Brinkman-Stokes makes it possible to capture the smooth velocity transition boundary effects in porous media which proves the interface continuity in this equation. If we do a velocity line integration along the x direction for these two models, a fluid rate is derived. Although the boundary layer thickness is very small, an oil rate (m^2/s) due to boundary layer effects will be higher slightly in this single-fracture Brinkman-Stokes system, especially for a larger fracture aperture (Figure 6-4).

Therefore, the Brinkman-Stokes approach, a unified equation combining both Darcy and Stokes flow, avoids additional slip interface problems as in the Darcy-Stokes coupling. It is convenient to describe the multi-physical flow accurately in carbonates with large-scale fractures using this unified equation.

(a) Brinkman-Stokes Coupling **(b) Darcy-Stokes Coupling**

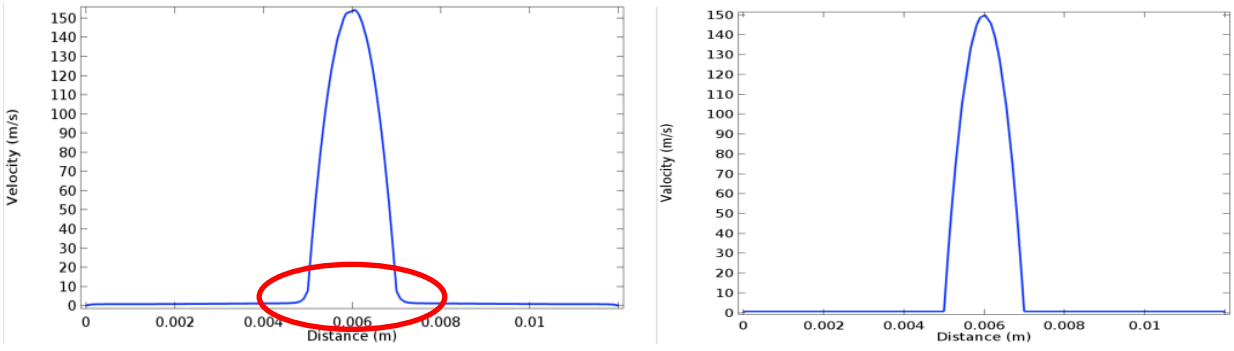

Figure 6-3 Oil velocity along the observation line AB for (a) Brinkman-Stokes coupling, (b) Darcy-Stokes coupling

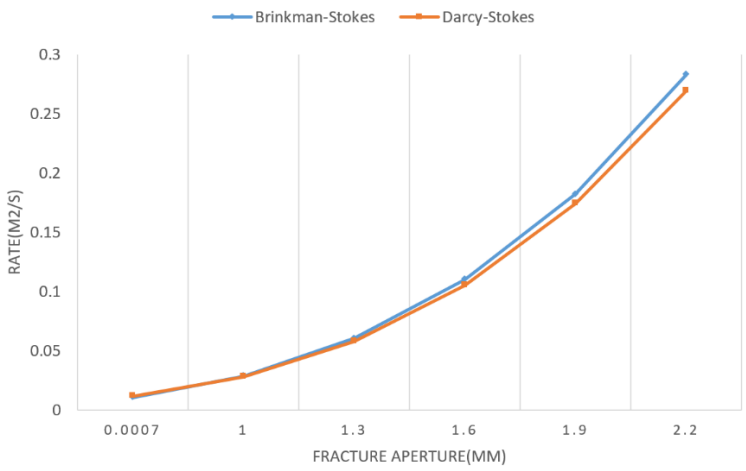

Figure 6-4 Oil rate comparison for Brinkman-Stokes and Darcy-Stokes models

6.3 2D Cases Simulation Results Discussion

The Brinkman-Stokes model will be studied in a synthetic reservoir with four stochastically distributed fractures for simplification. It is assumed that reservoir properties are homogeneous and isotropic and each fracture has a constant width. A two-dimensional multi-physical flow model with some fractures is created and simulated by COMSOL finite element software. Reservoir properties and other simulation inputs are listed in Table 6-1. Four 15mm fractures are placed stochastically around the middle producing well in this 2m*2m study region and two of them are connected (Figure 6-5). Reservoir pressure is 3000 kPa and wellhead pressure is set at the atmospheric pressure. After simulation, the velocity field with streamlines and pressure of the Brinkman-Stokes multi-physical flow model are shown in Figure 6-6.

Table 6-1 Multi-physical flow model reservoir properties

Parameter	Value
Oil Density, kg/m^3	1010
Oil Viscosity, cP	15
Matrix Permeability, mD	100
Matrix Porosity	0.25
Fracture Permeability, mD	10000
Reservoir Pressure, kPa	3000
Well Radius, m	0.1

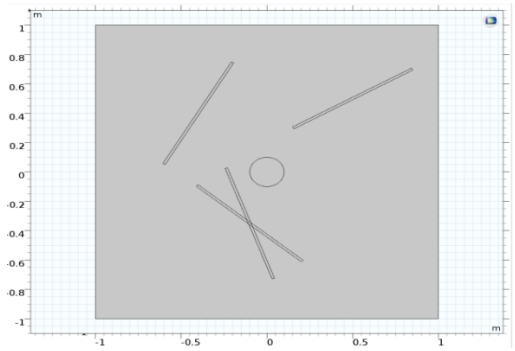

Figure 6-5 2D case model configuration

(a) Velocity Field with Streamlines **(b) Pressure Field Contours**

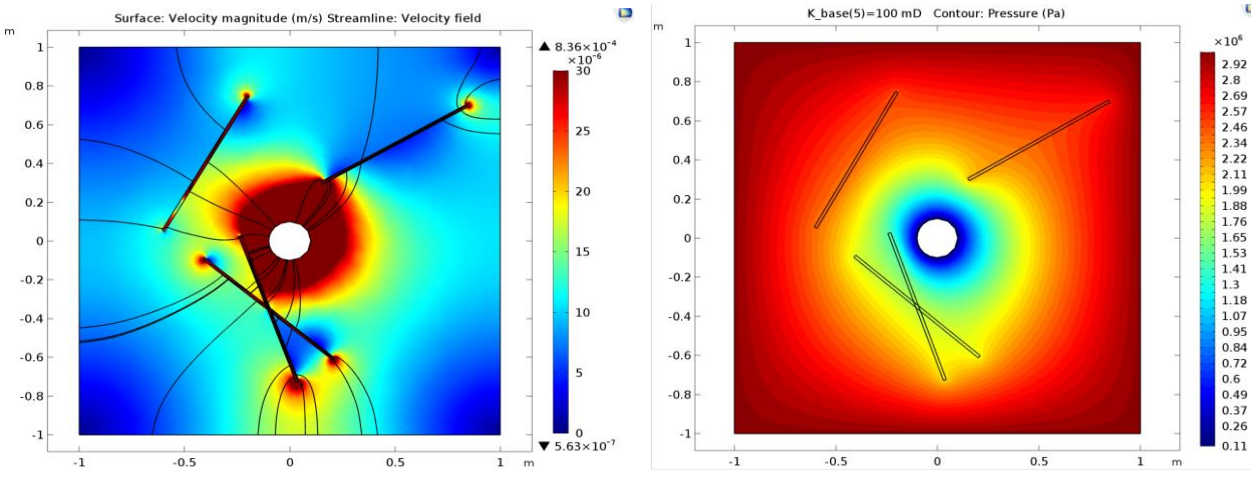

Figure 6-6 Brinkman-Stokes model (a) Velocity Field with Streamlines and (b) Pressure Field Contours simulation results

From the results, large-scale fractures have a significant influence on the flow routes and pressure field distribution, and hence should be characterized accurately in carbonate reservoir numerical simulation. It displays that the existing of large interconnected fractures distort velocity field profiles remarkably compared with other fractures alone. The fluid prefers flowing to more permeable regions as mentioned before and hence the flow velocity is faster apparently in the free flow fractures than that in porous areas. Although each fracture has the same aperture, velocity inside is different because of various slopes and positions of the fractures. It is observed that streamlines are not continuous when contacting the fractures due to fluid seepage inside the fractures. Furthermore, a pressure radial pattern is altered by large-scale fractures and a pressure drop inside the fractures is not significant as a result of faster pressure propagation in high permeability regions. If the reservoir height is assumed to be 10m, a relationship curve between the oil production volumetric rate per hour in the middle producing well and fracture permeability for the Brinkman-Stokes model is derived (Figure 6-7). It is observed that the production rate is promoted as fracture permeability increases. However, the oil rate difference is 0.15 m^3/h when the permeability of fractures varies from 10D to 100D, and if fracture permeability keeps rising larger than 100D, the production rate difference is only around 0.03 m^3/h which is assumed to be negligible. Therefore, when the fracture permeability of a carbonate reservoir is relatively large, to estimate an exact value of permeability is meaningless using this Brinkman-Stokes multi-physical flow model. For a heterogeneous carbonate reservoir, it is difficult to measure an accurate value of fracture permeability. Therefore, the Brinkman-Stokes model is more convenient when

there is limited information about the fracture properties, because accurately estimating the value of higher fracture permeability has a relatively small influence on the oil production rate.

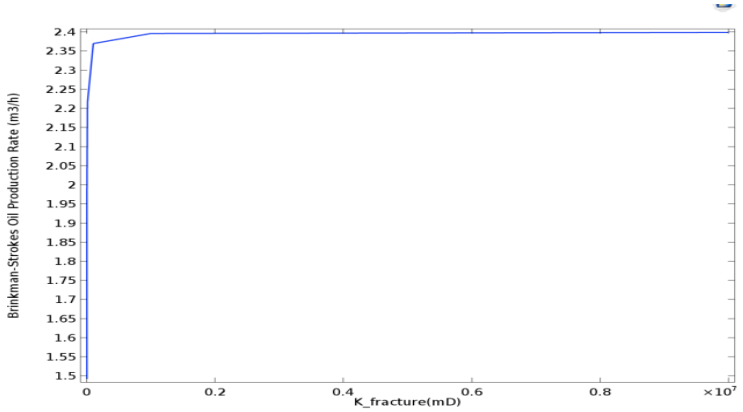

Figure 6-7 Relationship between oil production volumetric rate and fracture permeability

In the previous dual permeability/dual porosity model, Darcy's law is applied to describe the fluid flow in both fractures and porous media. Therefore, a Darcy-Darcy model will be tested with identical reservoir parameters. Also, simulation results will be compared to investigate the optimal range or conditions when the Brinkman-Stokes model should be employed. Solutions of the Darcy-Darcy model velocity field with streamlines and pressure plots are shown in Figure 6-8. Actually, only a slight difference can be seen from the plot compared with Figure 6-6. Under the same grid condition, the Darcy-Darcy velocity is smooth whereas the Brinkman-Stokes model has a slightly oscillating velocity solution. This phenomenon was reported by others as well (Salinger, 1994) and finer mesh resolution may improve the velocity solution oscillation in the Brinkman-Stokes model; however, the mesh resolution problem is out of the topics of this thesis. Instead, the

performance comparison of two models with identical conditions will be investigated. When the Brinkman-Stoke pressure minus the Darcy-Darcy pressure generates a distinct pressure difference contours (Figure 6-9), it is observed that pressure difference at the same position between two models is up to $10^4\ Pa$. Particularly, the Brinkman-Stokes model has a higher-pressure distribution and the difference becomes more evident especially around the producing well.

(a) Velocity Field with Streamlines **(b) Pressure Field Contours**

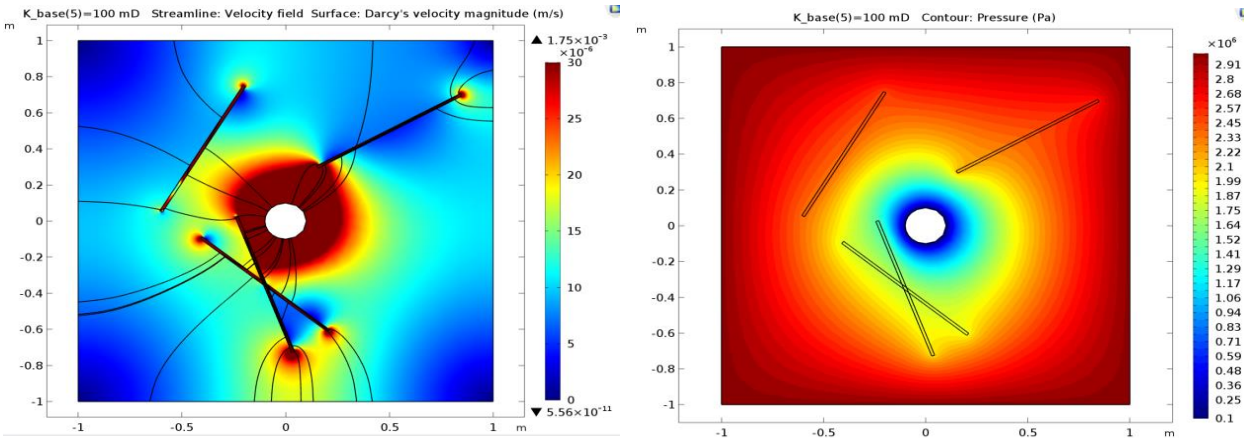

Figure 6-8 Darcy-Darcy model Velocity Field and Pressure Field Contours results

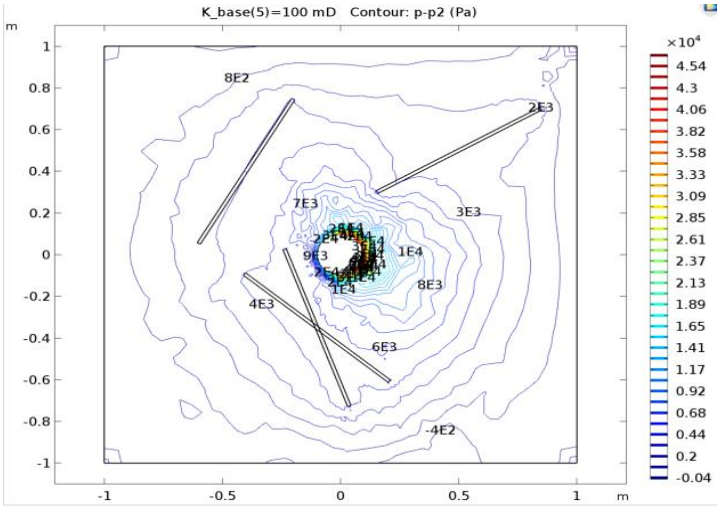

Figure 6-9 Pressure difference contours between two models

Further examination of the difference between the two models will be constructed through the oil production rate in the middle well (Figure 6-10). With a growth of matrix permeability, the middle well production rate of both the Brinkman-Stokes and Darcy-Darcy models keeps increasing monotonically due to a higher matrix permeability effect. Moreover, the difference of production between these two models is accelerated when matrix permeability enhances, though fracture permeability is kept at the same value (10000 mD). To better understand the influence of permeability and achieve a reasonable application range of the Brinkman-Stokes model, a relationship between the production difference error of these two models and matrix permeability is depicted in Figure 6-11. Each curve represents a relationship curve at a different fracture permeability value. From plot 6-11(a), it is observed that the difference error becomes larger with continuously increasing matrix permeability no matter which fracture permeability value is chosen. It is noteworthy that a rise of the difference error is not obvious at relatively large fracture permeability values. If we amplify the plot and get visible local curves at relatively larger fracture permeability values (Figure 6-11(b)), the difference error for K_f=1000D starts increasing at $K_m = 0.01D$ while the difference error for K_f=10000D is not enhanced until $K_m = 0.1D$. Thus, when the permeability ratio $\frac{K_f}{K_m}$ is less than $10\text{^}5$, a difference error between the two models becomes much more evident. This situation indeed exists in a severely karstified carbonate reservoir with cm-scale vugs. Although the error variation with matrix permeability is small, it will have an apparent production difference in the long-term exploitation. Therefore, a permeability ratio $\frac{K_f}{K_m} \approx 10\text{^}5$ is found below which the Brinkman-Stokes model should be

employed to describe the multi-physical flow on a karstified carbonate reservoir other than Darcy-Darcy model.

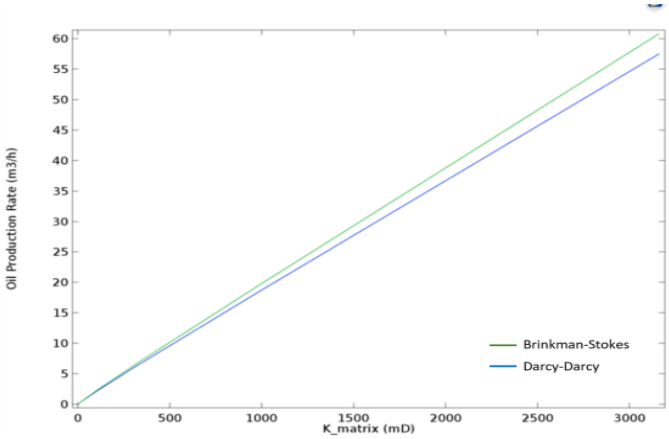

Figure 6-10 Oil production rate (m^3/h) vs. matrix permeability curves for two models

(a) **(b)**

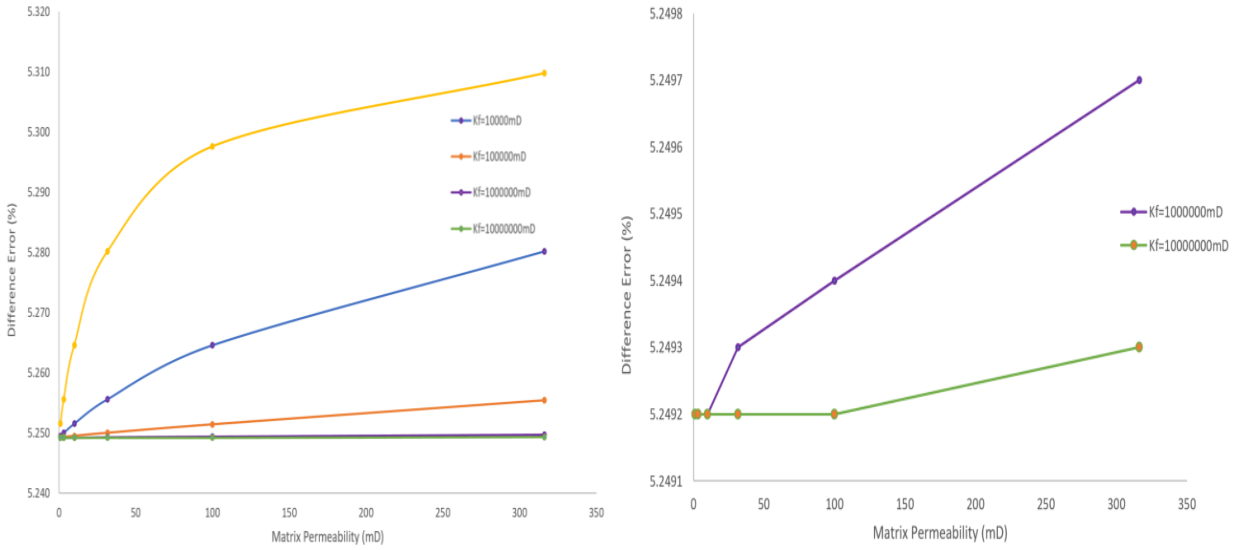

Figure 6-11 Relationship curves between the difference error and matrix permeability

Actually, relatively finer triangular grids inside or around fractures were created in our model with a maximum element size of 0.002m. If the mesh resolution is adjusted to a 0.005m maximum element size and hence fewer grids are inside the fractures (Figure 6-12), simulation results will change accordingly due to a coarser resolution. The difference error between these two models becomes larger when the mesh resolution gets coarser even though the fracture permeability is the same at 10000mD (Figure 6-13). Moreover, coarser grids around fractures are not able to capture the legible difference variation as matrix permeability increase. Absolutely, grid refining enhances the computation time, but it will provide more accurate production comparison between the Brinkman-Stokes and Darcy-Darcy models.

(a) 0.005m maximum element size **(b) 0.002m maximum element size**

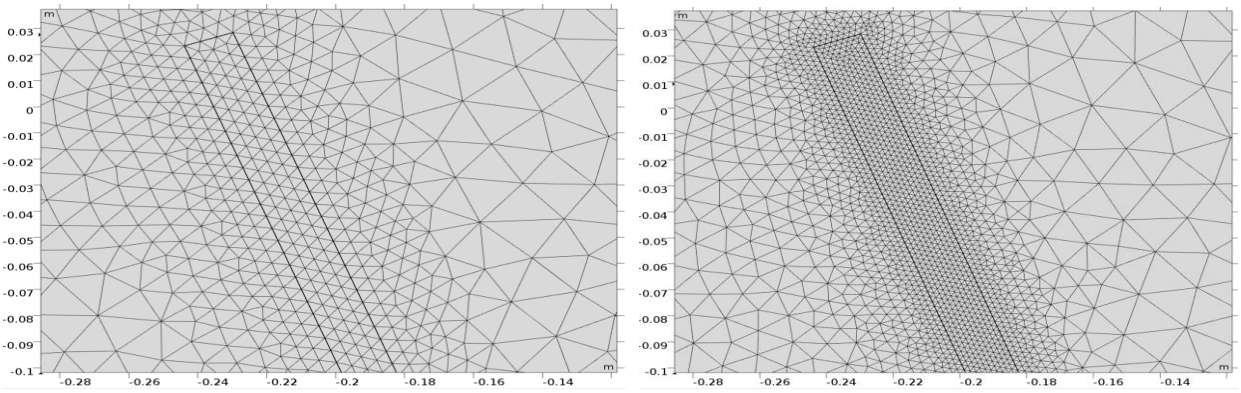

Figure 6-12 Grid resolution comparison of (a) 0.005m, (b) 0.002m maximum element size

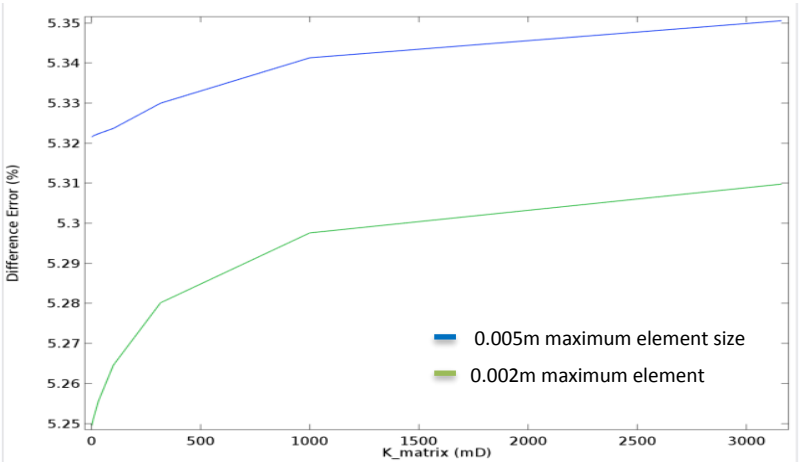

Figure 6-13 Difference error comparison for different grid resolution

In conclusion, large-scale fractures have a significant influence on the flow routes and pressure distribution. A fluid prefers flowing to more permeable regions. In addition, the flow velocity is faster apparently in fractures, and hence the Brinkman-Stokes model is feasible to describe the multi-physical flow in karstified carbonates, especially with large-scale vugs. It is more convenient without accurately estimating the value of fracture permeability. Also, a permeability ratio $\frac{K_f}{K_m} \approx$ 10^5 is found below which a difference error between the Brinkman-Stokes model and Darcy-Darcy model becomes more evident and hence the Brinkman-Stokes model should be employed to describe the multi-physical flow on a karstified carbonate reservoir. Furthermore, coarser grid resolution around fractures will also change the difference of production between the two models.

6.4 Application of Brinkman-Stokes Model in Future Work

In a real heterogeneous carbonate reservoir with complex fractures and vugs, there would be too many fine grids in the flow modeling which requires tremendous computations. The Brinkman-

Stokes equations are solved to achieve velocity and pressure distributions on the fine scale in Section 6.3. Although this synthetic model is small and simple, there are more than 80000 triangular grids in total. To solve this highly ill-conditioned system, the fine-scale multi-physical flow should be scaled up to a coarse-scale (Popov, 2009). Usually, effective permeability is presented to represent the property of the whole 2m*2m region and then Darcy's flow could be calculated on this coarse-scale. For example, if a pressure difference is placed in the horizontal direction and periodic velocity boundary conditions are set up on the 2m*2m block in Figure 6-14:

$$u(x, y = 1) \cdot n_1 = -u(x, y = -1) \cdot n_3, \quad P(x = -1, y) = \mathrm{P(x = 1, y)} - \mathrm{L}\frac{\partial P}{\partial x} \tag{6-4}$$

Effective permeability tenser of K_{xx} and K_{xy} is derived as below:

$$K_{xx} = \frac{\mu \overline{u_x} * L}{P_x} \qquad K_{xy} = \frac{\mu \overline{u_y} * L}{P_x} \tag{6-5}$$

where $\overline{u_x}$ is the average of the x component of the Brinkman-Stokes velocity and L is the length of a block.

Similarly, when a pressure difference is applied in the vertical direction:

$$u(x = -1, y) \cdot n_2 = -u(x = 1, y) \cdot n_4, \quad P(x, y = -1) = \mathrm{P(x, y = 1)} - \mathrm{L}\frac{\partial P}{\partial y} \tag{6-6}$$

Effective permeability tenser of K_{yy} and K_{xy} is derived also:

$$K_{yy} = \frac{\mu \overline{u_y} * L}{P_y} \qquad K_{yx} = \frac{\mu \overline{u_x} * L}{P_y} \tag{6-7}$$

Reservoir parameters are kept the same as mentioned before. Therefore, effective permeability tenser K for this entire 2m*2m region is calculated:

$$K = \begin{bmatrix} 115.73 & 2.99 \\ 2.99 & 123.06 \end{bmatrix} mD$$

More numbers of large fractures or vugs in a block will present a higher effective permeability. Once CT scan images of fracture distributions are acquired, effective permeability for each coarse-scale grid will be calculated and flow modeling in a larger region can be finished. This upscaled treatment not only considers the effects of large fractures to the entire flow field but also solves the tremendous grid numbers problem. It has been verified as a possible treatment to apply the B-S equations in future numerical simulation.

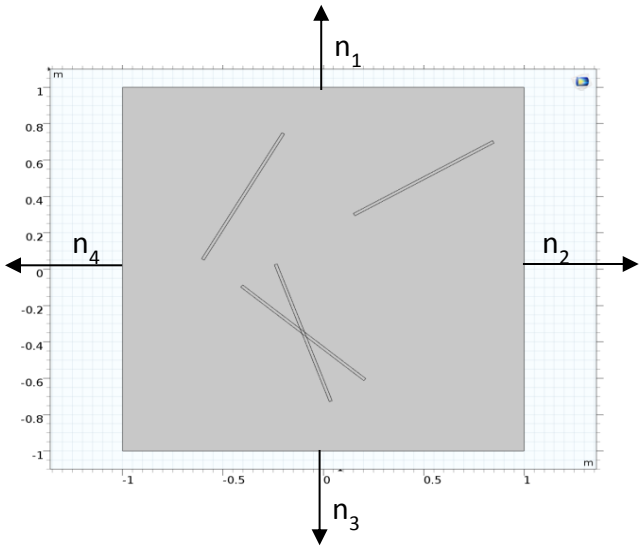

Figure 6-14 Periodic velocity boundary conditions of the entire study region

6.5 Conclusions

It is shown that the Brinkman-Stokes model should be employed to describe the multi-physical flow on karstified carbonates with free flow fractures and porous media. Brinkman-Stokes reduces to either the Stokes equation or Darcy's equation when some parameters vary. This unified equation makes it possible to capture smooth velocity transition boundary effects in porous media and hence provides the interface continuity in this equation and avoids additional complex slip interface conditions as in the traditional Darcy-Stokes coupling method. A 2D synthetic flow model is built to investigate that large-scale fractures have a significant influence on the flow routes and pressure distribution. During the Brinkman-Stokes multi-physical flow modeling, estimating an accurate value of fracture permeability has a relatively small influence on an oil production rate. Moreover, it is found that there is a permeability ratio $\frac{K_f}{K_m} \approx 10\text{^}5$ below which the Brinkman-Stokes model is preferable to describe the multi-physical flow in carbonates due to higher difference errors, compared with the conventional Darcy-Darcy model. Different grid resolution around fractures will also change the difference of production between these two models. Furthermore, the upscaled treatment through effective permeability calculations will solve more complicated flow problems in a real carbonate. However, more research should be conducted in terms of a coarse-scale 3D heterogeneous flow model.

CHAPTER 7 : CONCLUSIONS AND FUTURE WORK

7.1 Conclusions

A 3D heterogeneous numerical model representing the Grosmont carbonate has been built and validated by history matching of the vertical well Mclean pilot. This model includes various porosity types and high permeability conduits separated by discontinuous marl layers. Unavailable properties are decided by stochastic simulation in a reasonable range and tuned by history matching and optimization. Severe inter-well communications impact the bottom-hole pressure matching results. Several recovery strategies have been investigated in this model and a multi-physical flow has been tested on a seriously karstified carbonate. The following conclusions are derived:

1. The Brinkman-Stokes model can be employed to describe a multi-physical flow in a karstified carbonate with free flow fractures and porous media. Large-scale fractures have a significant influence on the flow routes and pressure distribution. Estimating an accurate value of fracture permeability has a relatively small influence on an oil production rate. Moreover, a permeability ratio $\frac{K_f}{K_m} \approx 10\text{^}5$ is found below which the Brinkman-Stokes model is preferable to describe the multi-physical flow compared with the conventional Darcy-Darcy model. Different grid resolutions around fractures also change a production rate.

2. Sensitivity assessments of the vertical well CSS process indicate that fracture spacing, rock compressibility, rock heat capability and a rock-in-fracture fraction have relatively large influences on the production and BHP results. Also, fracture properties are more sensitive in a higher fracture permeability reservoir.

3. The vertical well CSS process in Grosmont has severe steam overriding and limited sweep efficiency because of high vertical permeability and high-pressure injection. Therefore, well placements and operations should be noticed in the case of steam effectivity affected.

4. During the SAGD process, a moderate steam injection rate and steam trap at 10^{o}C should be chosen to obtain the optimal result in this model. Although a higher injection pressure can promote a growth of its steam chamber and overcome the marl barriers initially, it accelerates an earlier steam breakthrough.

5. SAGD has a stable, improved and longer production period. However, the performance of SAGD in the Grosmont carbonate varies dramatically when wells are placed near severe karst regions or operations change. A steam chamber which is extremely sensitive to the SAGD process is hardly formed during simulation because of reservoir heterogeneity and limited cored data.

6. The improved hybrid SAGD in a staggered pattern promotes the lateral and downward sweep and retains more heat regardless of a steam chamber shape. The recovery factor is 17% in a shorter time compared with 14% for Base-SAGD when the amounts of steam injected are the same. Well placements can be patterned by drilling additional vertical wells to promote heat distribution and oil production.

7. The optimal cycle numbers when switching to a continuous production period are the time that cyclic production become declined. Moreover, a shorter cycle length initially may be economic to save the steam injection and a longer cycle later may be effective for the whole hybrid SAGD operation. A moderate well spacing distance will be positive for thermal communication and heat distribution.

8. Initial solution gas in a heterogeneous carbonate impedes bitumen production dramatically due to weakened heat transfer. Nevertheless, insulation gas films prevent steam or solvents channeling to the high permeability conduits and lead to a lower solvent retention in the reservoir.

9. Several drainage mechanisms: heat transfer, gravity effects, solvent dilution and accumulation, steam channeling relieved by gas films and solvent rich zones make the

solvent-aided process to achieve a 7% more bitumen recovery factor with less steam injection than Base-SAGD during the same time.

10. Bitumen recovery is not proportional to a solvent volume fraction, because the ultimate recovery is decided by the combination effects of solvent accumulation and thermal transfer. Also, a higher concentration is not favorable to the solvent recycle. A lighter solvent like C_5 is thought to be more suitable in an actual Grosmont carbonate in terms of phase behavior evolution or geological environment. Volatile solvents like C_4 are detrimental to the whole solvent-aided process. In addition, heavier solvents larger than C_{10} will not have a satisfied recycle result during the blowdown process due to their higher saturation temperature.

7.2 Recommendations for Future Work

1. A larger and more detailed geostatistical carbonate model needs to be built including water layers and karst related regions. Inter-well communications which have a relatively important influence on five-spot or multi-well patterns should be considered in a larger carbonate reservoir model. More sensitivity analysis to improve steam overriding in this carbonate with high permeability conduits can be developed. Moreover, solvent mixture

injection and economical examination of solvent retention will provide a practical significance to the solvent-aided process in carbonates.

2. The application of the Brinkman-Stokes multi-physical flow should be studied in a more complicated derived carbonate model including the practical characteristics of vugs and fractures. Assuming single phase steady-state flow can be extended to a multiphase transient flow. With the upscaled treatments on a coarser scale, it is possible to apply Brinkman-Stokes in the future commercial reservoir simulator.

References

Al-Hadhrami, H.S. and Blunt, M.J. 2001. Thermally Induced Wettability Alteration to Improve Oil Recovery in Fractured Reservoirs. *SPE Reservoir Evaluation & Engineering*.

Marciales, A. and Babadagli, T. 2014. Solvent-Selection Criteria Based on Diffusion Rate and Mixing Quality for Steam/Solvent Applications in Heavy-Oil and Bitumen Recovery. *Society of Petroleum Engineers*.

Gulbransen, A., Hauge, V and Lie, K. 2009. A Multiscale Mixed Finite-Element Method for Vuggy and. Naturally-Fractured Reservoirs. *Society of Petroleum Engineers.*

Yazdani, A., Alvestad, J., Kjonsvik, D. and Gilje, E. 2012. A Parametric Simulation Study for Solvent-Coinjection Process in Bitumen Deposits. *Journal of Canadian Petroleum Technology.*

Beavers, G.S. and Joseph, D.D. 1967. Boundary Conditions at a Naturally Permeable Wall. *Journal of Fluid Mechanics*, 30, 197-207.

Buschkuehle, B. E., Hein, F. J. and Grobe, M. 2006. An overview of the geology of the Upper Devonian Grosmont carbonate bitumen deposit, northern Alberta, Canada. *Natural Resources Research.*

Bi, L. 2009. A unified multi-physics model for flow through naturally fractured carbonate karst reservoirs. *Thesis (Ph.D.) --University of Wyoming.*

Butler, R.M. 1985. A new approach to the modeling of steam-assisted gravity drainage. *J Can Pet Technol* 24 (3): 42–51.

Bryan, J., Huang, H. and Kantzas, A. 2014. Recovery of Bitumen in a Heterogeneous Carbonate through Application of Warm Solvent. *SPE Heavy Oil Conference, Calgary, Canada*.

Ji, D. 2014. Simulation Study of Steam-Solvent Phase Behavior in Solvent Aided SAGD Process and Its Effect on Oil Recovery. *http://dx.doi.org/10.5072/PRISM/27788*.

Ghanbari, E., Mighani, S., Shaabani, E. and Alipour, R. 2011. Improving SAGD performance combining with CSS. *International petroleum technology conference.*

ERCB. 2011. Alberta's energy reserves 2010 and supply/demand outlook 2011-2020, *Energy Resources Conservation Board*.

ERCB. 2011. Potential of EOR in Alberta Oil Pools, *Energy Resources Conservation Board*.

Ezeuko C.C, et al. 2013. Simulation Analysis of Steam-Based EOR Using MultiObjects Grosmont Models. *SPE Heavy Oil Conference-Canada.*

Ezeuko C.C, et al. 2013. Object Characterization and Simulation of Thermal Recovery from Karstified, Brecciated and Fractured Bitumen Carbonate Reservoirs. *International Petroleum Technology Conference.*

Ezeuko C.C, et al. 2015. Towards the Development of Bitumen Carbonates: An Integrated Analysis of Grosmont Steam Pilots. *Oil & Gas Science and Technology*.

Coskuner, G. 2009. A New Process Combining Cyclic Steam Stimulation and Steam-Assisted Gravity Drainage: Hybrid SAGD. *Journal of Canadian Petroleum Technology*, 48(1): 8–13

Machel, H. G. et al. 2012. Grosmont: the world's largest unconventional oil reservoir hosted in carbonate rocks. *Geological Society, London, Special Publications*, 370, 49-81.

Brinkman, H. C. 1947. A Calculation of the Viscous Force Exerted by a Flowing Fluid on a Dense Swarm of Particles, *Journal of Applied Sciences Research*.

Warren, J. E. and Root, P. J. 1963. The Behavior of Naturally Fractured Reservoirs, *SPE Journal*, Vol. 3, No. 3, pp. 245-255.

He, J., Killough, J. E., Fadlelmula, F., Mohamed, M. and Fraim, M. 2015. A Unified Finite Difference Model for The Simulation of Transient Flow in Naturally Fractured Carbonate Karst Reservoirs. *SPE Reservoir Simulation Symposium*.

Marcin, K., Ligaarden, I. S., Lie, K. A. and Schmid, D. W. 2011. On the Importance of the Stokes-Brinkman Equations for Computing Effective Permeability in Karst Reservoirs. *Communications in Computational Physic*s, vol. 10, issue 05.

Luo, P. and Machel, H. G. 1995. Pore size and pore-throat types in a heterogeneous dolostone reservoir, Devonian Grosmont Formation, Western Canada Sedimentary Basin. *American of Petroleum Geologists Bulletin*.

Laptev, V. 2003. Numerical solution of coupled flow in plain and porous media. *Ph.D. Doctoral Thesis.*

Keshavarz, M., Okuno, R. and Babadagli, T. 2015. Optimal Application Conditions for Steam/Solvent Coinjection. *Society of Petroleum Engineers*.

Mohebati, M. H., Maini, B.B. and. Harding, T.G. 2010. Numerical Evaluation of Hydrocarbon Additives to Steam in the SAGD Process. *Journal of Canadian Petroleum Technology*.

Mohebati, M. H., Maini, B.B. and. Harding, T.G. 2010. Optimization of Hydrocarbon Additives with Steam in SAGD for Three Major Canadian Oil Sand Deposits. Paper. Canadian Unconventional Resources and International Petroleum Conference.

Mohebati, M. H. et al. 2014. Thermal Recovery of Bitumen from the Grosmont Carbonate Formation - Part 1: The Saleski Pilot. Journal of Canadian Petroleum Technology.

Naderi, K., Babadagli, T. and Coskuner, G. 2013. Bitumen Recovery by the SOS-FR (Steam-Over-Solvent Injection in Fractured Reservoirs) Method: An Experimental Study on Grosmont Carbonates, *Energy and Fuels.*

Naderi, K. and Babadagli, T. 2014. Use of Carbon Dioxide and Hydrocarbon Solvents during the Method of Steam-Over-Solvent Injection in Fractured Reservoirs for Heavy-Oil Recovery from Sandstones and Carbonates, *SPE Reservoir Evaluation & Engineering*.

Naderi, K. and Babadagli, T. 2016. Solvent Selection Criteria and Optimal Application Conditions for Heavy-Oil/Bitumen Recovery by Hybrid Thermal and Solvent Methods: A Review and Comparative Analysis. *J. of Energy Resources Technology*.

Neale, G. and Nader, W. 1974. Practical Significance of Brinkman's Extension of Darcy's Law Coupled Parallel Flows within a Channel and a Bounding Porous Medium. *The Canadian Journal of Chemical Engineering*.

Qi, J., Yuan, J-Y. 2013. History Matching Grosmont C Carbonate Thermal Production Performance. *SPE Heavy Oil Conference-Canada.*

Xu, J. et al. 2014. Numerical Thermal Simulation and Optimization of Hybrid CSS/SAGD Process in Long Lake with Lean Zones. *SPE Heavy Oil Conference-Canada.*

Liu, J., Ren, F., Bao, L., Yang, L., Ma, D. 2003. Gravity Drainage as a Potential. Follow-Up Process for CSS. *Canadian International Petroleum Conference.*

Li, J., Zhao, X., Chen, Z., 2011. Design and numerical study of a new hybrid CSS-SAGD process using horizontal wells for recovering heavy oil. *Petroleum Science and Technology.*

Ardali, M., Mamora, D. D., Barrufet, M. 2010. A comparative simulation study of addition of solvents to steam in SAGD process. *Canadian Unconventional Resources and International Petroleum Conference*.

Novak J., Edmunds N., Cimolai M. 2007. A history match of. CSS recovery in the Grosmont, *8th Canadian International Petroleum Conference*, SPE.

McDougall, M., Alvarez J. M., and Isaacs, E., 2008. Alberta Carbonates - the Third Trillion. *19th World Petroleum Congress*, 19-0925.

Edmunds, N. et al. 2009. Prospects for Commercial Bitumen Recovery from the Grosmont Carbonate, Alberta, *J. Can. Petrol. Technol*.

Popov, P., Qin, G., Bi, L., Efendiev, Y., Kang, Z. and Li, J. 2009. Multiphysics and Multiscale Methods for Modeling Fluid Flow through Naturally Fractured Carbonate Karst Reservoirs, *SPE Reservoir Evaluation & Engineering*, 12(2):218-231.

Govind, P. A., Das, S. K. Srinivasan, S., Wheeler, T. J. 2008. Expanding solvent SAGD in heavy oil reservoirs. *International Thermal Operations and Heavy Oil Symposium*.

Jiang, Q. and Youck, D. 2006. Improving Recovery from Partially Depleted Reservoirs after Cyclic Steam Stimulation (CSS) Operations. *World Heavy Oil Conference, Beijing*.

Jiang, Q. et al. 2009. Evaluation of Recovery Technologies for the Grosmont Carbonate Reservoirs. *Journal of Canadian Petroleum Technology* 49(05).

Song, Q. et al. 2015. Steam Injection Schemes for Bitumen Recovery from the Grosmont Carbonate Deposits. *SPE Canada Heavy Oil Technical Conference.*

Jha, R. K. et al. 2013. New Insights into Steam/Solvent-Co-injection Process Mechanism. *SPE Journal.*

Russel-Houston, J. and Gray, K. 2014. Paleokarst in the Grosmont Formation and Reservoir Implications, Saleski Alberta. *Society of Exploration Geophysicists*.

Zimmerman, R.W., Bodvarsson, G.S. 1996. Hydraulic conductivity of rocks fractures. *Transport in Porous Media*.

Saghir, M. Z., Nejad, M., Vaziri, H. H. and Islam, M. R. 2001. Modeling of heat and mass transfer in a fractured porous medium. *International Journal of Computational Fluid Dynamics*.

Salinger, A. G.; Aris, R. and Derby, J. J. 1994. Finite element formulations for large-scale coupled flows in adjacent porous and open fluid domains. *International Journal for Numerical Methods Fluids*.

Saltelli A., Annoni P., Azzini I., Campolongo F., Ratto M., Tarantola S. 2010. Variance based sensitivity analysis of model output. Design and estimator for the total sensitivity index, *Computer Physics Communications*.

Das, S. 2007. Application of thermal processes in heavy oil carbonate reservoirs. *15th SPE Middle East Oil & Gas Show*.

Arbogast, T. and Lehr, H. 2006. Homogenization of a Darcy-Stokes system modeling vuggy porous media. *Computational Geosciences*.

Nasr, T.N., Beaulieu, G., Golbeck, H. and Heck, G. 2003. Novel expanding solvent-SAGD process ES-SAGD. *Journal of Canadian Petroleum Technology*.

UNOCAL Report 1168, 1990. Geological Description of Upper Grosmont 3.

UNOCAL Report 648, 1987. Grosmont Thermal Recovery Project: A Summary of Project Knowledge.

Pathak, V., Babadagli, T. and Edmunds, N.R. 2012. Mechanics of Heavy-Oil and Bitumen. Recovery by Hot Solvent Injection. *Society of Petroleum Engineers.*

Li, W. 2010. Drainage Mechanism of Steam with Solvent Coinjection under Steam Assisted Gravity Drainage (SAGD) Process. *International Oil and Gas Conference and Exhibition in China.*

Peng, X.; Du, Z.; Liang, B.; Qi, Z. 2009. Darcy-Stokes streamline simulation for the Tahe-fractured reservoir with cavities. *SPE Journal*.

Yang, D., Hosseininejad Mohebati, M., Brand, S. et al. 2014. Thermal Recovery of Bitumen from the Grosmont Carbonate Formation - Part 2: Pilot Interpretation and Development Strategy. *Journal of Canadian Petroleum Technology*.

Yang, L. 2006. Field Test of SAGD as Follow-Up Process to CSS in Liaohe Oil Field of. China. *Journal of Canadian Petroleum Technology.*

Yuan, J-Y, et al. 2010. Evolving Recovery Technologies Directed Towards Commercial Development of the Grosmont Carbonate Reservoirs. *Canadian Unconventional Resources and International Petroleum Conference*.